

August 2022

Adsorption of Per- and Polyfluoroalkyl Substances on Functionalized Minerals: Effects of Modifier Property and Mineral Structure

Qianqian Dong
University of Wisconsin-Milwaukee

Follow this and additional works at: <https://dc.uwm.edu/etd>



Part of the [Environmental Engineering Commons](#)

Recommended Citation

Dong, Qianqian, "Adsorption of Per- and Polyfluoroalkyl Substances on Functionalized Minerals: Effects of Modifier Property and Mineral Structure" (2022). *Theses and Dissertations*. 2991.
<https://dc.uwm.edu/etd/2991>

This Dissertation is brought to you for free and open access by UWM Digital Commons. It has been accepted for inclusion in Theses and Dissertations by an authorized administrator of UWM Digital Commons. For more information, please contact scholarlycommunicationteam-group@uwm.edu.

ADSORPTION OF PER- AND POLYFLUOROALKYL
SUBSTANCES ON FUNCTIONALIZED MINERALS: EFFECTS OF
MODIFIER PROPERTY AND MINERAL STRUCTURE

by

Qianqian Dong

A Dissertation Submitted in
Partial Fulfillment of the
Requirements of the Degree of

Doctor of Philosophy
in Engineering

at

The University of Wisconsin-Milwaukee

August 2022

ABSTRACT

ADSORPTION OF PER- AND POLYFLUOROALKYL SUBSTANCES ON FUNCTIONALIZED MINERALS: EFFECTS OF MODIFIER PROPERTY AND MINERAL STRUCTURE

by

Qianqian Dong

The University of Wisconsin-Milwaukee, 2022
Under the Supervision of Professor Yin Wang

Per- and polyfluoroalkyl substances (PFAS) are a large group of manmade chemicals widely used in various consumer and industrial products. The adverse effect of PFAS exposure includes bioaccumulation, organ damage and birth defects. Although the primary feedstock perfluorooctanoic acid (PFOA) and perfluorooctanesulfonic acid (PFOS) has been phased out since the 2000s, PFAS are worldwide detectable in water bodies due to the historical production, accumulation and endless substitution of long-chain PFAS in the environment. Removal of PFAS represents a special challenge for water/wastewater treatment because of their diverse structures and unique physicochemical properties such as high-water solubility and high stability of the C-F bond. Therefore, it is urgent to find a cost-effective way to deal with PFAS contamination.

Compared to the destructive approaches, adsorption is a safe and economical way to treat PFAS through physical separation. Clay mineral-based adsorbent shows great potential in PFAS removal due to its environmental friendliness, small particle size, layered structure, cation exchangeability and abundant active grafting sites. Ionic liquid, as a green solvent, has not been studied for the PFAS removal through the intercalation with clay minerals. Ionic liquid and silane with various functional groups and chain lengths can be used for clay modification through ionic exchange or

post-grafting reactions. Enlarging the surface area of clay minerals with exfoliation could provide more active sites for post-grafting. The covalent bond between silane and clay minerals also benefits the regeneration and reuse of spent adsorbents. Besides, clay minerals such as montmorillonite and vermiculite possess different structures and compositions which play important roles in adsorption. Overall, the objective is to develop organically functionalized clay materials with high adsorption capacity, fast adsorption kinetics and good regeneration ability for PFAS removal. The effect of organic modifier composition, clay mineral structure, PFAS structure and clay/modifier ratio are systematically investigated.

This dissertation entails (1) the review of current technology on PFAS treatment including destructive and non-destructive methods, (2) the development and characterization of ionic liquid-modified montmorillonite with enhanced adsorption of PFOA and PFOS and the elucidation of the impact of ionic liquid chain length on PFOA and PFOS removal, (3) the characterization and comparison of ionic liquid-modified clays prepared using various clay substrates for the adsorption of eight representative PFAS, (4) and removal of perfluoroalkyl acids (PFAAs) and precursors with silylated clay: efficient adsorption and enhanced reuse.

© Copyright by Qianqian Dong, 2022
All Rights Reserved

TABLE OF CONTENTS

ABSTRACT	ii
TABLE OF CONTENTS	v
LIST OF FIGURES	vii
LIST OF TABLES	ix
ACKNOWLEDGMENTS	x
Chapter 1 Introduction and Research Objectives	1
1.1 Background	1
1.2 Current technology in PFAS removal	3
1.2.1 Destructive technology	3
1.2.2 Nondestructive Technology	4
1.3 Clay-based adsorbents in PFAS removal	6
1.5 Research objectives and outlines	8
Chapter 2 Efficient Sorption of Perfluoroalkyl Acids by Ionic Liquid-Modified Natural Clay.....	11
2.1 Introduction	11
2.2 Materials and methods	15
2.2.1 Materials and chemicals	15
2.2.2 IL-modified clay preparation and characterization	16
2.2.3 Batch sorption experiments	17
2.3 Results and discussion	21
2.3.1 Effect of IL chain length on PFOA and PFOS sorption	21
2.3.2 Characterization of IL-modified clays	23
2.3.3 Sorption kinetics and isotherms of PFOA and PFOS by CaMTC16	28
2.3.4 Effects of water chemistry	33
2.3.5 Regeneration and reuse	36
2.3.6 Removal of multiple PFAS compounds	37
2.3.7 Practical considerations	38
2.4 Conclusions	39
Chapter 3 Adsorption of PFAS on Ionic Liquid-Modified Clays: Effect of Clay Mineral Structure and PFAS Nature	41
3.1 Introduction	41
3.2 Material and Methods	44

3.2.1 Chemicals.....	44
3.2.2 Synthesis and characterization of IL-modified clays	46
3.2.3 PFAS adsorption experiments.....	47
3.2.4 PFAS measurement.....	47
3.2.5 Data analysis	50
3.3 Results and Discussion.....	52
3.3.1 Characterization of IL-modified clay minerals	52
3.3.2 Adsorption isotherms of PFAS by IL-modified clays.....	54
3.3.3 Discussion of the PFAS structural impact on adsorption.....	61
3.3.4 Adsorption of low-concentration PFAS mixture in various water matrices	68
3.4 Conclusions.....	70
Chapter 4 Removal of Perfluoroalkyl Acids and Precursors with Silylated Clay: Efficient Adsorption and Enhanced Reuse.....	72
4.1 Introduction.....	72
4.2 Materials and Methods.....	75
4.2.1 Materials	75
4.2.2 Preparation of organically functionalized clays.....	77
4.2.3 Material Characterization.....	78
4.2.4 Batch Sorption Experiments	79
4.2.5 PFAS measurement.....	80
4.3 Results and Discussion.....	82
4.3.1 Material characterization.....	82
4.3.2 Adsorption kinetics	85
4.3.3 Adsorption isotherms	88
4.3.4 Effect of water chemistry parameters	91
4.3.5 Regeneration and reuse	94
4.4 Conclusion	96
Chapter 5 Conclusions and Recommendations.....	98
5.1 Conclusions.....	98
5.2 Recommendations for future work	100
Reference	101
CURRICULUM VITAE.....	117

LIST OF FIGURES

Figure 2.1 Sorption of PFOA and PFOS by raw (CaMT) and IL-modified clays prepared using ILs with different alkyl chain lengths (CaMTC4 – CaMTC16). Experiments were conducted at pH 5 with an initial PFOA or PFOS concentration of 1 mg/L, a sorbent loading of 0.25 g/L.....	22
Figure 2.2 XRD patterns of raw and IL-modified clays prepared using ILs with different alkyl chain lengths at 2theta in the range of 3 – 10 degrees.	24
Figure 2.3 FTIR spectra of raw and IL-modified clays prepared using ILs with different alkyl chain lengths. Error bars represent one standard deviation of duplicate experiments. Error bars represent one standard deviation of duplicate experiments.....	26
Figure 2.4 Zeta potentials of raw and IL-modified clays prepared using ILs with different alkyl chain lengths at pH 3 – 11. Error bars represent one standard deviation of duplicate experiments.	26
Figure 2.5 Sorption kinetics of PFOA and PFOS by CaMTC16. Experiments were conducted at pH 5 with an initial PFOA or PFOS concentration of 1 mg/L and a sorbent loading of 0.25 g/L. Dash lines represent pseudo-second order kinetics model fit.	29
Figure 2.6 Sorption isotherms of (a) PFOA and (b) PFOS by CaMTC16 and their Langmuir model fits. Experiments were conducted at pH 5 with a sorbent loading of 0.25 g/L and a contact time of 24 h. Error bars represent one standard deviation of duplicate experiments.....	31
Figure 2.7 Effects of (a) solution pH (3 – 11), (b) common anions (1 mM), and (c) NOM (1 – 10 mg C/L) on the sorption of PFOA and PFOS by CaMTC16. Experiments were conducted at pH 5 (except panel a) with an initial PFOA or PFOS concentration of 1 mg/L, a sorbent loading of 0.25 g/L, and a contact time of 24 h. Error bars represent one standard deviation of duplicate experiments.	35
Figure 2.8 Removal of a mixture of ten PFAAs with a nominal concentration of 10 µg/L for each PFAA in pure water and lake water with the use of CaMTC16 (0.25 g/L). Error bars represent one standard deviation of duplicate experiments.	38
Figure 3.1 The structure of 1-hexadecyl-3-methylimidazolium chloride (IL).....	46
Figure 3.2 FTIR (a), XRD (b), and zeta potential (c) measurement of unmodified and IL-modified clays.	53
Figure 3.3 Adsorption isotherms fitted with Sips model of (a) PFBA, (b) PFBS, (c) PFHxA, (d) PFHpA, (e) PFHxS, (f) PFOA, (g) PFNA, and (h) PFOS onto the three IL-modified clays. Experiments were conducted at pH 7 with a sorbent loading of 0.25 g/L and a contact time of 24h. Dash lines represent Sips model fits.	56
Figure 3.4 Removal efficiency of PFOA and PFOS on raw clays.....	56
Figure 3.5 Comparison of adsorption capacities of eight PFAAs by three IL-modified clays (Based on Sips isotherm, $C_e = 50$ mg/L).....	58
Figure 3.6 The linear regression of CEC values of raw clays vs the estimated PFAS adsorption capacity Q_s (at $C_e = 50$ mg/L) onto the corresponding IL-modified clays.	59
Figure 3.7 The linear regression of Q_s (at $C_e = 50$ mg/L) vs IL loadings (a), d spacing (b), and zeta potential (c) of the IL-modified clays.	60
Figure 3.8 K_d values as a function of C_e for individual PFAS based on Sips isotherm calculation.....	62

Figure 3.9 Fitted K_d values with $\log D_{ow}$ of PFAS for three IL-modified clays at representative C_e values ($C_e = 0.1, 1$ and 10 mg/L).	64
Figure 3.10 Fitted K_d values with $\log K_{ow}$ of PFAS for three IL-modified clays for representative C_e values ($C_e = 0.1, 1$ and 10 mg/L).	66
Figure 3.11 Linear relationship between the number of CF_2 (and CF_3) moiety and the adsorption free energy of PFAS at $C_e = 1$ mg/L onto three IL-modified clays. PFCA group and PFSA group were fitted separately and were shown with the solid and dash lines, respectively.	67
Figure 3.12 PFAS removal efficiency by three IL-modified clays (0.25 g/L) in low-concentration PFAS mixture experiments (1 μ g/L for each PFAS) under different water matrices.	69
Figure 4.1 FTIR (a), small-angle XRD pattern (b) and zeta potential (c) of raw and organically modified clays.	83
Figure 4.2 Wide angle XRD pattern (a) and simulated isotherms for nitrogen (b) of clay substrate and organically functionalized clay.	84
Figure 4.3 Removal of PFOA, PFOS, 6:2FTS and 5:3FTCA ($C_0=10$ mg/L) on clay substrate. Experiments were conducted at pH 7 with a sorbent loading of 0.25 g/L and a contact time of 24 h.	86
Figure 4.4 Pseudo-second-order fitted kinetics of PFOA, PFOS, 6:2FTS and 5:3FTCA on ZrMC (a) and ZrMD (b).	86
Figure 4.5 Adsorption isotherms of (a) PFOA, (b) PFOS, (c) 5:3FTCA, and (d) 6:2FTS onto ZrMD and ZrMC. Experiments were conducted at pH 7 with an organoclay loading of 0.25 g/L. Dash lines represent Langmuir model fits.	89
Figure 4.6 (a) Fitted adsorption capacity (mg/g) of 5:3FTCA, 6:2FTS, PFOA and PFOS on ZrMD and ZrMC. (b) The linear regression of $\log D_{ow}$ and $\log Q_m$ (fitted adsorption capacity by Langmuir mode) of selected PFAS on ZrMD and ZrMC.	90
Figure 4.7 Effect of common anions (1 mM) and NOM (1 mM as C) on the adsorption of PFAS onto (a) ZrMD and (b) ZrMC. Experiments were conducted at pH 7 with a PFAS concentration of 1 mg/L and organoclay loading of 0.25 g/L.	91
Figure 4.8 Removal of PFOS, PFOA, 6:2FTS, and 5:3FTCA by ZrMC (a) and ZrMD (b) with different ionic strengths (provided by NaCl).	92
Figure 4.9 Removal of PFOS, PFOA, 6:2FTS, and 5:3FTCA by ZrMC (a) and ZrMD (b) in a wide range of pH (3-11).	93
Figure 4.10 Regeneration of (a) PFAS-loaded ZrMD using 50%/50% methanol/water mixture with varied concentrations of NaCl and (b) PFAS-loaded ZrMC using 50%/50% methanol/water mixture with 10% NaCl.	95
Figure 4.11 Reuse of (a) ZrMD and (b) ZrMC for PFAS removal (1 mg/L) at pH 7 with an adsorbent loading of 0.25 g/L. The organoclays were regenerated after PFAS adsorption in each cycle using a 50%/50% methanol/water mixture with 10% NaCl.	95

LIST OF TABLES

Table 2.1 pH and major anion composition of Lake Michigan water.....	18
Table 2.2 MS/MS conditions and detection limits for the ten PFAAs using LC-MS/MS.....	20
Table 2.3 Langmuir model fitting parameters and calculated adsorption capacities for PFOA and PFOS at $C_e = 0.1$ mg/L by various adsorbents reported in literature.	33
Table 3.1 Characteristics and components of raw clays.	45
Table 3.2 PFAS chemical list for adsorption experiments.....	45
Table 3.3 Major water composition of the natural groundwater and river water samples.....	48
Table 3.4 PFAS analytical conditions for each PFAS and their isotope labelled internal standards using LCMS-8060.	50
Table 3.5 Key characterizing parameters of clay minerals.	54
Table 3.6 Isotherm fitting parameters of adsorption of eight PFAAs onto three IL-modified clays (including Langmuir, Freundlich, and Sips nonlinear fitting results).....	57
Table 3.7 PFAS examined in this study, their octanol-water partition coefficients (K_{ow}), and octanol-water distribution coefficient (D_{ow}) at pH 7.....	63
Table 4.1 Key characteristics of the clay mineral.....	76
Table 4.2 PFAS chemical list for adsorption experiments.....	76
Table 4.3 Structure and key parameters of PFAS and organic modifiers.....	77
Table 4.4 Surface area of functionalized clay.....	84
Table 4.5 Kinetics and isotherm fitting parameters for PFAS adsorption onto ZrMC and ZrMD.	87

ACKNOWLEDGMENTS

At the end of my student life, many memories crowded in upon my head. First and foremost, I am immensely thankful to my supervisor professor Yin Wang, who gives me his excellent scientific inputs, continuous funding support, and great patience during my PhD study. Dr. Wang's immense knowledge and plentiful experience have encouraged me in all the time of my academic research and daily life. The training of critical thinking and logical rigorous writing I received from Dr. Wang would be beneficial to my future life adventure.

I would also like to thank Dr. Jin Li, Dr. Qian Liao Dr. Shangping Xu and Dr. Woojin Chang for serving on my dissertation committee and providing critical insights to improve my research. I am also grateful for all the members in Dr. Junhong Chen's lab when he served at UW-Milwaukee. Their efficient work and interdisciplinary research inspire me to be a multitasker and to think in different aspects. I really appreciate the assistance from Dr. Anna Benko, Mr. Patrick Anderson, Dr. Steven Hardcastle, and Mr. Timothy Wahl, and School of Freshwater Science, Department of Mechanical Engineering, Shimazu Laboratory for Advanced and Applied Analytical Chemistry, Advanced Analysis Facility, Water Technology Accelerator at UWM.

UWM was a fun place to spend five years among intelligent and passionate peers. I want to say thanks to my lab mates in Dr. Wang's research group, in particular Dr. Jingwan Huo, Dr. Xiaopeng Min for their mentor in experimental details and material characterizations, as well as Yanan Zhao, Wenxin Zhang who helped take care of my son and me when I was not feeling well before the preliminary exam, my considerate neighbors at the lab bench, Dr. Junwei Wang and Zhiqin Qiang who stayed the whole afternoon with me in the emergency room, my groupmates Adam Schmitt. I am grateful to my dear friend Dr. Guihua Zhou for calming me and distressing me from being a student parent. Life is always full of cheerful voice with the accompany of Xiaoyu Liu, Daqing Jiang and Weilin Xia. Thanks for my neighbor, Yale Wang, Weipeng Yang and Tianyao Ding sharing the delicious food and fantastic homemade drinks.

My current work was also owing partially to my previous advisor Qinghui Huang and his group at Tongji University, who introduced me in the research area, encouraged me to gain more academic

training from the exchanging program and international conference, and his support and encouragement to my Ph.D. study at UWM.

Finally, but most importantly, I'd like to thank my parents, who have less access to education resources but have a long-term view and commitment to my education and growth. I thank my mother-in-law who left her small town for the first time and flew over 16 hours to support my graduation during the pandemic. My deepest thanks to my diligent and conscientious husband and my lovely son, who brings me more joy than any Ph.D. student could. They make me realize my strength and limitations.

Chapter 1 Introduction and Research Objectives

1.1 Background

The manufacturing and application of per- and polyfluoroalkyl substances (PFAS) in the past 60 years seeds the nowadays environmental problems. Back in the 1940s, polytetrafluorethylene (PTFE), the first compound in the PFAS family, was accidentally invented by Roy J. Plunkett. Since then, the main feedstock perfluorooctanoic acid (PFOA) used to be called C8 was widely and quickly introduced to people's daily items such as cookware coating, food packaging, carpeting, floor wax remover and treated apparel etc. (Fluoride Action Network Pesticide Project 2006). Besides, aqueous film-forming foam (AFFF) containing various PFAS was used in military sites, civilian airports, and firefighting training centers worldwide since the 1970s (Michael Hawthorne 2003). The manufacturer has been dumping large quantities of C8-related waste to the air and water since 1980s (Fluoride Action Network Pesticide Project 2006; Michael Hawthorne 2003). Although PFOA has been phased out in early 2000s, the adverse effect of PFAS will last for several decades due to their toxicity, the long half time and recalcitrance to natural degradation (Evich et al. 2022; Wanninayake 2021). Meanwhile, the family of PFAS is growing bigger and more than 4700 PFAS have been existed in the global market till now (Cousins et al. 2020).

The residue of PFAS produces a long-term and accumulate toxic effect on human health and aquatic life. In 1954, the toxicity of C8 became a concern for the manufactory workers (Michael Hawthorne 2003). Cattle death, birth defects and organ damage were linked to C8 through a years' epidemiological analysis (Nicole 2013; Podder et al. 2021). With the development of analytical technology, PFAS now are detected across the globe in the groundwater, drinking water, human blood, serum, etc. (Lang et al. 2017; F. Xiao 2017; Mahinroosta and Senevirathna 2020; Z. Zhou

et al. 2013; Bartell et al. 2010). Even in the secluded Arctic Ocean, PFOA was found either by the atmospheric oxidation of volatile precursor compounds, such as the fluorotelomer alcohols (FTOHs), or the long-range oceanic transport of directly emitted perfluorinated carboxylic acids (PFCAs) (Ateia, Maroli, et al. 2019). More and more evidence showed that the exposure of PFOA and other related PFAS is not tolerable. Therefore, in 2016, the U.S. Environmental Protection Agency (EPA) established the health advisory level of 70 ng/L for PFOA and perfluorooctane sulfonate (PFOS) in drinking water, both individually and combined (US EPA 2016a). PFOA, PFOS, and their precursors have also been listed under the Stockholm Convention on Persistent Organic Pollutants (UNEP 2019).

Removal of PFAS from water is a big challenge for environmental protection due to the unique properties of PFAS. C-F bond is labeled as the strongest in organic chemistry with a bond dissociation energy of up to 544 kJ/mol which is rising from the significant polarity/dipole moment of the electron. PFAS share both the high solubility and hydrophobicity characteristics which varied with the carbon chain length. Technologies for PFAS treatment can generally be divided into destructive and non-destructive approaches (Appleman et al. 2014; Kucharzyk et al. 2017). Destructive technologies aim to break the strong C-F bonds and convert PFAS to smaller and benign molecules (ideally fluoride, carbon dioxide and water). Numerous destructive technologies have been investigated for the treatment of PFAS including PFOA and PFOS, such as advanced oxidation, advanced reduction aided by the UV light or catalysts, electrochemical degradation, sonochemical treatment, hydrothermal reaction, plasma treatment, and thermal destruction (J. Cui, Gao, and Deng 2020; B. Wu et al. 2019; Vecitis et al. 2009; Merino et al. 2016). These technologies have demonstrated some initial success for the destruction and defluorination of PFOA and/or PFOS, mostly under lab-scale investigations. Meanwhile, adoption of these early-stage

technologies requires more intensive investigation on various aspects, such as intermediate and end products identification, degradation pathway analysis, energy consumption evaluation, field demonstration, etc. (R. K. Singh et al. 2019; Tichonovas et al. 2017; D. Wu et al. 2017; Ye et al. 2019). On the other hand, nondestructive technologies, such as sorption, reverse osmosis and nanofiltration, aim to rapidly remove and concentrate PFAS through physical separation (Q. Yu et al. 2009; Boyer et al. 2021). They may be applied as a stand-alone approach or be combined with destructive technologies for complete PFAS treatment (D. Lu et al. 2020). Particularly, granular and powdered activated carbon (GAC/PAC) sorption and ion exchange are so far the most widely used approaches for PFOS and PFOA removal and have been successfully employed in some field applications (Gagliano et al. 2020; Deng et al. 2015).

1.2 Current technology in PFAS removal

Current PFAS treatment methods could be categorized into destructive technology and nondestructive technology.

1.2.1 Destructive technology

Various destructive methods including advanced oxidation, advanced reduction, electrochemical degradation, sonochemical degradation, hydrothermal reaction, and plasma technology have been applied for PFAS treatment in water. Destructive methods aim conversion of PFAS to less toxic products, which is also a good choice for the treatment train design. However, some technical issues hinder them for practical application. For instance, since PFOA has negligible absorption at the UVA and UVB, the degradation of PFOA requires the short-wavelength UVC which is the most damaging type of UV radiation (R. R. Giri et al. 2011; Rabindra Raj Giri et al. 2012). Even

with the catalyst, such as ferric ion, PFOS could absorb UV light at around 280 nm, but the defluorination rate was very low (Y. Wang et al. 2008). Incomplete defluorination, in almost all UV radiation systems, brought secondary contaminants like shorter-chain PFCAs (e.g., perfluoroheptanoic acid (PFHpA), perfluorohexanoic acid (PFHxA), perfluoropentanoic acid (PFPeA) and perfluorobutanoic acid (PFBA)) (Verma et al. 2021; D. Wu et al. 2017; Tang et al. 2012; Chen et al. 2016; Tichonovas et al. 2017). In electrochemical degradation, the short-chain PFAS need a longer treatment time and correspondingly high energy consumption (Fang, Megharaj, and Naidu 2017). High electricity and electrode consumption also increases the operation and maintenance cost in practice. (Radjenovic et al. 2020). In addition to the high energy consumption and low defluorination rate, the application of emerging technologies such as sonochemical degradation, plasma technology, and thermal destruction needs extra protection from the inert gas to prevent the volatile PFAS or other gaseous byproducts emitting to the air (Moriwaki et al. 2005; Fernandez et al. 2016; R. K. Singh et al. 2019; Watanabe et al. 2016).

Destructive approaches can be robust and efficient towards the removal of PFAS from water sometimes. However, considering the environmental application, scale up will be a big problem for applying electrochemical oxidation, sonication, hydrothermal degradation, plasma treatment, and thermal destruction. The non-environmental-friendly chemical use, high energy consumption, and unpleasant operation environment hinder their general use in practice. Apparently, they are good alternatives for secondary treatment of concentrated waste.

1.2.2 Nondestructive Technology

Nondestructive methods such as ion exchange, filtration, and adsorption are widely used in practice for PFAS treatment.

Anion exchange resins can effectively remove PFAS through the adsorption and ion exchange process. Commercial ion exchange resins such as Amberlite™HPR4200, Purolite A860, Purolite A592E and Amberlite™PSR2 Plus have been used for PFAS removal due to their effectiveness (Winchell et al. 2021). The uptake capacity ranges from 1 - 6134 $\mu\text{mol/g}$ depending on the functional group and polymeric matrix of ion exchange resins and the structure difference of PFAS (Deng et al. 2010; Taylor et al. 2010; Gao et al. 2017; Z. Du et al. 2015). The slow adsorption kinetics are an apparent disadvantage of ion exchange resins. Besides, the presence of organic matter impairs the ability of ion exchange in a real water matrix by blocking the pores on the surface (Dixit, Barbeau, and Mohseni 2018).

Adsorption is a safe and popular way to treat PFAS in the industry. Various types of adsorbents such as carbonous materials, metal oxides, polymers, clay minerals, and novel synthetic materials have been studied for PFAS removal. Activated carbon (AC) has a relatively high adsorption capacity among these materials, which is related to their large surface area and proper particle size (Z. W. Du et al. 2014). Yet, the used AC is not easily regenerated with methanol or ethanol which are common regenerating agents. The adsorption on Fe-based metal organic frameworks (MOFs) also indicates that smaller pores are important in the adsorption process. The Fe center and benzene of organic ligands react as electron acceptors and donors respectively in the adsorption process (Y. Yang et al. 2020). Synthetic materials such as β -cyclodextrin polymer and poly(ethylenimine)-functionalized cellulose micro- crystals show effectiveness on the removal of low-concentration PFAS through the electrostatic and hydrophobic interactions (Alsbaiee et al. 2016; Ateia et al. 2018). However, the material preparation process is complicated.

Although the adsorption mechanisms vary among different adsorbents in PFAS removal, the adsorption behavior may be generally compared through the adsorption isotherm and kinetics studies. Langmuir and Freundlich isotherm models are commonly used to fit the isotherm data to obtain the adsorption capacity. The PFAS adsorption kinetics can generally be fitted with the pseudo-second-order kinetics model.

1.3 Clay-based adsorbents in PFAS removal

Clay minerals are naturally abundant and environmentally friendly materials. Their layered structure allows strong physical and chemical interactions with dissolved species, which are due to electrostatic interaction, crystallinity, adsorption, or specific cation exchange reactions. Some commonly used clay minerals in environmental remediation include montmorillonite, vermiculite, etc. Montmorillonite is a 2:1 clay with an Mg/Fe octahedral layer sandwiched between two Si-Al tetrahedral layers. The isomorphous change of Si with Al results in the negative charge of the surface, which is balanced by the interlayer exchangeable ions such as Ca^{2+} or Na^+ . Besides, the hydration of Ca^{2+} or Na^+ could expand the interlayer of montmorillonites, also called swellable mica (Barshad 1955). The clays from different regions have different compositions and properties (Sato, Watanabe, and Otsuka 1992). Likewise, vermiculite, a 2:1 clay, is composed of a $\text{MgO}_2(\text{OH})_4$ octahedra sheet symmetrically coupled to a tetrahedral sheet of Si/Al, but the cation exchange capacity and layer charge is quite different from montmorillonites (Sato, Watanabe, and Otsuka 1992).

Clay minerals have been directly used in the adsorption of heavy metal ions through the ion exchange reaction. Zeta potential of clay minerals indicates the negative surface charge that was

found to positively correlate with the octahedral Al^{3+} and Mg^{2+} (Şans et al. 2017). The surface charge density plays an important role in the adsorption of different adsorbates such as sulfonamide, heavy metals, dyes, pesticides etc. (Ismadji, Soetaredjo, and Ayucitra 2015; T. Wang et al. 2018). Compared with AC, clay exhibits a faster adsorption towards copper (Weng et al. 2007).

To improve the performance of clay on adsorption, several modification methods have been explored to increase its adsorption capacity, kinetics, and regeneration ability. For example, milling and the thermal treatment of natural clay have been reported to enhance the adsorption of Cr (III) through enlarging the specific surface area (Jia et al. 2019). The acid treatment increases the pore volume and decreases the zeta potential of natural clay, resulting a higher cation exchange capacity (X. Wang et al. 2012). Increased interlayer spacing is observed through the intercalation of ZrO_2 and surfactant, ionic liquids, polymer, and organosilane into natural clay. The organic modifier could also change the surface charge and hydrophobicity of natural clay which enhances the adsorption of PFAS. Specifically, several previous studies suggested that organically modified clays (i.e., organoclays) show some success in the fast, efficient and selective removal of PFAS at relatively high concentrations (Q. Zhou et al. 2010; Z. Du et al. 2016). Due to the economic and environmental compatibility of clay minerals, organoclay with higher adsorption capacity and regeneration ability deserves comprehensive study.

1.4 Knowledge gaps

Most previous studies on novel adsorbent design have focused on non-competitive adsorption of PFOA or PFOS in synthetic water, and the effectiveness of PFAS adsorption and material

regeneration for the treatment of more complex water matrices remains insufficiently understood. Different PFAS may have substantially varied water solubility and sorption behavior, and thus the reported adsorption material designed for the two legacy C8 compounds might not exhibit satisfying adsorption capability towards other PFAS. In addition, previous efforts on clay-based adsorbents have mostly focused on the use of montmorillonite modified with cetyltrimonium bromide (CTAB), a model cationic surfactant. Clay minerals with varied properties (e.g., swelling property, cation exchange capacity) may have distinct ability to accommodate various organic modifiers, but their performance remains unexplored for PFAS adsorption. Regarding the potential use in practice, the water matrix effect such as pH, organic matter, and co-existing ions also deserves more detailed investigation. The regeneration ability of organoclays is also critical to the real water application.

1.5 Research objectives and outlines

The overall objective of the thesis research was to develop and evaluate a series of organoclay adsorbents for PFAS adsorption. Specifically, the ideal organoclays aimed to achieve a satisfactory adsorption capacity, fast adsorption kinetics, and good regeneration ability. We hypothesized that the interaction between PFAS and organoclays was governed by PFAS structure and organoclay property. Tuning the properties of organoclays (e.g., clay structure, clay cation exchange capacity, and structure and functional groups of organic modifiers) could lead to the development of a class of innovative materials with selective and tunable adsorption capability towards a suite of PFAS in a range of water treatment-relevant conditions. To achieve the overall objective, three research tasks were outlined below.

Task 1: Develop ionic liquid-modified clay with enhanced adsorption of PFAS (Chapter 2)

We assumed that the adsorption of PFOA and PFOS on ionic liquid (IL)-modified clays relied on the electrostatic and hydrophobicity interactions. The hydrophobicity increased with the chain length of ionic liquids. Therefore, a wide array of organoclay adsorbents were prepared with ILs of varying chain lengths. The impact of alkyl chain length of IL (i.e., C4 –C16) on the removal efficiency of PFOA and PFOS was examined. The optimum material formulation was selected through comparing the isotherms and kinetics of PFOA and PFOS adsorption. The removal of a low-concentration PFAS mixture was examined in lake water. The varied performance of different IL-modified clays was investigated through a series of characterization tools including X-ray diffraction (XRD), Fourier-transform infrared spectroscopy (FTIR), and zeta potential measurement.

Task 2: Investigate the role of clay substrate on the performance of IL-modified clay for PFAS sorption (Chapter 3)

We assumed that the adsorption capacity of PFAS was related to the structure of both PFAS and IL-modified clay. A series of IL-modified clays were prepared using representative natural clay substrates, including a Ca-rich montmorillonite (CaMT), a Na-rich montmorillonite (NaMT), and a vermiculite. Batch adsorption experiments were conducted to quantify the adsorption capacity of eight representative PFAS onto the IL-modified clay materials. The adsorption isotherm data was fitted with Langmuir, Freundlich and Sips models to obtain the adsorption capacity of individual PFAS pollutants. The performance of IL-modified clays was also examined using low-concentration PFAS mixture in complex environmental matrices.

Task 3: Develop organosilane-modified clay with enhanced reusability for PFAS removal
(Chapter 4)

We assumed that the exfoliation of clays could increase the adsorption site of clay minerals through enlarging the surface area. The grafting of organosilane could enhance the stability of organic functional groups due to the strong covalent bonding between silanes and clay minerals. Zirconium was used to pre-treat the clay substrates to enhance the surface area. The pillared clay substrates were modified with desired organic functional groups through post grafting reactions with organosilanes and were compared with an organoclay prepared through the cation exchange process with CTAB. The prepared organoclays were extensively characterized using various tools, and systematically examined for PFAS adsorption and material reuse.

Chapter 2 Efficient Sorption of Perfluoroalkyl Acids by Ionic Liquid-Modified Natural Clay

2.1 Introduction

Per- and polyfluoroalkyl substances (PFAS) are a large group of chemicals used in various consumer and industrial products (Kotthoff et al. 2015; Buck et al. 2011; Paul, Jones, and Sweetman 2009). Perfluorooctanoic acid (PFOA) and perfluorooctane sulfonate (PFOS) have been the two most extensively studied PFAS because of their intensive use in industry, widespread presence in the natural environment, and long-term environmental concern (Z. Wang et al. 2017). Since the early 2000s, the two major U.S. manufacturers have been phased out PFOA and PFOS; however, PFOA and PFOS are highly persistent in the environment, and have still been widely observed in aquatic systems (Post et al. 2009; B. Ji et al. 2020; Kunacheva et al. 2012). The major sources of PFAS contamination in drinking water aquifers including fire-fighting foams in military sites and airports, manufacturing facilities, and waste streams (X. C. Hu et al. 2016; Shin et al. 2011; Houtz et al. 2013, 2016; Lang et al. 2017). In 2016, the U.S. Environmental Protection Agency (EPA) established the health advisory level to 70 ng/L for PFOA and PFOS in drinking water, both individually and combined (US EPA 2016a). PFOA, PFOS, and their precursors have also been listed under the Stockholm Convention on Persistent Organic Pollutants (UNEP 2019). Currently, PFAS removal encounters a special challenge for water/wastewater treatment, because of their diverse structures, varied chain lengths of the per- and polyfluoroalkyl moieties, and unique physicochemical properties (e.g., high water solubility, high stability of C-F bond) (Rahman, Peldszus, and Anderson 2014; Arvaniti and Stasinakis 2015; F. Xiao 2017; F. Li et al. 2020).

Technologies for PFAS treatment can generally be divided into destructive and nondestructive approaches (Merino et al. 2016; Saleh et al. 2019). Destructive technologies aim to break the strong C-F bonds and convert PFAS to smaller and benign molecules (ideally fluoride, carbon dioxide and water) (Merino et al. 2016). Numerous destructive technologies have been investigated for the treatment of PFAS including PFOA and PFOS, such as chemical oxidation, advanced reduction, electrochemical oxidation, photocatalysis, sonochemical treatment, hydrothermal reaction, plasma treatment, and thermal destruction (Trojanowicz et al. 2018; J. Cui, Gao, and Deng 2020; Radjenovic et al. 2020; S. Wang et al. 2017; Cao et al. 2020; B. Wu et al. 2019; F. Xiao et al. 2020). These technologies have demonstrated some initial success for destruction and defluorination of PFOA and/or PFOS, mostly under lab-scale investigations. Meanwhile, adoption of these early-stage technologies requires more intensive investigation on various aspects, such as intermediate and end products identification, degradation pathway analysis, energy consumption evaluation, field demonstration, etc. (Saleh et al. 2019; J. Cui, Gao, and Deng 2020; Ross et al. 2018; Kucharzyk et al. 2017; Wanninayake 2021).

On the other hand, nondestructive technologies, such as sorption, reverse osmosis and nanofiltration, aim to rapidly remove and concentrate PFAS through physical separation (Z. W. Du et al. 2014; J. Wang et al. 2018; Herkert et al. 2020). They may be applied as a stand-alone approach, or be combined with destructive technologies for complete PFAS treatment (D. Lu et al. 2020). Particularly, granular and powdered activated carbon (GAC/PAC) sorption and ion exchange are so far the most widely used approaches for PFOS and PFOA removal, and have been successfully employed in some field applications (Z. W. Du et al. 2014; Bartell et al. 2010; Arias Espana, Mallavarapu, and Naidu 2015). However, there are several limitations for conventional GAC/PAC and ion exchange resins, such as slow sorption kinetics, lack of selectivity, and reduced

performance in the presence of organic matter and other water constituent (Gagliano et al. 2020; D. Q. Zhang, Zhang, and Liang 2019). Various advanced adsorption materials have recently been developed, such as amine-modified carbonaceous materials, β -cyclodextrin-based polymers, and organic-inorganic hybrid materials (Ateia, Alsaiee, et al. 2019; Ateia et al. 2018; Klemes et al. 2019; L. Xiao et al. 2017; Z. Du et al. 2017). Notably, clay-based materials are receiving increasing interests as economic materials for pollution control, because of their earth abundance and compatibility with natural soils/sediments (Xu et al. 2017; Lee and Tiwari 2012; Huo, Min, and Wang 2021). However, natural clays typically carry negative surface charges under circumneutral conditions, and thus they may not be suitable to remove anionic PFAS including PFOA and PFOS (L. Zhao et al. 2014). A few pioneering efforts have reported the modification of natural clays with quaternary ammonium cations, and the resulting materials showed high efficiency for PFAS sorption (Yan et al. 2020; Z. Du et al. 2016; Q. Zhou et al. 2010). Thus, natural clays modified with a cationic organic modifier may be a promising sorbent for PFAS removal.

Ionic liquids (ILs), including both room temperature ILs and molten salts, are organic salts consisting of organic cations balanced by one or more types of anions (Wilkes 2002). Due to their low vapor pressure, exceptional solvation, miscibility, thermal stability, and tunable physicochemical properties, ILs are gaining great attention in various fields, such as catalysis, liquid extraction, and material synthesis (S. K. Singh and Savoy 2020; Dai et al. 2017). The organic cations of ILs, such as imidazolium-type cations, may be employed in water pollution control to target the treatment of anionic pollutants (Lv et al. 2014; R. Zambare, X. Song, S. Bhuvana, J.S. Antony Prince 2017). Badruddoza et al. prepared magnetic nanoparticles modified with β -cyclodextrin-IL polymer for adsorption of anionic pollutants, including PFOA and PFOS. They found that introducing an imidazolium-type IL substantially improved the capture of PFOA and

PFOS, with the maximum adsorption capacities reaching 2.5 and 13.2 mg/g for PFOA and PFOS, respectively (Badrudodoza, Bhattarai, and Suri 2017). It has been reported that imidazolium-type ILs can adsorb onto mineral surfaces through cation exchange (Stepnowski, Mrozik, and Nichthauser 2007). Thus, in principle, imidazolium-type ILs may be adopted as a modifier of natural clays to enhance the capture of anionic PFAS. However, the efficiency of IL-modified natural clays on the sorption of PFOA and PFOS remains unexplored. Further, it has been reported that the alkyl chain length of organic cations plays a critical role in manipulating the organic cation intercalation capacity and arrangement within the clay interlayer (L. Wu, Yang, et al. 2014), which may subsequently affect the sorption of anionic pollutants. However, the effect of alkyl chain length of ILs on the modified natural clays for PFOA and PFOS removal is insufficiently understood.

The objectives of this study were to (1) modify natural clays with imidazolium-type ILs for the sorption of PFOA and PFOS; (2) characterize and determine the effect of alkyl chain length of imidazolium cations on the performance of the IL-modified clays; (3) investigate the impact of water chemistry parameters on PFOA and PFOS sorption by clay modified with the optimal IL; and (4) evaluate the performance of the optimal IL-modified clay for simultaneous removal of a range of perfluoroalkyl acids (PFAAs) with different chain lengths of the perfluoroalkyl moiety. Because of their high environmental relevance, PFOA and PFOS were selected as representative anionic PFAS for detailed investigation of the adsorption behaviors (Z. Wang et al. 2017; Kunacheva et al. 2012). A natural montmorillonite with high cation exchange capacity (CEC) and good expansion property was selected as a model clay for modification with four imidazolium-type ILs with varied alkyl chain lengths.

2.2 Materials and methods

2.2.1 Materials and chemicals

Natural clay originated from Manning formation, Texas, USA (STx-1) was purchased from the Clay Minerals Society and used as a representative clay in the present work. The primary composition of the clay was Ca-rich montmorillonite (CaMT) (Ermut, Ano, and Cartagena 2001). The high CEC (84.4 meq/100g) and charged layered structure make the clay suitable for modification with ILs (Dogan et al. 2006). PFOA was purchased from Alfa-Aesar. PFOS in potassium salt, perfluorobutanoic acid (PFBA), perfluorobutanesulfonic acid (PFBS), perfluoroheptanoic acid (PFHpA), perfluorohexanesulfonic acid (PFHxS) in potassium salt, and perfluorononanoic acid (PFNA) were purchased from Sigma-Aldrich. Perfluoropentanoic acid (PFPeA), perfluorohexanoic acid (PFHxA), and perfluorodecanoic acid (PFDA) were acquired from Oakwood Chemical. The CAS number and purify of the PFAAs were shown in the Supplementary Material (Table S1 of Supplementary Material). Analytical grade sodium chloride (NaCl), sodium bicarbonate (NaHCO₃), sodium sulfate (Na₂SO₄), and sodium nitrate (NaNO₃) were purchased from Fisher-Scientific. Suwannee River natural organic matter (NOM) was purchased from the International Humic Substances Society. A NOM stock solution of 50 mg C/L was prepared and calibrated with a Shimadzu TOC analyzer. Sodium hydroxide (NaOH) was purchased from DOT-Scientific. Hydrochloric acid and HPLC grade methanol were purchased from VWR-BDH. LCMS grade acetonitrile and methanol were purchased from Fisher Scientific. 1-Hexadecyl-3-methylimidazolium chloride (C16) and 1-Decyl-3-methylimidazolium chloride (C10) were purchased from Acros-Organics. 1-Hexyl-3-methylimidazolium chloride (C6) and 1-Butyl-3-methylimidazolium hexafluorophosphate (C4) was purchased from Tokyo Chemical Industry. Ultrapure water (resistivity > 18.2 MΩ) was used for all experiments. Lake water was

collected from Lake Michigan and filtered with 0.22 μm polyether-sulfone (PES) membrane (Millipore) before use.

2.2.2 IL-modified clay preparation and characterization

The IL-modified clays were prepared with a fixed IL loading at 1:1CEC of the clay mineral (i.e., 5 g of CaMT with 4.22 mmol of IL). In a typical synthesis, clay mineral was first ground to fine powder and screened through a 53- μm sieve. Then, 5 g of clay mineral was dispersed in 100 mL of water and stirred at room temperature for 24 h. Then aliquots of an IL solution with the desired amount (i.e., 4.22 mmol) were added into the clay-water mixture and stirred for another 24h. Solids were then collected by centrifugation, washed with water 5 times, and oven dried at 60 $^{\circ}\text{C}$. The obtained IL-modified clay was denoted as CaMTC $_n$ where n was the number of carbons in the alkyl chain of the IL (i.e., $n = 4, 6, 10$ or 16).

Powder X-ray diffraction (XRD) patterns of raw and IL-modified clays were recorded on Bruker D8 Discover X-ray Diffractometer with Cu-K α radiation equipped with a Lynx-Eye detector. The shape and morphology of raw and IL-modified clays were determined by scanning electron microscopy (SEM) using a Hitachi Model S4800. Fourier transform infrared spectroscopy (FTIR) measurements were conducted on a Shimadzu IRTracer100 Spectrometer. FTIR spectra (4000-600 cm^{-1}) were collected using IR solutions 6.0 Software for Windows with resolution of 2 cm^{-1} by co-adding 64 scans for each spectrum. Zeta potential measurements were performed in the pH range from 3 to 11 using a Malvern Zetasizer Nano ZS 90. Nitrogen and carbon contents were analyzed on Fisons NA 1500 NCS elemental analyzer.

2.2.3 Batch sorption experiments

PFOA and PFOS sorption experiments were conducted under batch mode and ambient temperature (22 ± 2 °C) with a sorbent loading of 0.25 g/L. The initial concentration of PFOA or PFOS was fixed at 1 mg/L for most experimental conditions, unless otherwise specified. The selected PFOA and PFOS concentration was within the range of previous studies to allow for full examination of sorbent performance under batch mode (Q. Yu et al. 2009; Pan, Li, and Xu 2020; Chang, Jiang, and Li 2019), and was slightly higher than those observed in contaminated groundwater near source zone (McGuire et al. 2014; Backe, Day, and Field 2013). In each experiment, 10 mg of a sorbent was added into 40 mL of a PFOA or PFOS solution in a polypropylene tube, and the tube was placed immediately on a shaker (Thermo Scientific, 300 rpm) to initiate the experiment. The solution pH was ~ 5 and was stable over the course of the experiment. Experiments were conducted for 24 h to ensure that PFOA and PFOS sorption reached equilibrium, except for the kinetic studies where samples were collected at a series of pre-determined time intervals (i.e., 1 min – 24 h). Sorption isotherm studies were performed with PFOA or PFOS concentrations in the range of 1 – 50 mg/L. A separate set of experiments were performed to determine the effect of solution pH (3 – 11), common anions (chloride, nitrate, bicarbonate, sulfate, 1 mM) and NOM (1 – 10 mg C/L). Additionally, the performance of the best-performed IL-modified clay was evaluated for the simultaneous removal of ten PFAAs under more environmentally relevant concentrations, including seven perfluorinated carboxylic acids (PFBA, PFPeA, PFHxA, PFHpA, PFOA, PFDA, PFNA) and three perfluorinated sulfonates (PFBS, PFHxS, PFOS). Experiments were conducted both in a simple lab-prepared solution (i.e., ultrapure water) and natural water (i.e., Lake Michigan water) spiked with a mixture of the ten PFAAs with a nominal concentration of 10 $\mu\text{g/L}$ for each

PFAA. Water quality parameters of the natural water was provided in Table 2.1. Duplicate experiments were performed for all experimental conditions.

Table 2.1 pH and major anion composition of Lake Michigan water.

Ion	Lake Michigan water	
	Conc. (mg/L) ^a	Conc. (mM)
Cl ⁻	17.01	0.48
SO ₄ ²⁻	17.16	0.18
HCO ₃ ^{-b}	165.36	2.71
NO ₃ ⁻	0.29	0.005
DOC	2.16 ^c	0.18 ^d
pH	7.98 ^e	

^aConcentrations of Cl⁻, SO₄²⁻, and NO₃⁻ were determined using ion chromatography.

^bConcentration of HCO₃⁻ was determined based on alkalinity measurement using titration (Baird 2012).

^cConcentration of dissolved organic carbon (DOC) was determined using TOC analyzer and was reported as mg C/L

^dConcentration of DOC here was reported as mM of C.

^epH value is unitless

Regeneration of the best-performed IL-modified clay was investigated using three regenerants that include a 50-mM NaCl solution, a 500-mM NaCl solution, or a methanol/water (50%/50%) mixture. Sorption experiment was first performed using a sorbent loading of 0.25 g/L and a PFOA or PFOS concentration of 1 mg/L. After 24 h of contact time, the PFOA- or PFOS-loaded sorbent was collected from solution by centrifugation, and was regenerated using a regenerant for 24 h. Reuse of the IL-modified clay was evaluated by conducting the sorption/regeneration experiments for three cycles with the use of 50%/50% methanol/water mixture as the regenerant.

Samples collected in all experiments were immediately filtered with 0.22- μ m PES syringe filters (SLGPX13NK, Millipore) and the filtrates were preserved for PFAS analysis based on protocols modified from published studies (Huang et al. 2018; Loos et al. 2013). During the filtering process, the first 3-mL sample was used to rinse the filter and wasted. No significant PFAS capture by the

filter was observed because of the small filter diameter (13 mm) and the use of the rinsing step. Additionally, sorbent-free control experiment suggested negligible PFAS loss/adsorption to containers and vials. The analysis of PFOA and PFOS from the single-sorbate sorption experiments was carried out on an ultra-high-performance liquid chromatography (UHPLC) system coupled with a single quadrupole mass spectrometry (LCMS-2020, Shimadzu). The analysis of the ten PFAS compounds from the PFAS-mixture sorption experiments was performed on a UHPLC system coupled with a triple quadrupole mass spectrometry (LCMS-8040, Shimadzu). Detailed liquid chromatography and mass spectrometry conditions were described as below.

The analysis of PFOA and PFOS from the single-sorbate sorption experiments (initial PFOA or PFOS concentration ≥ 1 mg/L) was carried out on an ultra-high-performance liquid chromatography (UHPLC) system coupled with a single quadrupole mass spectrometry (LCMS-2020, Shimadzu). Chromatography was performed using a XB-C18 column (Kinetex® 1.7 μm , 100 Å, 100 x 2.1 mm, Phenomenex). The mobile phase consisted of (A) Milli-Q water and (B) acetonitrile (Optima LCMS grade, Fisher Scientific), each amended with 0.1% formic acetate (Fisher Scientific). The gradient of mobile phase started at 80% acetonitrile and jumping to 100% acetonitrile at 2 min and then reversing to the original condition at 4 min and maintaining to 6 min at a flow rate of 400 $\mu\text{L}/\text{min}$. Mass spectrometry (MS) analysis was performed using the single quadrupole MS with an ESI source operated in a negative polarity mode (SIM⁻). MS operating conditions were as follows: interface voltage -4.5 kV; desolvation temperature 250 °C; heat block temperature 400 °C; drying gas flow rate 15 L/min; and nebulizing gas flow 1.5 L/min. LabSolutions V6.82 (Shimadzu) was used for instrument control, acquisition, and mass analysis. Matrix-matched calibration standards for PFOA and PFOS were used to minimize any matrix-induced effects. The method detection limit for PFOA and PFOS was 2 $\mu\text{g}/\text{L}$.

Table 2.2 MS/MS conditions and detection limits for the ten PFAAs using LC-MS/MS.

Analyte	Precursor ion (m/z)	Product ion (m/z)	Collision energy (V)	Detection limit (ng/L)
PFBA	213	169	9	100
PF	263	219	8	100
PFH _x A	313	269	8	50
PFBS	299	80	33	50
PFHpA	363	319	9	50
PFOA	413	369	9	50
PFH _x S	399	80	46	50
PFNA	463	419	10	100
PFOS	499	80	45	50
PFDA	513	469	10	50

The analysis of the ten PFAS compounds from the PFAS-mixture sorption experiments was performed on a UHPLC system coupled with a triple quadrupole mass spectrometry (LCMS-8040, Shimadzu). Chromatography was performed using a XB-C18 column (Kinetex® 1.7 μm, 100 Å, 100 x 2.1 mm, Phenomenex). The mobile phase consisted of (A) Milli-Q water and (B) methanol (Optima LCMS grade, Fisher Scientific) amended with 5-mM ammonium formate (Fisher Scientific). Samples were injected at 10 μL volumes with a loading pump delivering at 500 μL/min of the mobile phase consisting of 70% B. The column temperature was held constant at 50 °C. Electrospray ionization was operated in a negative mode with the parameters set as capillary voltage at -4.5kv, desolvation temperature at 250 °C, and heat block temperature at 400 °C. Nitrogen (>99.99% purity, Airgas) was used as the desolvation gas and nebulizing gas with flow rates of 15 L/min and 2 L/min, respectively. LabSolutions V6.82 (Shimadzu) was used for instrument control, acquisition, and mass analysis. Matrix-matched calibration standards for the

ten PFAS mixture were used to minimize any matrix-induced effects. MS/MS condition and detection limit of each PFAS were listed in Table 2.2.

The amount of adsorbed PFOA or PFOS, q (mg/g), was determined based on Equation (2.1):

$$q = \frac{(C_0 - C_e) * V}{W} \quad (2.1)$$

where C_0 (mg/L) is the initial PFOA or PFOS concentration prior to sorption, C_e (mg/L) is the concentration of PFOA or PFOS after sorption reaches equilibrium, V (L) is the volume of the solution, and W (g) is the mass of the sorbent.

2.3 Results and discussion

2.3.1 Effect of IL chain length on PFOA and PFOS sorption

Four IL-modified clays were prepared using imidazolium-type cations with different alkyl chain lengths (C4 – C16). A set of sorption experiments were first performed to evaluate the effect of alkyl chain length of ILs on the sorption of PFOA and PFOS by IL-modified clays. The unmodified clay showed minimal sorption of both PFOA and PFOS, and <10% of PFOA and PFOS was captured by the raw clay under the experimental condition (Figure 2.1). Intercalation of imidazolium-type ILs remarkably improved PFOS removal by the modified clays. Specifically, >98% PFOS removal was observed for CaMTC16 and CaMTC10 under the experimental condition, and even clays modified with short-chain ILs ($C_n \leq 6$) showed >70% removal of PFOS (Figure 2.1).

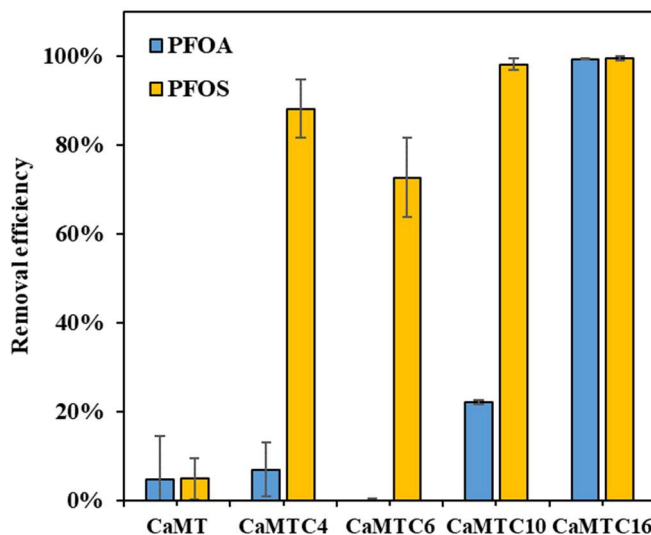


Figure 2.1 Sorption of PFOA and PFOS by raw (CaMT) and IL-modified clays prepared using ILs with different alkyl chain lengths (CaMTC4 – CaMTC16). Experiments were conducted at pH 5 with an initial PFOA or PFOS concentration of 1 mg/L, a sorbent loading of 0.25 g/L.

Meanwhile, alkyl chain length of ILs had a more substantial effect on PFOA sorption. Particularly, CaMTC16 was efficient for PFOA capture with the removal efficiency reaching >99%, while PFOA removal dropped significantly using clay modified with shorter-chain ILs. CaMTC10 showed ~20% PFOA removal, and <10% PFOA removal was achieved for CaMTC4 and CaMTC6, which was similar to the unmodified clay (Figure 2.1). The overall better performance for PFOS sorption than PFOA by IL-modified clays may be attributed to the structural differences between PFOS and PFOA. Both hydrophobic and electrostatic interactions may play important roles in PFOS and PFOA sorption (Z. W. Du et al. 2014; Dixit et al. 2021). PFOS and PFOA sorption may also be affected by the surface properties of IL-modified clays, such as the surface charge. Compared to PFOA, PFOS had both stronger hydrophobicity and a higher total negative atomic charge because of its longer perfluoroalkyl moiety and the electron-rich sulfonate group (Higgins and Luthy 2006; Park, Daniels, et al. 2020). Better removal of PFOS than PFOA had also been

reported in previous studies using various carbon- and mineral-based sorbents (Deng et al. 2015; D. Zhang et al. 2016; Z. Du et al. 2016). Overall, our result suggested that (1) modification with IL improved PFOA and PFOS sorption by clay; (2) the alkyl chain length of the intercalated IL strongly affected the capture of PFOA and PFOS by IL-modified clay; and (3) CaMTC16 showed high removal efficiency for both PFOA and PFOS.

2.3.2 Characterization of IL-modified clays

Both raw and IL-modified clays were extensively characterized using a series of characterization tools to investigate the key role of ILs in the composition and properties of the IL-modified clays that may affect their performance. The basal spacing and crystalline structure of raw and IL-modified clays were determined using XRD. Montmorillonite is a 2:1 layered clay with each structural layer containing an octahedral alumina sheet sandwiched between two tetrahedral silica sheets, and exchangeable cations were positioned within the interlayer of two structural layers (Drits 2003). The d-spacing the basal layer (i.e., one structural layer + interlayer) can be determined based on the position of the (001) reflection peak, according to Bragg's law (Huo, Min, and Wang 2021). The raw montmorillonite clay had a strong (001) peak at 2θ of 5.8° , corresponding to a basal spacing (d_{001}) of 15.2 \AA (Figure 2.2). Clear shifts of (001) peak was found for all IL-modified clays, suggesting that IL modification altered the clay basal spacing. No new peaks or peak splitting were observed for any IL-modified clays, which indicated the uniform intercalation of ILs into the clay interlayer (Figure 2.2). Compared to raw montmorillonite, the (001) peaks of CaMTC4 and CaMTC6 shifted to higher 2θ values, suggesting a slight decrease of their basal spacing. Meanwhile, the basal spacing of CaMTC10 and CaMTC16 increased by 0.8 \AA and 4.4 \AA in comparison to raw montmorillonite, respectively. Previous studies also reported

that the basal spacing of swelling clays increased with the higher chain length of the organic modifiers (L. Wu, Yang, et al. 2014; Klapyta, Fujita, and Iyi 2001). The interlayer spacing of two adjacent structural layers of the IL-modified clays can be estimated based on the difference of the basal spacing and the thickness of one structural layer (9.6 Å) (Golubeva and Gusarov 2007). For example, the interlayer spacing of CaMTC16 was calculated as 10.0 Å, which was smaller than the size of the organic cation (23.4 Å) (L. Wu, Liao, et al. 2014). Consistent with previous experimental and simulation results, our observation suggested that the intercalated ILs may be positioned in the clay interlayer with a certain angle (L. Wu, Liao, et al. 2014; M. Zhao et al. 2019). Furthermore, intercalation of ILs into the clay did not substantially change the clay crystalline structure or surface morphology, evidenced by the similar features of the XRD patterns at a wider range of 2θ degrees and the SEM images between the raw and IL-modified clays.

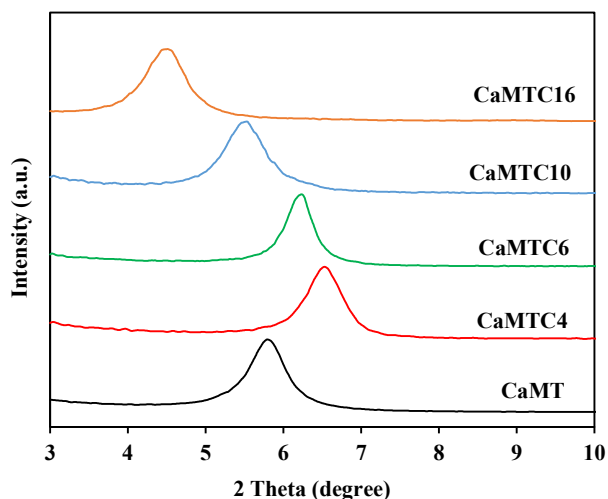


Figure 2.2 XRD patterns of raw and IL-modified clays prepared using ILs with different alkyl chain lengths at 2θ in the range of 3 – 10 degrees.

The functional groups of IL-modified clays were determined based on FTIR characterization (Figure 2.3). Compared to the raw clay, two new peaks were observed at 2850-2950 cm^{-1} for IL-

modified clays, which were attributed to the symmetric stretching and asymmetric mode of C-H (L. Wu, Yang, et al. 2014). Notably, these peaks are very sensitive, and any conformational disorder may slightly shift the peak positions (Venkataraman and Vasudevan 2002). The peak intensities were higher for clays modified with long-chain ILs (C16 and C10) than those modified with short-chain ILs (C6 and C4). Additionally, two small but distinguishable peaks were observed at $\sim 1560\text{ cm}^{-1}$ and $\sim 1460\text{ cm}^{-1}$ for IL-modified clays but not the raw clay, which were related to C=C stretching and C=N-H stretching of the imidazolium ring (L. Wu, Yang, et al. 2014)(Ahmed et al. 2018a). Thus, FTIR results further confirmed the successful intercalation of ILs within the IL-modified clays. The IL loadings were then quantified based on carbon and nitrogen elemental analysis. In general, the IL loading increased with increasing alkyl chain length, and CaMTC16 had the highest IL loading of 0.71 mmol per gram of clay. Interestingly, the IL loading appeared to exhibit a linear relationship to the carbon number of the IL alkyl chain ($R^2 = 0.95$). A similar observation was found in a previous study that modified montmorillonite from a different origin using imidazolium cations with different alkyl chain lengths (C2 – C8) (M. Zhao et al. 2019). In the present work, the increased loading of long-chain ILs may suggest their stronger interaction with the clay substrate than the short-chain ones. Nevertheless, even CaMTC4 had an IL loading of 0.60 mmol/g of clay, which was only 15% lower than that of CaMTC16. The different IL loading alone thus is unlikely the primary factor that account for the dramatic different performance of the IL-modified clays for PFOA and PFOS removal.

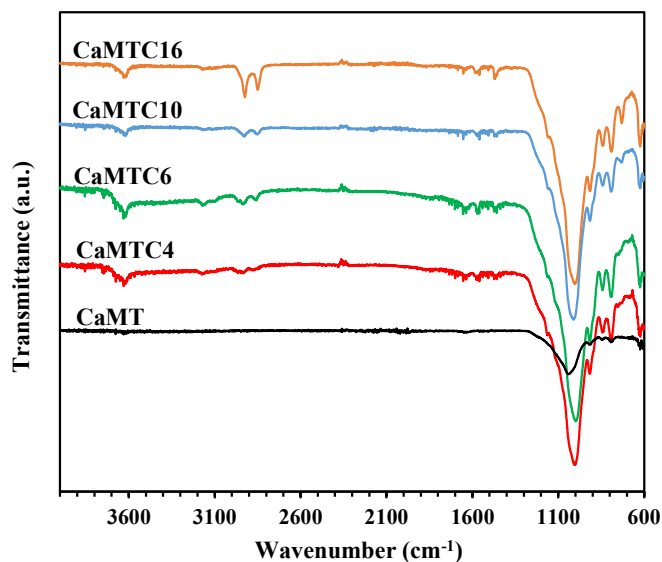


Figure 2.3 FTIR spectra of raw and IL-modified clays prepared using ILs with different alkyl chain lengths. Error bars represent one standard deviation of duplicate experiments. Error bars represent one standard deviation of duplicate experiments.

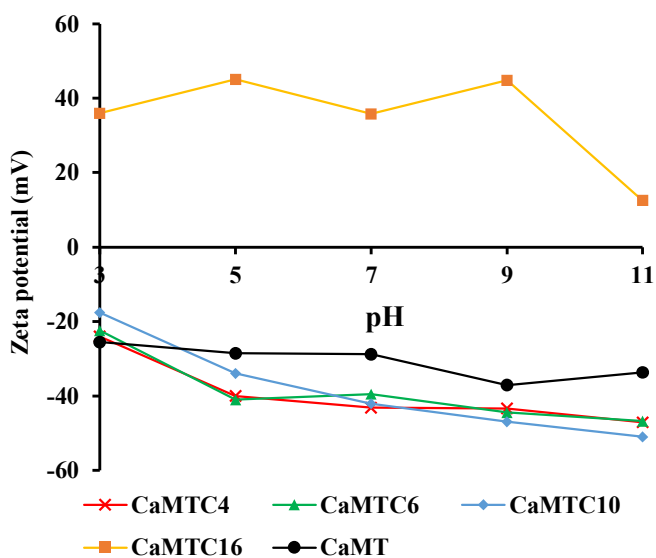


Figure 2.4 Zeta potentials of raw and IL-modified clays prepared using ILs with different alkyl chain lengths at pH 3 – 11. Error bars represent one standard deviation of duplicate experiments.

The surface charge of the raw and IL-modified clays was determined based on zeta potential measurement. The surface of the raw clay was negatively charged under pH 3 – 11 (Figure 2.4), which can be attributed to the isomorphous replacement of Si with Al within the clay structural layer, structure imperfection, and deprotonation of the surface hydroxyl groups of clay (Drits 2003). After IL modification, the surface of CaMTC16 became positively charged, while the zeta potentials of the clays were modified with shorter-chain ILs (i.e., CaMTC4, CaMTC6, CaMTC10) remained negative under the experimental pH range. Since all the four imidazolium-type cations had the same charged functional head group, this observation suggested that the C16 imidazolium cation ($C_{16}mim^+$) had a stronger interaction with the clay substrate than the shorter-chain ones. It is well known that the hydrophobicity of the ILs increased with the increasing alkyl chain length (Blesic et al. 2007). Thus, modification of clay with long-chain IL would improve the hydrophobic lateral interaction of the clay substrate to bind more IL cations within the shear plane, resulting in a switch of the zeta potential from negative to positive (R. Zhang and Somasundaran 2006). In contrast, short-chain ILs may act similarly to free cations such as Ca^{2+} and Na^+ and only had weak interaction with the clay substrate (Blesic et al. 2007). Based on molecular dynamics simulation, Wu et al. also suggested that long-chain ILs had stronger interaction with the clay substrate than short-chain ones, and clay modified with long-chain ILs had more stable structure because of the favorable intercalation energy and interlayer IL arrangement (L. Wu, Yang, et al. 2014). Furthermore, the strong interaction of $C_{16}mim^+$ with the clay substrate may also be related to the weak positive inductive effect of its alkyl chain. The positive inductive effect of alkyl chain was caused by its electron repelling properties, and the extent decreased with increasing alkyl chain length (Elsherbiny, Salem, and Ismail 2012). Compared to the shorter-chain ILs, the imidazolium head of $C_{16}mim^+$ retained a high positive charge because of the reduced positive inductive effect

of its long alkyl chain, making its intercalation more favorable with the negatively charged clay surface. Thus, the substantially improved performance of CaMTC16 over the other IL-modified clays for PFOA sorption may be attributed to its positive surface charge along with the increased hydrophobicity of C16mim+. As for PFOS, the IL-modified clays generally exhibited better removal efficiencies than for PFOA, which may be attributed to the stronger hydrophobicity of PFOS than PFOA.

2.3.3 Sorption kinetics and isotherms of PFOA and PFOS by CaMTC16

Since CaMTC16 exhibited favorable performance for both PFOA and PFOS sorption, detailed batch sorption experiments were conducted to further determine the sorption behaviors of PFOA and PFOS by CaMTC16. Rapid uptake of PFOA and PFOS by CaMTC16 was observed from kinetics studies. Specifically, nearly complete PFOA removal was found within just 1 min of contact time, suggesting the superfast PFOA sorption kinetics (Figure 2.5). Meanwhile, ~90% PFOS removal was observed after 6 min of contact time, and PFOS sorption reached equilibrium within 60 min. Previous research also reported fast PFOA and PFOS sorption kinetics by clay minerals, which may be attributed to the layered structure along with the easily accessible mineral-water interface of clays (L. Zhao et al. 2014). The faster kinetics of PFOA than PFOS might be related to the smaller size of PFOA that resulted in less steric hinderance during the sorption process (Z. W. Du et al. 2014). Additionally, because of the larger size of PFOS and the strong nucleophilic property of the sulfonate group, PFOS sorption may occur both on the external surface and within the interlayer of CaMTC16, and its diffusion to the interlayer might slow down the sorption kinetics. Meanwhile, the nearly instantaneous PFOA removal indicated that PFOA sorption might mainly occur on the external surface of CaMTC16 under the experimental condition.

Notably, the longer perfluoroalkyl moiety of PFOS may also impact the free energy and entropy of the sorption at mineral-water interface (WARD; L.TORDAI 1946). It is suggested that the sorption kinetics can be affected by the binding energy between the sorbent and sorbate, and lower binding energies would result in faster sorption kinetics (Gao et al. 2017b). Our result thus implied that PFOS might have a higher binding energy with CaMTC16 than that of PFOA.

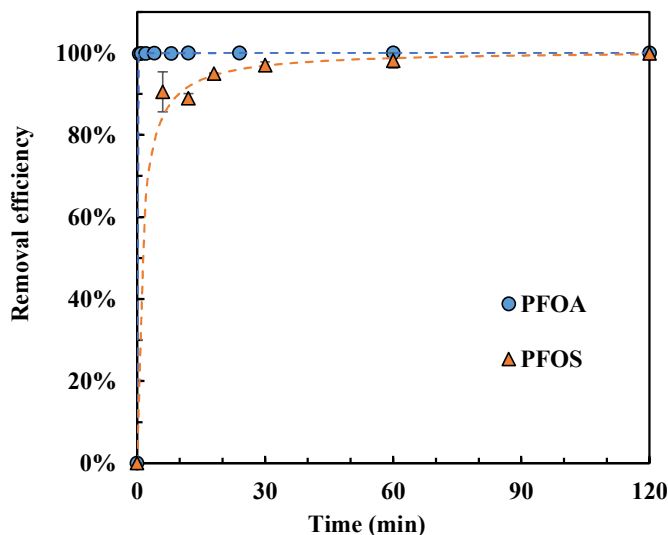


Figure 2.5 Sorption kinetics of PFOA and PFOS by CaMTC16. Experiments were conducted at pH 5 with an initial PFOA or PFOS concentration of 1 mg/L and a sorbent loading of 0.25 g/L. Dash lines represent pseudo-second order kinetics model fit.

Both PFOA and PFOS sorption kinetics can be well fitted using the pseudo-second-order kinetics model (Figure 2.5) and, which assumed that chemisorption (i.e., chemical interaction between sorbent and adsorbate) was involved in the sorption process, and the sorption rate depended on the available sites on the sorbent surface (Simonin 2016; Min et al. 2020; Ho and McKay 1999). It should be noted that the sorption kinetics may be affected by parameters such as concentrations of sorbents and sorbates, as well as the water chemistry conditions (Z. W. Du et al. 2014). Thus,

cautions should be made when directly comparing sorption kinetics parameters among various studies because of the different experimental conditions. Nevertheless, previous studies reported that it usually took several hours for PFOA and PFOS sorption to reach equilibrium with PAC. The equilibrium time could be up to several days using GAC and ion exchange resins (D. Q. Zhang, Zhang, and Liang 2019; Dixit et al. 2021). Therefore, the fast kinetics with CaMTC16, therefore may be a favorable feature for potential application of the sorbent. Also, the leaching of the IL from CaMTC16 was negligible under experimental conditions.

The sorption isotherms of PFOA and PFOS by CaMTC16 were determined to investigate the equilibrium sorption behavior of PFOA and PFOS between aqueous and sorbent phases (Figure 2.6). Data were fitted with the Langmuir and Freundlich isotherm models, expressed by Equations 2.2 and 2.3, respectively (Foo and Hameed 2010).

$$q_e = \frac{Q_{max}K_L C_e}{1 + K_L C_e} \quad (2.2)$$

$$q_e = K_F C_e^{\frac{1}{n}} \quad (2.3)$$

where q_e (mg/g) is the amount of adsorbed PFOA or PFOS per unit mass of sorbent, and C_e (mg/L) represents the concentration of PFOA or PFOS in solution once sorption reached equilibrium. K_L (L/mg) in Equation 2 is the Langmuir sorption constant, and Q_{max} (mg/g) is the maximum sorption capacity. In Equation 3, K_F (mg/g·(L/mg)^{1/n}) is the Freundlich constant and $1/n$ is a dimensionless indicator related to the sorbent surface heterogeneity.

PFOA and PFOS sorption isotherms were adequately fitted by both Langmuir and Freundlich models, and the Langmuir model showed a slightly better fit than the Freundlich model. Based on the Langmuir model, high K_L values were obtained for PFOA (1.54 L/mg) and PFOS (4.40 L/mg), suggesting the strong sorption affinity between CaMTC16 and PFOA/PFOS, which can also be

reflected by the sharply increased PFOA and PFOS sorption capacities under low equilibrium concentrations (Figure 2.6).

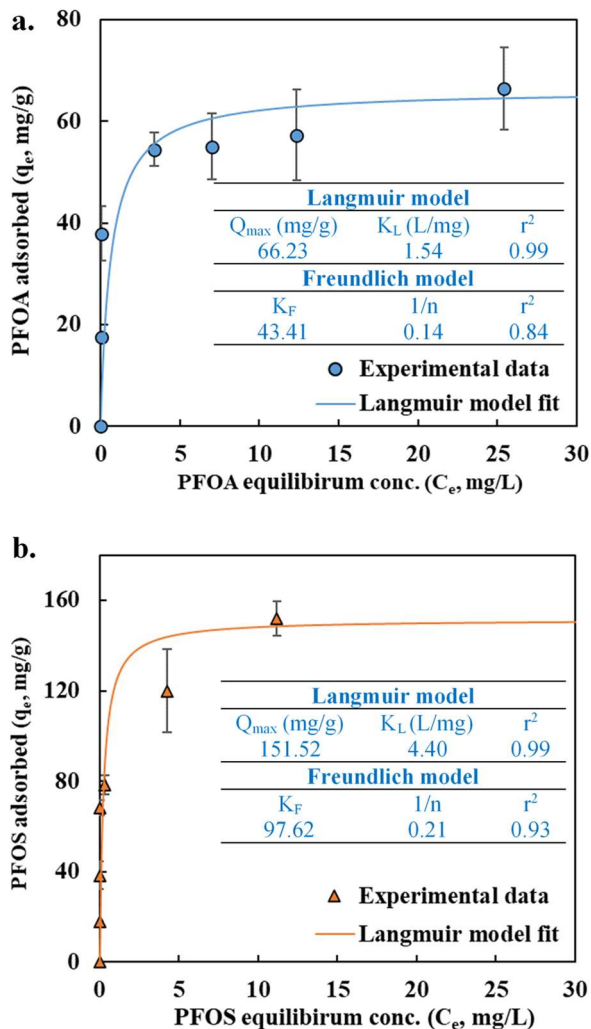


Figure 2.6 Sorption isotherms of (a) PFOA and (b) PFOS by CaMTC16 and their Langmuir model fits. Experiments were conducted at pH 5 with a sorbent loading of 0.25 g/L and a contact time of 24 h. Error bars represent one standard deviation of duplicate experiments.

Although Q_{\max} represents the maximum sorption capacity, this value would only be achievable with a very high equilibrium PFOA or PFOS aqueous concentration. PFOA and PFOS concentrations in natural and polluted water and wastewater are generally in the range of ng/L to

$\mu\text{g/L}$, and can be up to a few hundred $\mu\text{g/L}$ in contaminated groundwater near source zone (Kunacheva et al. 2012; Houtz et al. 2013; Backe, Day, and Field 2013). The sorption capacities of PFOA and PFOS under relatively low equilibrium aqueous concentrations would be determined by both Q_{max} and K_L . For instance, with sufficiently low equilibrium aqueous concentrations ($K_L \cdot C_e \ll 1$), Equation 2 can be simplified to $q_e = Q_{\text{max}} K_L C_e$, where the sorption capacity has a linear dependence with both Q_{max} and K_L . In the present work, PFOA and PFOS sorption capacities by CaMTC16 were calculated with equilibrium aqueous concentrations (i.e., C_e) of $100 \mu\text{g/L}$ for illustration purposes and to represent PFAS concentrations in highly contaminated sources (McGuire et al. 2014; Backe, Day, and Field 2013). The calculated capacities, along with Q_{max} and K_L , were compared with several representative sorbents reported in literature (Table 3). CaMTC16 showed comparable PFOA and PFOS sorption capacities to fluorinated alkyl chain-modified and choline-amended clays (Z. Du et al. 2016; M. Wang et al. 2021), and outperformed various materials such as GAC, PAC, and metal-organic framework (Q. Yu et al. 2009; D. Zhang et al. 2016; Clark et al. 2019; K. Liu et al. 2015). The improved performance of CaMTC16 may be attributed to its strong affinity with PFOA and PFOS. Additionally, CaMTC16 exhibited higher sorption capacities for PFOS than PFOA, which was consistent with various classes of sorbents reported in earlier studies (Badruddoza, Bhattarai, and Suri 2017; D. Zhang et al. 2016; M. Wang et al. 2021).

Table 2.3 Langmuir model fitting parameters and calculated adsorption capacities for PFOA and PFOS at $C_e = 0.1$ mg/L by various adsorbents reported in literature.

Adsorbent	Adsorbate	Langmuir parameters		q_e (mg/g) at $C_e = 0.1$ mg/L	Reference
		Q_{max} (mg/g)	K_L (L/mg)		
choline-modified montmorillonite	PFOS	324.4	1.94	52.71	(M. Wang et al. 2021)
	PFOA	206.5	0.61	11.87	
CaMTC16	PFOS	151.5	4.40	46.30	this work
	PFOA	66.2	1.54	8.84	
fluorinated alkyl chain-modified montmorillonite	PFOS	124.1	5.05	41.64	(Z. Du et al. 2016)
	PFOA	80.9	1.50	10.55	
calcined hydrotalcite	PFOA	1587.0	0.064	10.09	(Chang, Jiang, and Li 2019)
magnetic nanoparticle amended with β -cyclodextrin-IL polymer	PFOS	8.1	113	7.44	(Badruddoza, Bhattarai, and Suri 2017)
	PFOA	3.1	40	2.48	
powdered activated carbon	PFOS	520.0	0.11	5.66	(Q. Yu et al. 2009)
	PFOA	277.4	0.14	3.91	
quaternary ammonium-modified montmorillonite	PFOS	746.0	0.071	5.26	(Q. Zhou et al. 2010)
carnitine-modified montmorillonite	PFOS	304.4	0.14	4.20	(M. Wang et al. 2021)
	PFOA	181.7	0.35	6.14	
ion exchange resin Al400	PFOS	210.0	0.14	2.90	(Q. Yu et al. 2009)
	PFOA	1208.9	0.17	20.21	
ion exchange resin IRA-900	PFOS	1272.4	0.012	1.53	(Clark et al. 2019)
MIL-101-based MOF	PFOA	753.5	0.02	1.50	(K. Liu et al. 2015)
granular activated carbon	PFOS	185.0	0.078	1.43	(Q. Yu et al. 2009)
	PFOA	161.5	0.043	0.69	
powdered activated carbon	PFOS	319.4	0.037	1.18	(Clark et al. 2019)
granular activated carbon	PFOS	72.2	0.07	0.50	(D. Zhang et al. 2016)
	PFOA	52.8	0.05	0.26	
UiO-66-based metal organic framework (MOF)	PFOS	618.8	0.008	0.49	(Clark et al. 2019)

2.3.4 Effects of water chemistry

Sorption of PFOA and PFOS by CaMTC16 was further determined in the presence of various water chemistry parameters. Consistently high PFOA and PFOS removal efficiency was observed in the range of pH 3 to 11 (Figure 2.7a), suggesting that pH had negligible effect on the performance of CaMTC16 under experimental conditions. The robust performance of CaMTC16 may be related to its positively charged surface under pH 3 – 11 (Figure 2.4) which provided strong electrostatic interaction with PFOA and PFOS anions. Additionally, the long alkyl chain of $C_{16}mim^+$ could also favor the capture of PFOA and PFOS by CaMTC16 through hydrophobic interactions (L. Wu, Liao, et al. 2014). Similarly, a previous study reported that pH had little effect on PFOS sorption by quaternary ammonium-amended montmorillonite (Q. Zhou et al. 2010). Since the pH of natural waters is generally under slightly acidic to slightly basic conditions, our result indicated that CaMTC16 may be effective for PFOA and PFOS removal under environmentally relevant pH conditions.

The presence of common inorganic anions also had no inhibitory effect on PFOA and PFOS sorption by CaMTC16. As shown in Figure 2.7b, nearly complete removal of PFOA and PFOS was achieved in the presence of 1 mM of chloride, sulfate, bicarbonate, or nitrate. Inorganic anions, particularly sulfate, have been found to reduce PFOA and PFOS sorption by sorbents that primarily rely on electrostatic interaction as the PFAS capture mechanism. For instance, Hu et al. found that the presence of 1 mM of sulfate reduced PFOS sorption by nitrate-intercalated layer double hydroxide by ~70%, due to the lack of hydrophobic interactions between PFOS and the sorbent (Z. Hu et al. 2017). Sulfate has also been reported to negatively impact PFOS capture by various anion exchange resin materials (Gao et al. 2017b; Deng et al. 2010). No anion inhibition was observed in the present work, which may suggest the important role of hydrophobic interactions in PFOA and PFOS sorption by CaMTC16, in addition to that of electrostatic interaction.

The impact of NOM on PFOA and PFOS sorption was investigated using Suwannee River NOM with various concentrations. The presence of NOM had no effect on PFOS sorption by CaMTC16, and nearly complete PFOS removal was observed under all NOM levels (Figure 7c). Meanwhile, PFOA removal was not affected in the presence of up to 5 mg C/L of NOM, while increasing NOM concentration to 10 mg C/L had a minor reduction of PFOA removal efficiency by ~15%.

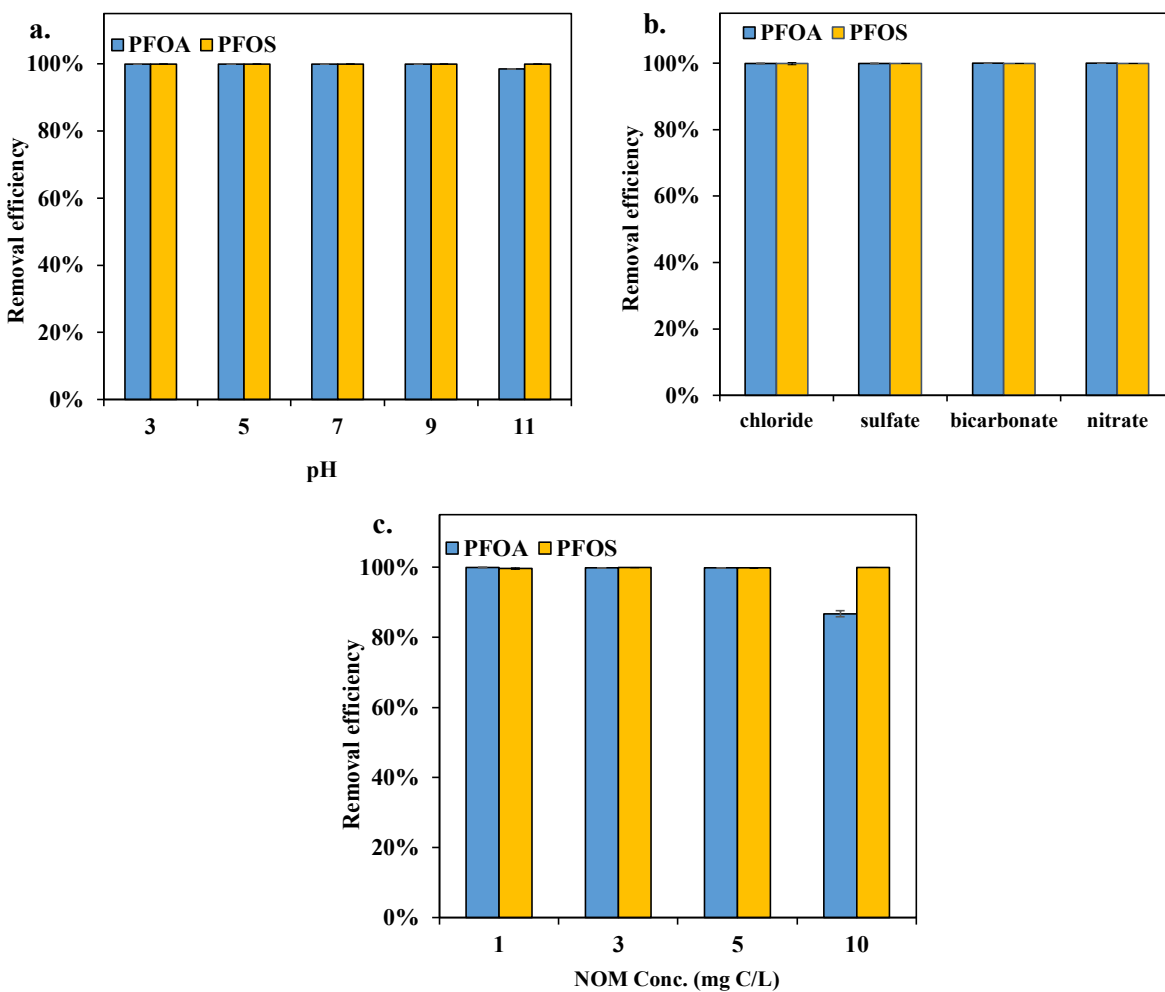


Figure 2.7 Effects of (a) solution pH (3 – 11), (b) common anions (1 mM), and (c) NOM (1 – 10 mg C/L) on the sorption of PFOA and PFOS by CaMTC16. Experiments were conducted at pH 5 (except panel a) with an initial PFOA or PFOS concentration of 1 mg/L, a sorbent loading of 0.25 g/L, and a contact time of 24 h. Error bars represent one standard deviation of duplicate experiments.

NOM may inhibit PFAS sorption by various mechanisms such as competition of sorption sites, pore blockage, and/or alternation of sorbent surface properties (D. Q. Zhang, Zhang, and Liang 2019). Previous studies reported that NOM, as well as dissolved inorganic carbon (DOC) from other sources, had substantially reduced PFOS and PFOA sorption by various sorbents, such as activated carbon and ion exchange resins (Gagliano et al. 2020; J. Yu et al. 2012). In the present work, NOM had a mild inhibitory effect on PFOA sorption but not PFOS, which was consistent with the longer perfluoroalkyl moiety of PFOS along with its electron-rich sulfonate group that may result in stronger interactions between CaMTC16 and PFOS than PFOA (Higgins and Luthy 2006; Park, Daniels, et al. 2020). It should be noted that NOM represents a highly complex matrix of organic chemicals, and NOM from different sources may have different compositions. Thus, systematic investigation of the NOM effect on PFAS sorption by CaMTC16 may worth further research.

2.3.5 Regeneration and reuse

Regenerability and reusability are important aspects for the practical application of sorbents in *ex-situ* water treatment. Regeneration of PFOA- or PFOS-loaded CaMTC16 was first evaluated using three regenerants, including 50 mM of NaCl, 500 mM of NaCl, and 50%/50% mixture of methanol/water solutions. The use of 50 and 500 mM of NaCl resulted in minimal desorption of PFOA or PFOS, indicating that these solutions were not effective for CaMTC16 regeneration. In contrast, nearly complete desorption of PFOA or PFOS was achieved with the use of the 50%/50% methanol/water mixture, suggesting efficient regeneration of the PFOA- or PFOS-loaded CaMTC16. Thus, the 50%/50% methanol/water mixture was used as the reagents for CaMTC16 reuse experiments. As shown in Figure 2.8, CaMTC16 maintained a high PFOS removal efficiency

(>98%) after using for three times, while the removal efficiency for PFOA gradually decreased after regeneration and reuse. The better performance for PFOS removal may be attributed to the stronger affinity between CaMTC16 and PFOS than PFOA. During each regeneration process, a small amount of the IL modifier may be lost from CaMTC16 to regenerate because of the use of methanol, which might contribute to the reduced performance for PFOA removal. In general, our results showed that CaMTC16 may be regenerable by solvent extraction and reusable multiple times.

2.3.6 Removal of multiple PFAS compounds

In addition to PFOA and PFOS, numerous PFAS compounds may co-exist in the field. To provide an initial evaluation of the simultaneous removal of multiple PFAS compounds, the performance of CaMTC16 was determined in a mixture of seven perfluorinated carboxylic acids and three perfluorinated sulfonates with a nominal concentration of 10 µg/L for each of the PFAAs. As shown in Figure 8, CaMTC16 was very effective for the removal of a range of PFAAs with varied chain lengths and end functional groups in pure water, showing >97% removal efficiency for most of the examined PFAAs. Even for PFBA, CaMTC16 achieved >85% removal efficiency. Additionally, CaMTC16 also exhibited robust performance under the lake water matrix consisting of various constituents such as chloride, bicarbonate, sulfate, nitrate, and DOC. Nearly complete removal was observed for PFHxS, PFOA, PFNA, PFOS, and PFDA in lake water. The removal efficiencies for PFHpA, PFHxA, and PFBS were slightly reduced compared to those in pure water, while the performance of CaMTC16 substantially decreased for the removal of PFBA and PFPeA (Figure 2.8), which may be attributed to the presence of a relatively high level of anions and a moderate level of DOC in the source water that might compete for the sorption sites. Sorption of

short-chain PFAS, like PFBA, has been identified as a unique challenge because of their reduced affinity with various classes of sorbents (Vu and Wu 2020). Due to their shorter perfluoroalkyl moieties, PFBA and PFPeA may be less preferentially captured by CaMTC16 than the other PFAAs. Nevertheless, our result suggested that CaMTC16 may be potentially applied as an efficient sorbent for the treatment of various PFAS compounds.

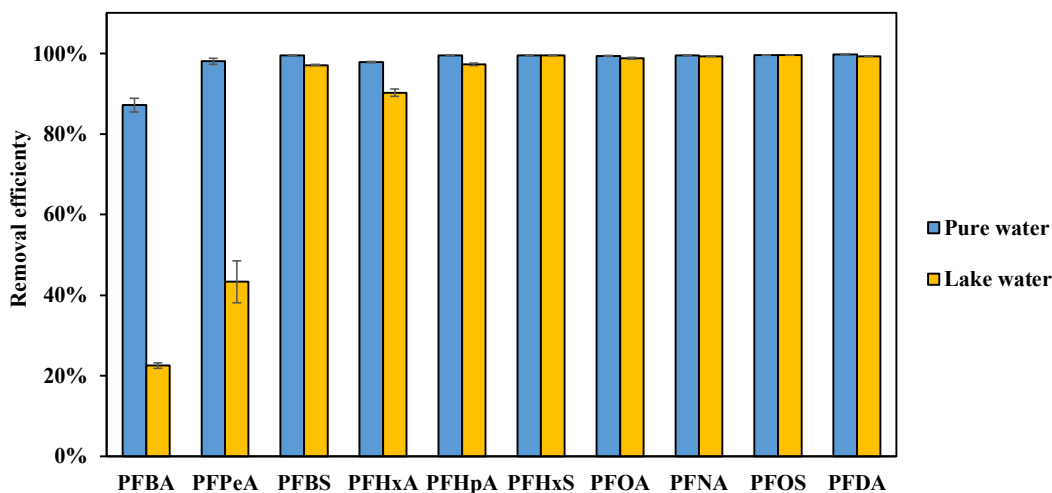


Figure 2.8 Removal of a mixture of ten PFAAs with a nominal concentration of 10 $\mu\text{g/L}$ for each PFAA in pure water and lake water with the use of CaMTC16 (0.25 g/L). Error bars represent one standard deviation of duplicate experiments.

2.3.7 Practical considerations

The present work provided an initial assessment of IL-modified clay for PFAS sorption. In practice, IL-modified clay may possibly be used as an efficient sorbent for ex situ treatment of waters contaminated with PFAS. Proper handling of PFAS-loaded sorbents and/or PFAS-containing regenerants is critical for ex situ treatment applications. Development of a treatment train approach with the inclusion of a PFAS destruction technology may allow for complete treatment of PFAS-laden sorbents or regenerants for safe disposal and reuse (D. Lu et al. 2020). In addition, IL-

modified clay may potentially be a suitable medium for in situ remediation of PFAS contamination sites, due to its compatibility with natural soils and sediments. For instance, IL-modified clay may be employed as an amendment for soil remediation, and/or be used alone or together with other media to develop technologies like permeable adsorptive barrier to remediate PFAS-impacted groundwater. A Ca-rich montmorillonite (CaMT) was used as a model clay substrate in the present study, while IL-modified clay may be prepared practically by locally sourced clays. The effect of composition and properties of different clay substrates on the IL accommodation and PFAS removal warrants further investigation.

2.4 Conclusions

In this chapter, a family of IL-modified clays was prepared using imidazolium-type ILs with varied alkyl chain lengths and evaluated for the sorption of PFOA and PFOS for the first time. The alkyl chain length of the IL strongly affected the surface charge and interlayer spacing of the corresponding IL-modified clay, and thus the sorption of PFOA and PFOS. Compared to clays modified with shorter-chain ILs (C4, C6 and C10), CaMTC16 exhibited high removal efficiency for both PFOA and PFOS, probably due to the strong hydrophobic and electrostatic interactions. Detailed sorption experiments revealed that CaMTC16 had fast sorption kinetics and high affinity with PFOA and PFOS, as well as robust performance under various water chemistry conditions. In addition, CaMTC16 was very effective for the simultaneous removal of numerous PFAAs. Our results highlighted the important role of IL structure in the performance of the IL-modified clay, and clay modified with the optimal IL may be an efficient sorbent for PFAS capture and removal. To promote technology development, future research may focus on (1) systematic investigation of the sorption behaviors of PFAS with a variety of structures and end functional groups; (2)

elucidation of the effect of clay structure and property on PFAS sorption by IL-modified clay; (3) development of improved strategies to promote the reuse of IL-modified clay; and (4) determination of the long-term performance of IL-modified clay with settings relevant to field applications.

Acknowledgements

This research was financially supported by the Department of Defense (DoD) Strategic Environmental Research and Development Program (SERDP, ER18-1289). All opinions expressed in this work are the authors' and do not necessarily reflect the views of DoD. We acknowledge the use of XRD and SEM in the Advanced Analysis Facility and the Department of Biology at University of Wisconsin – Milwaukee (UWM), respectively. FTIR and Zeta potential measurements were performed in the Water Technology Accelerator at UWM. LC-MS and LC-MS/MS analyses were conducted in the Shimadzu Laboratory for Advanced and Applied Analytical Chemistry at UWM. We thank Ms. Leah Stewart for her assistance with some PFAS sorption experiments. We are grateful to Mr. Patrick Anderson at UWM for his help with the carbon and nitrogen elemental analysis. The authors declare no competing financial interest.

Chapter 3 Adsorption of PFAS on Ionic Liquid-Modified Clays: Effect of Clay Mineral Structure and PFAS Nature

3.1 Introduction

Per- and polyfluoroalkyl substances (PFAS) are a large group of manmade aliphatic compounds containing at least one fluorinated methyl or methylene carbon atom (Z. Wang et al. 2021). The vast production and application of PFAS-related products such as coatings, surfactants, fire-fighting foams, and pesticides lead to a substantial environmental challenge because of the persistence and recalcitrance of PFAS caused by the combination of robust C-F bonds and functional groups (OECD 2018). Nowadays, PFAS are ubiquitously found in the water bodies worldwide via the product emission, landfill leachate and indirect photolysis of PFAS-containing products (Lenka, Kah, and Padhye 2021; L. Yang, Zhu, and Liu 2011; Kim et al. 2011; Post et al. 2009; F. Li et al. 2020; US EPA 2016a). As a subclass of the PFAS family, perfluoroalkyl acids (PFAAs) are particularly persistent in nature because of the sp^3 C-F bonds. More and more evidence shows that PFAAs with varying chain lengths are highly stable and accumulative in the environment, causing a long-lasting effect on both humans and wildlife (Lenka, Kah, and Padhye 2021; Z. Wang et al. 2017). In 2016, the U.S. Environmental Protection Agency (USEPA) set up a health advisory level for perfluorooctanoic acid (PFOA) and perfluorooctanesulfonic acid (PFOS) in drinking water, which has been tightened recently (US EPA 2016a).

Adsorption is an established technology for substantial PFAS removal due to its high efficiency and low cost (Wang 2019; Pauletto and Bandosz 2022). Both the electrostatic and hydrophobic effects are observed as the main force governing the PFAS adsorption on activated carbon, ion

exchange resins, etc. (L. Liu et al. 2020; Park, Daniels, et al. 2020b; Q. Zhou et al. 2010). Clay minerals with layered structure are naturally abundant and green materials which have been developed as charge carriers, drug delivery, and adsorbents. (L. Wang et al. 2016; M. Wang et al. 2021; X. Ji et al. 2021; Sharma and Bajpai 2018). Among them, vermiculite and montmorillonite with the intercalation of organic and/or inorganic modifiers are commonly used for PFAS adsorption (Y. M. Li and Zhang 2014; Haouzi et al. 2018; Lee and Tiwari 2012; Huo, Min, and Wang 2021). Surface modifications enhanced the hydrophobicity and surface charge of clay minerals, and thus improved the removal efficiency of PFAS. For example, hexadecyltrimethylammonium bromide (HDTMAB), polyfluoroalkyl quaternary ammonium (PFQA), carnitine, and choline-modified montmorillonite showed improved PFAS removal compared with raw clays (Q. Zhou et al. 2010; M. Wang et al. 2021; Z. Du et al. 2016). Our previous work also showed that clay minerals modified with ionic liquids (ILs) exhibited fast and efficient removal of PFOS and PFOA, which may be used as a promising *in situ* groundwater and soil remediate (Dong et al. 2021). Meanwhile, it has been reported that clay structure is critical to the adsorption of surfactant and humic acid (Sánchez-Martín et al. 2008). However, the impact of clay structural on the adsorption of PFAS remains largely unexplored. Vermiculite and montmorillonite are both classified as 2:1 clays; however, they have different expansion properties and their distinct crystalline structures and properties are highly dependent on their compositions (Grim, Bary, and Bradley 1937; Naidu et al. 1997). Therefore, it is necessary to investigate the impact of clay composition on the overall adsorption behavior of PFAS.

It has been observed that PFAS adsorption highly depended on the chain length and head group of PFAS. Due to the increased hydrophobicity, the long-chain PFOA has a later breakthrough on granular activated carbon column than the short-chain perfluorobutanoic acid (PFBA) and

perfluorohexanoic acid (PFHxA), which could be related to their octanol/water distribution coefficients (Park, Wu, et al. 2020; Appleman et al. 2013). Park et al. found the contribution of distinct negative atomic charge of perfluorinated sulfonic acids (PFSAs) to their high removal on magnetic ion exchange with the aid of modeling and computational methods (Park, Daniels, et al. 2020). In the sorption of the long-chain PFOS on the organically modified-montmorillonite, both electrostatic interaction and hydrophobic partitioning were involved (Q. Zhou et al. 2010). However, the removal of PFAS with varied chain lengths using organoclay is not fully understood at the moment. Furthermore, the effects of chain length and charge group on the distribution of PFAS between IL-modified clay and water have not yet to be sufficiently understood.

This research aimed to investigate the adsorption behavior of various PFAAs onto IL-modified clays and identify key clay properties that impacted PFAS adsorption. Specifically, three natural clays with different composition and properties were used for IL modification. The specific objectives of this study were to (1) modify different clay substates with imidazolium-type ILs for the sorption of PFAAs with different chain lengths; (2) characterize and compare the performance of IL-modified clays with varied compositions; (3) explore the impact of clay composition and PFAAs structure on PFAAs adsorption. The correlation was examined between the adsorption capacity, adsorption affinity, adsorption Gibbs free energy, and clay/PFAAs structure; and (4) evaluate the performance of IL-modified clays for simultaneous removal of multiple PFAAs in natural water. Eight representative PFAAs including PFBA, PFHxA, PFOA, PFOS, perfluorobutanesulfonic acid (PFBS), perfluoroheptanoic acid (PFHpA), perfluorohexanesulphonic acid (PFHxS), and perfluorononanoic acid (PFNA) were selected in this study based on their high occurrence and recalcitrance in the environment (Z. Zhou et al. 2013; L. Yu, Liu, and Hua 2022; Kolpin et al. 2021). Also, the selected PFAAs covered the short-chain and

long-chain PFAAs with varied hydrophobicity and charge density, which would allow for a comprehensive understanding on the adsorption behavior of PFAAs onto IL-modified clays.

3.2 Material and Methods

3.2.1 Chemicals

Three natural clay minerals with high cation exchange capacity (CEC) but different structures were used for IL modification, including Ca-rich montmorillonite (CaMT, Texas, USA), Na-rich montmorillonite (NaMT, Wyoming, USA), and vermiculite (VT, South Africa). CaMT and NaMT were purchased from the Clay Minerals Society and used as received. VT was purchased from the Strong Company (USA) and pretreated to remove impurities prior to the modification based on our approach described previously (Huo, Min, and Wang 2021). Specifically, 20 g vermiculite was added to 200 mL HNO₃ solution (0.1 M), and then the mixture was stirred at 90 °C for 3 h. The obtained solid was washed with water until reaching neutral pH. Then the solids were dispersed in 200 mL Na₂CO₃ solution (8 g/L) for cation exchange at 80 °C with vigorous agitation for 3 h. The obtained VT was washed with water until neutral pH and then dried at 105 °C overnight. The characteristic and components of raw clays were detailed in Table 3.1.

A list of PFAS chemicals used in the present work is detailed in Table 3.2. Analytical grade sodium chloride (NaCl), sodium bicarbonate (NaHCO₃), sodium sulfate (Na₂SO₄), and sodium nitrate (NaNO₃) were purchased from Fisher-Scientific. Sodium hydroxide (NaOH) was purchased from DOT-Scientific. Hydrochloric acid and HPLC grade methanol were purchased from VWR-BDH. LCMS grade acetonitrile, ammonium acetate and methanol were purchased from Fisher Scientific. 1-Hexadecyl-3-methylimidazolium chloride (IL) was purchased from Acros-Organics. Ultrapure

water (resistivity > 18.2 MΩ·cm) was used for all experiments. Natural water collected from a local river (i.e., Milwaukee River) and a groundwater well was filtered with 0.22 μm polyether-sulfone (PES) membrane (Millipore) before use.

Table 3.1 Characteristics and components of raw clays.

Characteristics and components	Weight (%)		
	CaMT	NaMT	VT
CEC (meq/100g)	84	76	143
AEC (meq/100g)	0.22	1.05	2.11
SiO ₂	74.54%	64.24%	41.73%
Al ₂ O ₃	14.46%	20.14%	9.91%
MgO	2.77%	2.41%	23.24%
CaO	1.79%	1.50%	1.50%
Fe ₂ O ₃	1.13%	3.95%	9.27%
Na ₂ O	0.28%	1.89%	1.21%
LoI	6.35%	6.18%	6.53%

Table 3.2 PFAS chemical list for adsorption experiments.

Analyte	Abbreviation	CAS #	Purity	Manufacturer
Heptafluorobutyric acid	PFBA	375-22-4	98%	Sigma-Aldrich
Perfluorohexanoic acid	PFHxA	307-24-4	97%	Oakwood-Chemical
Nonafluorobutane-1-sulfonic acid	PFBS	375-73-5	97%	Sigma-Aldrich
Perfluoroheptanoic acid	PFHpA	375-85-9	99%	Sigma-Aldrich
Perfluorooctanoic acid	PFOA	335-67-1	95%	Alfa-Aesar
Tridecafluorohexane-1-sulfonic acid potassium salt	PFHxS	3871-99-6	≥ 98%	Sigma-Aldrich
Perfluorononanoic acid	PFNA	375-95-1	97%	Sigma-Aldrich
Heptadecafluorooctanesulfonic acid potassium salt	PFOS	2795-39-3	≥ 98%	Sigma-Aldrich

3.2.2 Synthesis and characterization of IL-modified clays

IL-modified clays were prepared by intercalating the three clay minerals with the 1-hexadecyl-3-methylimidazolium chloride (IL). The structure of IL was shown in Figure 3.1. The IL loading was fixed at 1.0 CEC of the clay minerals. The typical organoclay synthesis was detailed in our previous work (Dong et al. 2021). Briefly, a clay mineral solution of 5 g in 100 mL water was stirred for 24 hours at room temperature. Following this, aliquots of an IL solution with the desired amount (i.e., 4.22 mmol for CaMT, 3.80 mmol for NaMT, and 7.15 mmol for VT) were added to the clay-water mixture and stirred for another 24 hours. The solids were then centrifuged, washed with water for five times, and oven dried at 60 °C. The synthesized IL-modified CaMT, NaMT, and VT were denoted as CaMTIL, NaMTIL, and VTIL, respectively.

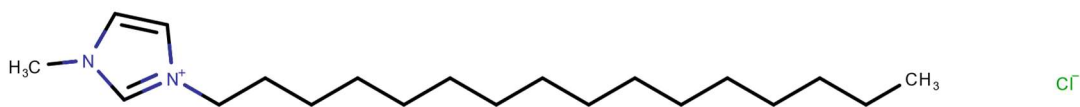


Figure 3.1 The structure of 1-hexadecyl-3-methylimidazolium chloride (IL)

In this study, the composition of raw and IL-modified clays was determined on a S4 pioneer X-ray fluorescence (XRF) spectrometer (Bruker AXS, Germany) equipped with a 4 kW Xray tube and Rh anode. The layered structure was determined on a Bruker D8 Discover X-ray diffractometer (XRD) with Cu-K α radiation equipped with a Lynx-Eye detector over the range of 2θ of 3-10⁰. Fourier transform infrared spectroscopy (FTIR) measurements were carried out using a Shimadzu IRTracer100 Spectrometer. The FTIR spectra (4000-600 cm⁻¹) were collected using

IR solutions 6.0 Software for Windows with a resolution of 2 cm^{-1} by adding 64 scans to each spectrum. A Malvern Zetasizer Nano ZS 90 was used to measure zeta potentials in the pH range of 3 to 11. Carbon and nitrogen contents were determined using a Fisons NA 1500 NCS elemental analyzer.

3.2.3 PFAS adsorption experiments

To fully examine the adsorption behavior of individual PFAS on IL-modified clays, adsorption isotherm experiments were carried out for each PFAS under batch mode and ambient temperature ($22 \pm 2\text{ }^\circ\text{C}$) with a sorbent loading of 0.25 g/L . The PFAS concentration ranged from 1 to 100 mg/L to cover the capacity. The solution pH was adjusted to 7 and was stable over the course of the experiment. The reactors were placed on a flat shaker at 300 rpm for 24 hours to ensure that adsorption reached equilibrium. Additionally, the performance of IL-modified clays was also examined under environmentally relevant conditions both in a simply lab-prepared solution (i.e., DI water) and two natural water matrices (river water and groundwater in Table 3.3). Specifically, the mixture of eight PFAS was spiked in each water matrix with a nominal concentration of $1\text{ }\mu\text{g/L}$ for each PFAS. All experimental conditions were run in duplicates.

3.2.4 PFAS measurement

In all experiments, the samples were immediately filtered using Millipore $0.22\text{-}\mu\text{m}$ PES syringe filters. In the filtering procedure, the first 3 mL of the sample were used for rinsing the filter before it was discarded. No significant PFAS capture by the filter was observed because of the small filter diameter (13 mm) and the use of the rinsing step. The filtrated samples were diluted to 50%/50%

water/methanol. For low-concentration PFAS mixture samples, acetic acid and isotope-labeled internal standards (200 ng/L) were also added based on modification of EPA Method 8327 (US EPA 2019).

Table 3.3 Major water composition of the natural groundwater and river water samples.

Ion	River water		Groundwater	
	Conc. (mg/L) ^a	Conc. (mM)	Conc. (mg/L) ^a	Conc. (mM)
Cl ⁻	101.07	2.85	9.53	0.27
SO ₄ ²⁻	26.37	0.27	12.99	0.14
NO ₃ ⁻	5.73	0.10	23.87	0.42
DOC	12.16 ^b	1.01 ^c	0.94 ^b	0.08 ^c
pH	7.6 ^d		7.98 ^d	

^a Concentrations of Cl⁻, SO₄²⁻, and NO₃⁻ were determined using ion chromatography.

^b Concentration of dissolved organic carbon (DOC) was determined using TOC analyzer and was reported as mg C/L

^c Concentration of DOC here was reported as mM of C.

^d pH value is unitless

The analysis of the eight PFAS from single-sorbate sorption experiments was carried out on a high-performance liquid chromatography (HPLC) system coupled with a single quadrupole mass spectrometer (ISQ-EM, Thermo Scientific). Mass spectrometry (MS) analysis was performed using the single quadrupole MS under ESI negative mode with the following operating conditions: ion transfer tube temperature 300 °C, vaporizer temperature 227 °C, source voltage -2046 V, sweep gas pressure 0.5 psig, aux gas pressure 4.8 psig, and sheath gas pressure 42.9 psig. Chromatography was performed using a XB-C18 column (Kinetex® 1.7 µm, 100 Å, 100 x 2.1 mm, Phenomenex). The mobile phase consisted of (A) Milli-Q water and (B) acetonitrile, both amended with 0.1% formic acid (Fisher Scientific). The gradient of mobile phase started at 40%

B, jumped to 90% B at 3 min and keep for 3 min, reversed to the original condition at 8 min, and maintained to 12 min at a flow rate of 400 $\mu\text{L}/\text{min}$.

The analysis of the eight PFAS compounds from the low-concentration PFAS mixture sorption experiments was performed on a UHPLC system coupled with a triple quadrupole mass spectrometry (LCMS-8060, Shimadzu), featuring an ultra-fast acquisition rate of 555 MRM/sec and which can operate without any compromise in sensitivity. Electrospray ionization was operated in a negative mode with the parameters set as capillary voltage at 4.5kV, desolvation temperature at 526 $^{\circ}\text{C}$, heat block temperature at 200 $^{\circ}\text{C}$. Nitrogen (>99.99% purity, Airgas) was used as nebulizing gas with the flow rate of 3 L/min. Drying gas flow 5 L/min, heating gas flow 13 L/min, nebulizing gas flow 3 L/min. Interface temperature 300 $^{\circ}\text{C}$. MS/MS condition was listed in Table 3.4. LabSolutions V6.90 (Shimadzu) was used for instrument control, acquisition, and mass analysis. Chromatography was performed using a XB-C18 column (Kinetex[®] 1.7 μm , 100 \AA , 100 x 2.1 mm, Phenomenex). An additional delay column (Nexcol C18 5 μm , 50 x 3.0 mm, Shimadzu) was placed in the mobile phase flow path before the sample injection valve to prevent contamination for LCMS-8060. The mobile phase consisted of (A) Milli-Q water amended with 20mM ammonium acetate (LCMS grade, Fisher, USA) (B) acetonitrile (Optima LCMS grade, Fisher, USA). Samples were injected at 40 μL volumes with a loading pump delivering at 400 $\mu\text{L min}^{-1}$ of the mobile phase consisting of 10% B, jumping to 30% at 2 min, further increasing to 55% at 9 min and then maintaining 80% at 11 min to 13 min, then going back to 10% at 14 min and ending at 15min. The column temperature was held constant at 40 $^{\circ}\text{C}$.

Table 3.4 PFAS analytical conditions for each PFAS and their isotope labelled internal standards using LCMS-8060.

Analyte	Transition monitored (<i>m/z</i>)	Collision energy (V)	Internal standard (IS)	IS transition monitored (<i>m/z</i>)	Detection limits (ng/L)
PFBA	213.4>169.2	11	MPFBA	217.2>172.1	10
PFBS	299.1>80.1	36	M3PFBS	302.2>80.0	10
PFHxA	313.4>269.1	8	M5PFHxA	318.1>273.2	10
PFHpA	363.0>319.0	10	M4PFHpA	367.2>322.1	10
PFHxS	399.0>80.0	42	M3PFHxS	402.0>80.0	10
PFOA	413.0>369.0	11	M8PFOA	421.2>376.0	10
PFNA	463.0>418.9	10	M9PFNA	472.1>427.1	10
PFOS	498.9>80.0	55	M8PFOS	507.1>80.0	10

3.2.5 Data analysis

The amount of adsorbed PFAS, q_e (mg/g), and removal efficiency (%) of PFAS was determined based on Equations 3.1 and 3.2, respectively:

$$q_e = \frac{(C_0 - C_e) \times V}{W} \quad (3.1)$$

$$Removal (\%) = \left(1 - \frac{C_e}{C_0}\right) \times 100\% \quad (3.2)$$

where C_0 (mg/L) is the initial PFAS concentration prior to sorption, C_e (mg/L) is the concentration of PFAS after sorption reaches equilibrium, V (L) is the volume of the solution, and W (g) is the mass of the sorbent.

Adsorption isotherms were fitted using the classic Langmuir (Equation 3.3) and Freundlich (Equation 3.4) models, as well as the Sips model (Equations 3.5), which is a combined form of Langmuir and Freundlich models.

$$q_e = \frac{Q_{max}K_L C_e}{1+K_L C_e} \quad (3.3)$$

$$q_e = K_F C_e^{\frac{1}{n}} \quad (3.4)$$

$$q_e = \frac{a C_e^n}{1+b C_e^n} \quad (3.5)$$

Where q_e (mg/g) and C_e (mg/L) refer to the same meaning with Equations 3.1 and 3.2. K_L in Equation 3.3 is the Langmuir adsorption constant and Q_{max} (mg/g) is the maximum sorption capacity. In Equation 3.4, K_F (mg/g·(L/mg)^{1/n}) is the Freundlich constant and $1/n$ is a dimensionless indicator related to the sorbent surface heterogeneity. Equation 3.5 is a simplified Sips model expression where a (mg/g· (L/mg)ⁿ) and b ((L/mg)ⁿ) are empirical adsorption constants, and n is the heterogeneity index (Tzabar and ter Brake 2016; He et al. 2019). It was worth noting that for Sips model, if $n = 1$, it would be Langmuir model; if $b = 0$, it would be Freundlich model.

The adsorbent-water partition coefficient K_d (L/kg) for individual PFAS at a given concentration is computed based on the following equation (F. Xiao et al. 2019).

$$K_d = \frac{q_e}{C_e} * 1000 \quad (3.6)$$

Where 1000 was a unit conversion factor between g and kg. Linear regression was performed between K_d values and the key characteristics of raw and IL-modified clays including the CEC value, IL loading, d-spacing, and zeta potential to evaluate the relation of these features with PFAS adsorption.

3.3 Results and Discussion

3.3.1 Characterization of IL-modified clay minerals

FTIR spectra showed the transmission of functional groups in the unmodified and IL-modified clays (Figure 3.2a). Compared with the unmodified clays, a significant change in FTIR spectra of IL-modified clays was observed in the region of 2900-3200 cm^{-1} , which was consistent with previous studies (L. Wu, Yang, et al. 2014; Ahmed et al. 2018; Cardona et al. 2016). The peaks between 2900-3200 cm^{-1} were related to the stretching vibration of C-H, which were not present in the as-received clays. Two peaks at ~ 1560 and ~ 1460 cm^{-1} that may result from the vibration of C=C and C=N-H asymmetric stretching of the imidazolium ring further confirmed the successful intercalation of ILs within the clays (Ahmed et al. 2018).

The layered structure of natural and IL-modified clays was compared using XRD with in small angle (Figure 3.2b). The natural clay had a strong peak at 2θ of 5.8° , 7.5° and 9.0° for CaMT, NaMT, and VT, respectively, corresponding to a basal spacing of 15.2 Å, 11.8 Å and 9.9 Å based on the Braggs equation (Oloyede et al. 2021). The layer expansion was smaller than the size of organic cation (23.4 Å) indicating an angular deployment of ILs in clay interlayers, which was also consistent with previous experimental and simulation results (L. Wu, Liao, et al. 2014). Notably, after the intercalation of IL, the (001) plane shifted to 4.5° and 5.0° for CaMTIL and NaMTIL, respectively, indicating a layer expansion within IL-modified montmorillonites (Table 3.5). VTIL formed two new peaks at 6.0° and 4.2° , which may be attributed to a superstructure that was composed of two different layers (Klapyta, Fujita, and Iyi 2001). The observation suggested heterogenous intercalation of ILs into VT, which resulted in a partial expansion of the interlayer of VT (L. Wang et al. 2016). Moreover, C/N content indicated that the intercalation

amount of ILs on three clays followed the order of VTIL > CaMTIL > NaMTIL, which was well related to the order of CECs of the raw clays.

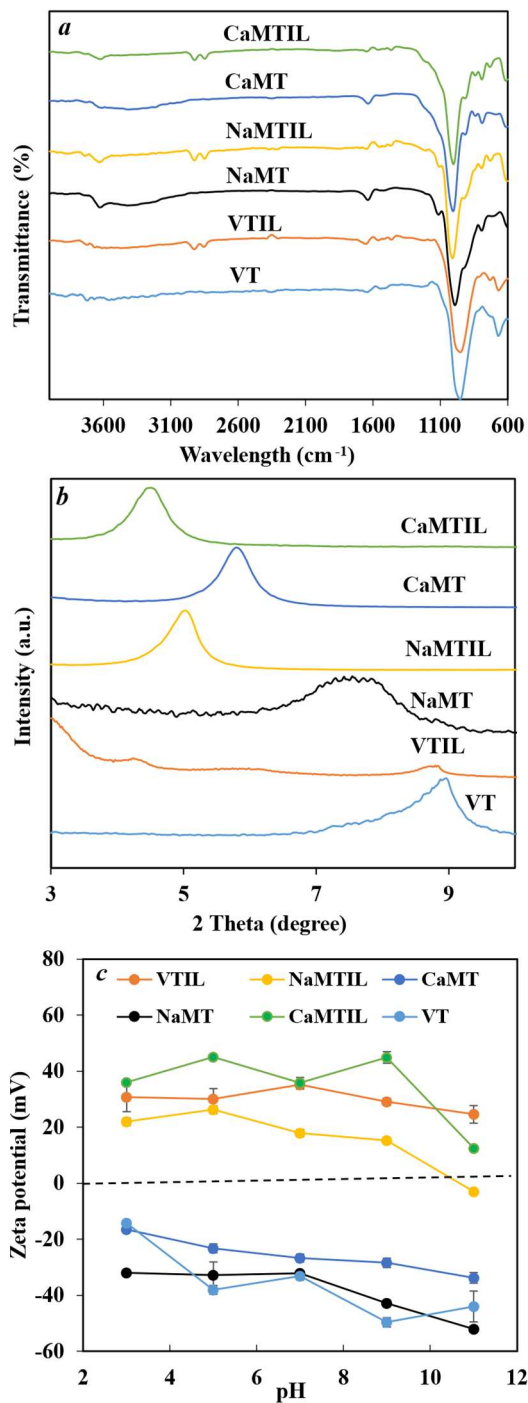


Figure 3.2 FTIR (a), XRD (b), and zeta potential (c) measurement of unmodified and IL-modified clays.

Zeta potential measurement was conducted for the raw and IL-modified clays in the pH range of 3 ~11 (Figure 3.2c). Zeta potential measures the charge in a shear plane resulting from isomorphous replacement of Si with Al within the clay structural, structure imperfection, and deprotonation of the surface hydroxyl groups of clay (Şans et al. 2017). Therefore, it is common that the zeta potential of three natural clays is negative. Modification with ILs reversed the surface charges of the clay substrates. At pH 7, zeta potential had a minor difference among the three modified clays with the following order that NaMTIL < VTIL \approx CaMTIL, and all IL-modified clays were positively charged.

Table 3.5 Key characterizing parameters of clay minerals.

Materials	Zeta potential mV^a	IL mmol/g	d spacing (nm)
CaMT	-26.7	NA	15.2
CaMTIL	37.3	0.59	19.6
NaMT	-32.2	NA	11.8
NaMTIL	17.9	0.54	17.7
VT	-33	NA	9.9
VTIL	35.2	0.77	10.1 ^c

^a Zeta potential value at pH 7.

^b Layout of ILs in the interlayer of clay minerals

^c d spacing calculated based on the strongest peak of VTIL.

3.3.2 Adsorption isotherms of PFAS by IL-modified clays

Adsorption isotherms of eight perfluorinated carboxylic acids (PFCAs) and PFASs with varying carbon chain lengths were determined to investigate the PFAS equilibrium sorption behavior between water and the three IL-modified clays. In general, the adsorbed PFAS increased quickly at low equilibrium concentrations, while gradually reached to the maximum capacity with the increase of PFAS concentration (Figure 3.3). Compared to other PFAS, the adsorbed PFBA increased slower at relatively low concentrations, indicating its less affinity with the IL-modified

clay sorbents. With the increasing chain length, the adsorbed PFAS increased on all three IL-modified clays, suggesting that PFAS structure may play important roles in the adsorption. Meanwhile, control experiments showed that PFAS adsorption was minimal onto the raw clays (Figure 3.4), indicating the role of IL modification for PFAS adsorption. Experimental data were fitted with the Langmuir, Freundlich, and Sips models (Equations 3.3 – 3.5). To reduce the propagation error, nonlinear regression fitting was applied to three models. The fitting parameters of three models with eight PFAS adsorption data on CaMT were shown in Table 3.6. Results showed that the Sips model performed better than the other two models, based on R^2 . Langmuir model did not fit well in some cases because of the heterogeneity of the IL-modified clays; Freundlich model did not perform well because of the plateau phase in some cases. Previous study also showed the advantage of Sips model over the Langmuir and Freundlich models to depict the heterogeneous adsorption at the low adsorbate concentration (Al-ghouti and Da 2020). Modification with ILs may provide a heterogeneous surface like the NOM preloaded activated carbon (Carter, Kilduff, and Weber 1995; Kłapyta et al. 2003). Therefore, it is necessary and rational to choose the Sips model for isotherm fitting in our study.

To compare the adsorption capacities of the PFAS under the experimental range, the estimated PFAS adsorption capacities (Q_s) at a sufficiently high equilibrium concentration ($C_e = 50$ mg/L) were calculated for the eight PFAS onto the three IL-modified clays based on the Sips model. As shown in Figure 3.5, the adsorption capacities for each PFAS followed the trend that VTIL > CaMTIL > NaMTIL, suggesting that PFAS adsorption strongly depended on the structural and compositional properties of the clay substrates. For a given organoclay, the PFAS adsorption capacities generally increased with the increasing chain length of the perfluoroalkyl moiety. Similar trends were found in the study using activated carbon and modified ion exchange resins

for PFAS mixture removal (Q. Yu et al. 2009; Gagliano et al. 2019). It should be noted that the maximum PFAS adsorption capacities derived from the Sips model were not used here because those values may only be achievable with a very high equilibrium PFAS aqueous concentration well beyond the experimental range of the present work.

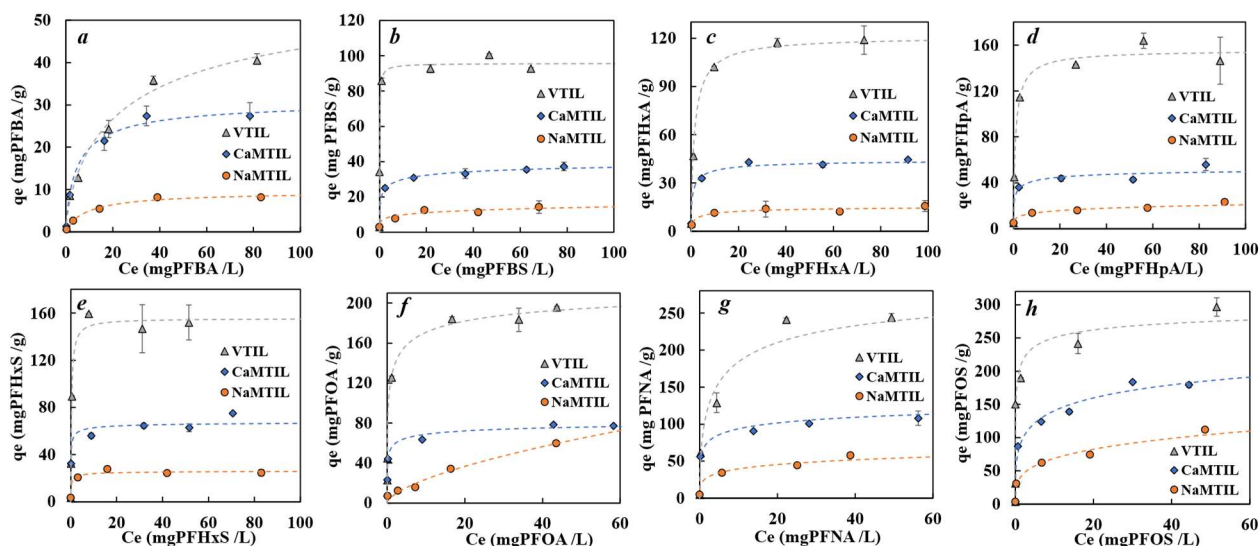


Figure 3.3 Adsorption isotherms fitted with Sips model of (a) PFBA, (b) PFBS, (c) PFHxA, (d) PFHpA, (e) PFHxS, (f) PFOA, (g) PFNA, and (h) PFOS onto the three IL-modified clays. Experiments were conducted at pH 7 with a sorbent loading of 0.25 g/L and a contact time of 24h. Dash lines represent Sips model fits.

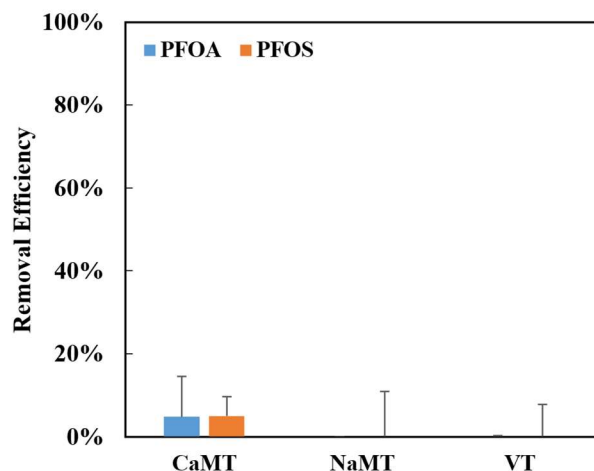


Figure 3.4 Removal efficiency of PFOA and PFOS on raw clays.

Table 3.6 Isotherm fitting parameters of adsorption of eight PFAAs onto three IL-modified clays (including Langmuir, Freundlich, and Sips nonlinear fitting results).

		Freundlich			Langmuir			Sips			
		K_f	$1/n$	R^2	K_L L/mg	Q_m mg/g	R^2	a	b	n	R^2
CaMTIL	PFBA	8.63	0.29	0.93	0.25	28.91	0.99	8.28	0.27	0.81	0.99
	PFHxA	22.48	0.15	0.86	0.78	43.23	0.97	55.21	1.23	0.62	0.98
	PFHpA	26.35	0.15	0.90	1.14	48.71	0.93	64.97	1.17	0.43	0.95
	PFOA	45.90	0.14	0.96	11.50	72.60	0.87	143.12	1.61	0.33	0.98
	PFNA	60.17	0.16	0.95	9.75	107.26	0.93	111.14	0.65	0.27	0.95
	PFBS	19.38	0.15	0.97	0.94	35.46	0.98	40.12	0.90	0.36	1.00
	PFHxS	38.89	0.15	0.93	28.14	64.74	0.95	252.92	3.69	0.48	0.95
	PFOS	82.89	0.21	0.97	1.30	166.65	0.92	111.02	0.31	0.31	0.98
VTIL	PFBA	7.50	0.40	0.97	0.07	47.32	0.98	2.89	0.05	1.02	0.99
	PFHxA	51.78	0.20	0.89	0.72	119.42	1.00	85.94	0.71	0.90	1.00
	PFHpA	70.46	0.19	0.89	1.19	153.37	0.99	174.19	1.12	0.88	0.99
	PFOA	105.11	0.17	0.97	28.20	174.15	0.91	267.50	1.16	0.39	0.99
	PFNA	98.99	0.22	0.94	0.31	256.41	0.96	135.70	0.44	0.53	0.97
	PFBS	60.36	0.13	0.83	17.34	94.60	0.99	928.61	9.70	0.83	1.00
	PFHxS	82.65	0.18	0.85	3.27	154.79	0.99	477.73	3.08	0.96	0.99
	PFOS	164.34	0.15	0.87	104.39	244.92	0.90	546.49	1.73	0.34	0.89
NaMTIL	PFBA	2.06	0.33	0.93	0.12	9.24	0.99	1.28	0.13	0.90	0.99
	PFHxA	6.36	0.19	0.88	1.06	13.72	0.90	9.85	0.61	0.56	0.93
	PFHpA	8.89	0.19	0.94	0.34	19.27	0.78	10.15	0.15	0.23	0.94
	PFOA	5.74	0.62	0.97	0.03	108.50	0.96	5.74	0.00	0.62	0.97
	PFNA	24.23	0.21	0.96	0.23	58.50	0.95	27.90	0.16	0.26	0.97
	PFBS	6.74	0.16	0.91	340.97	11.42	0.72	6.74	0.00	0.16	0.91
	PFHxS	15.58	0.13	0.82	1.68	25.83	0.94	68.31	2.58	0.57	0.96
	PFOS	37.90	0.26	0.98	0.14	120.06	0.89	37.90	0.00	0.26	0.98

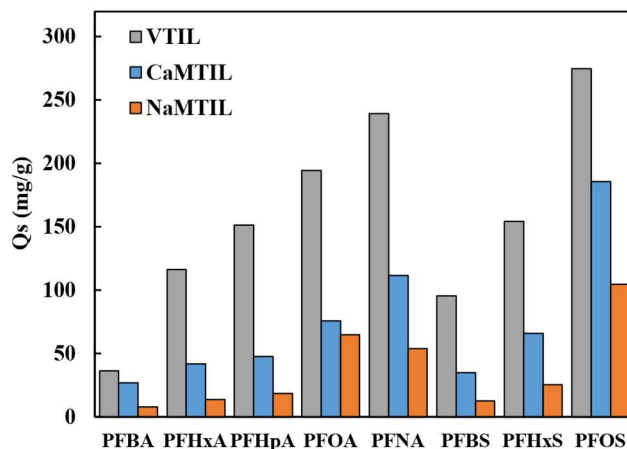


Figure 3.5 Comparison of adsorption capacities of eight PFAAs by three IL-modified clays (Based on Sips isotherm, $C_e = 50$ mg/L)

Linear regression analysis was performed between the estimated PFAS adsorption capacity (Q_s) and key clay characteristic parameters. As shown in Figure 3.6, Q_s generally showed a good linear relationship with the CEC values of raw clay for most PFAS, indicating the importance of clay compositions in PFAS adsorption. Compared to the longer chain PFAS, PFBA showed a poorer linearity between Q_s and CEC, which may be due to the relatively weak affinity between PFBA and the three IL-modified clays.

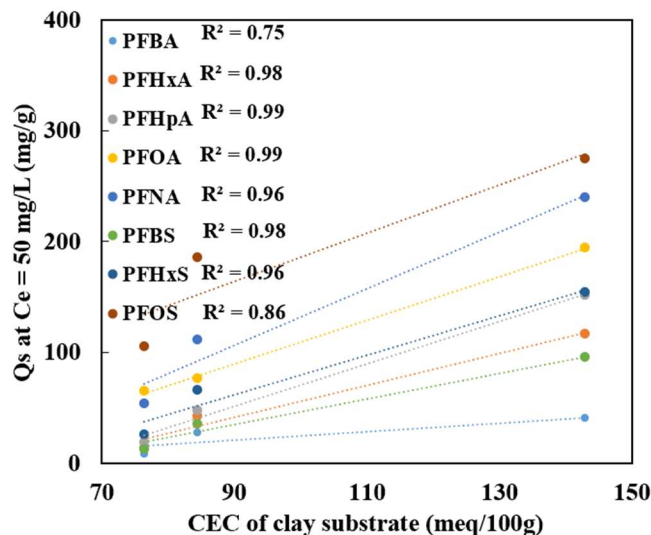


Figure 3.6 The linear regression of CEC values of raw clays vs the estimated PFAS adsorption capacity Q_s (at $C_e = 50$ mg/L) onto the corresponding IL-modified clays.

Moreover, the adsorption capacity has a positive correlation with the IL loading of the IL-modified clays that was closely related to the CEC values of the raw clays (Figure 3.7a). Notably, VTIL had a higher IL loading than CaMTIL and NaMTIL, which resulted in the highest PFAS adsorption capacity. Meanwhile, although the CEC values of CaMT and NaMT were very close, and the amount of intercalated ILs did not show a big difference between these two clays, the adsorption capacity of PFAS was much lower on NaMTIL, suggesting that factors other than IL loading may also play a role. It has been reported that CEC, zeta potential, and surface morphology play important roles in contaminant adsorption onto clay minerals (Alshameri et al. 2018; Sánchez-Martín et al. 2008). In the present study, however, no clear correlation was observed between d spacing of the IL-modified clays and their PFAS adsorption capacity (Figure 3.7b), which may be related to the heterogeneous nature of VTIL that could affect the calculated d spacing. Similarly, zeta potential also did not show good correlation with the Q_s values of PFAS on different organoclays (Figure 3.7c).

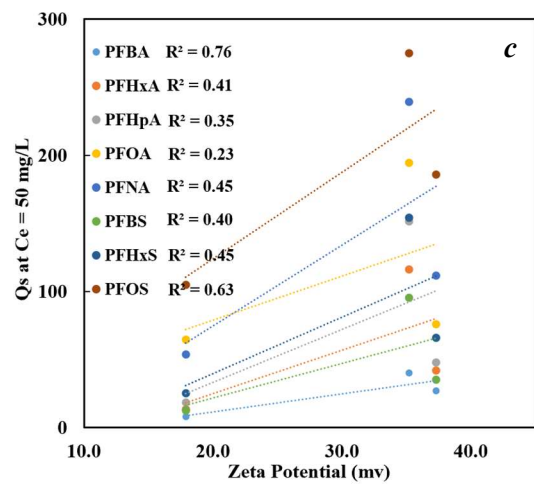
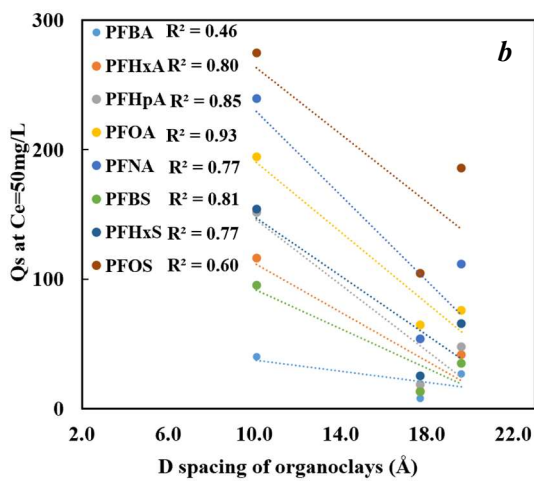
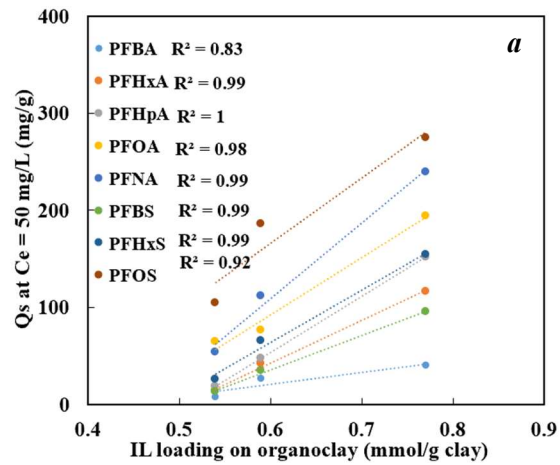


Figure 3.7 The linear regression of Q_s (at $C_e = 50$ mg/L) vs IL loadings (a), d spacing (b), and zeta potential (c) of the IL-modified clays.

3.3.3 Discussion of the PFAS structural impact on adsorption

Based on the Sips isotherm model, the adsorbent-water partition coefficient (K_d) can be calculated by combining Equations 3.5 and 3.6, as expressed in Equation 3.7:

$$K_d = \frac{aC_e^{n-1}}{1+bC_e^n} * 1000 \quad (3.7)$$

The K_d value indicates the partition of PFAS between the adsorbent and the aqueous phase at equilibrium, and a higher value indicates more favorable PFAS adsorption. For all PFAS, K_d values exhibited nonlinear responses versus C_e and generally decreased with increasing C_e values (Figure 3.8). At low concentrations, the adsorption sites of IL-modified were relatively abundant. Based on previous report, the adsorption sites of organoclays with high site energy was preferentially occupied by PFAS, resulting in relatively high K_d values with low PFAS concentrations (Yan, Wang, and Liu 2021). In general, for a given PFAS, the K_d values followed the trend that VTIL > CaMTIL > NaMTIL with high C_e concentrations (e.g., > 1 mg/L). Interestingly, the K_d values of CaMTIL became closer or even higher than those of VTIL with low C_e concentrations, suggesting the heterogeneous nature of the adsorption sites of the IL-modified clays. While VTIL may have more adsorption sites than CaMTIL because of the higher IL loading, CaMTIL may have more high energy sites, resulting in comparable or even higher affinity with PFAS than that of VTIL at low PFAS concentrations. Overall, our results suggested that the adsorption affinity could be different for all PFAS on different IL-modified clays.

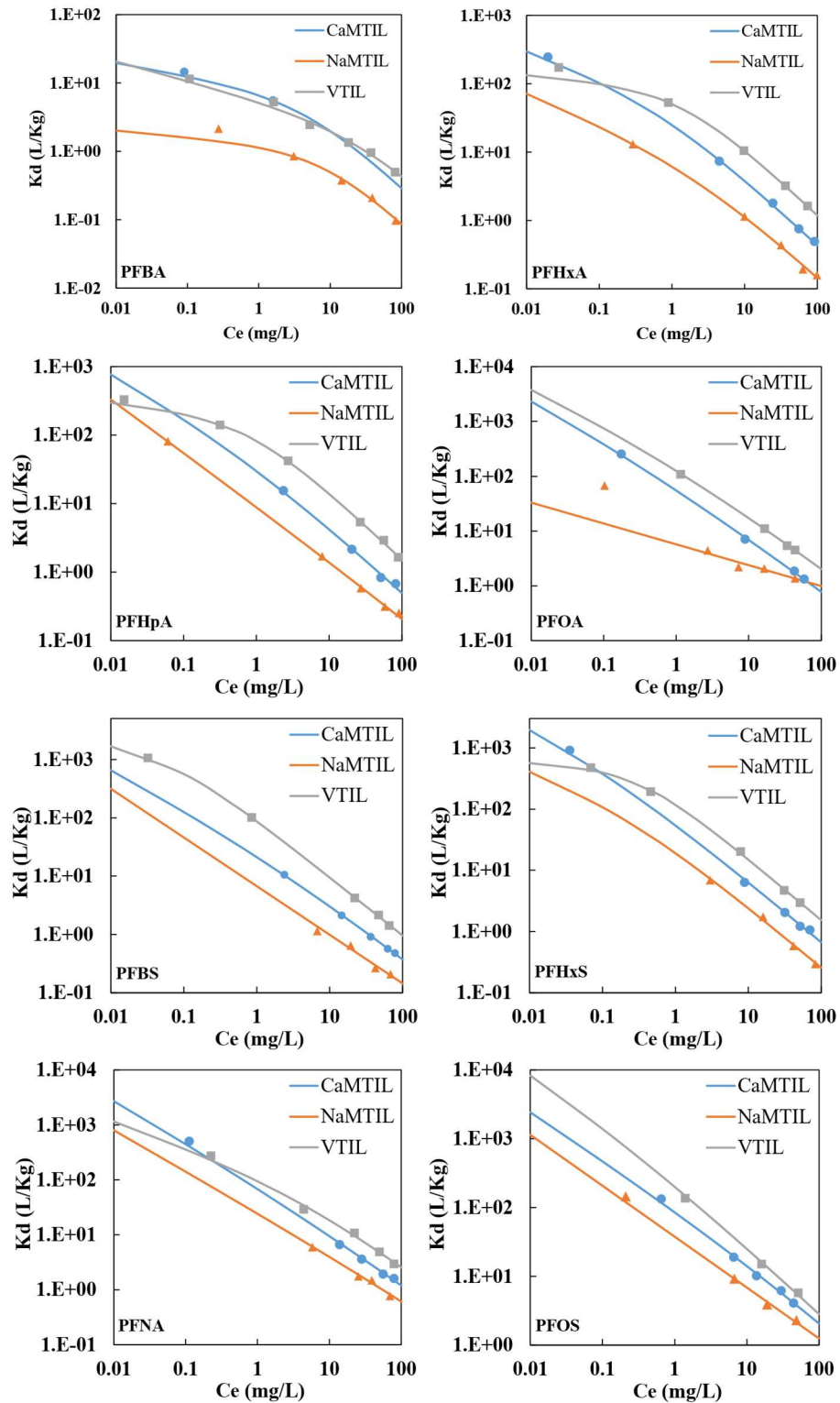


Figure 3.8 K_d values as a function of C_e for individual PFAS based on Sips isotherm calculation.

Martin et al. found that the removal efficiency of different types of emerging pollutants on organoclays increased significantly when the logarithmic value of octanol-water partition coefficient ($\log K_{ow}$) was greater than 2.5, which was also the case for all the PFAS studied in this work (Table 3.7) (Martín et al. 2018). Compared to K_{ow} , the octanol-water distribution coefficient (D_{ow}) at a given pH describes the ratio between the compound concentration in octanol and the compound concentration in water with the consideration of both neutral and ionized species. $\log D_{ow}$ increased with the increasing hydrophobicity of PFAS (Park, Wu, et al. 2020). Since PFAAs are primarily present as anions in aqueous solution under environmentally relevant pH, D_{ow} may be more suitable than K_{ow} to represent PFAS properties in aqueous solution. The $\log D_{ow}$ values of the eight PFAAs were listed in Table 3.7. For PFSA and PFCA with the same chain length of the perfluoroalkyl moiety (e.g., PFOS vs PFNA), the $\log D_{ow}$ values of the PFSA were usually higher than those of the PFCA, reflecting the stronger impact of the sulfonate than the carboxylate group.

Table 3.7 PFAS examined in this study, their octanol-water partition coefficients (K_{ow}), and octanol-water distribution coefficient (D_{ow}) at pH 7.

Analyte	Chemical formula	Log K_{ow} ^a	Log D_{ow} ^a
PFBA	CF ₃ (CF ₂) ₂ COOH	2.31	-1.22
PFHxA	CF ₃ (CF ₂) ₄ COOH	3.71	0.18
PFBS	CF ₃ (CF ₂) ₃ SO ₃ H	2.63	0.25
PFHpA	CF ₃ (CF ₂) ₅ COOH	4.41	0.88
PFHxS	CF ₃ (CF ₂) ₅ SO ₃ H	4.03	1.65
PFOA	CF ₃ (CF ₂) ₆ COOH	5.11	1.58
PFNA	CF ₃ (CF ₂) ₇ COOH	5.81	2.28
PFOS	CF ₃ (CF ₂) ₇ SO ₃ H	5.43	3.05

^aParameters were estimated using MarvinSketchTM.

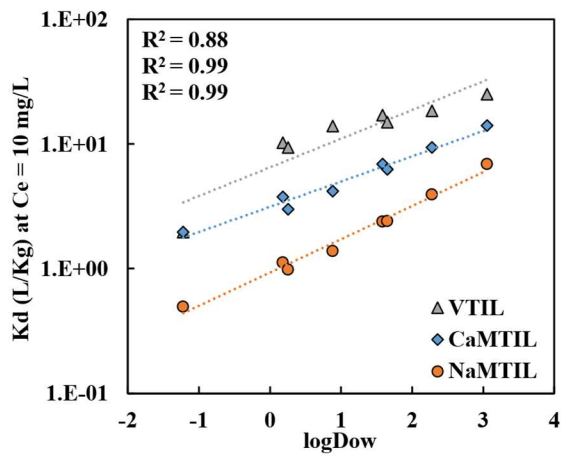
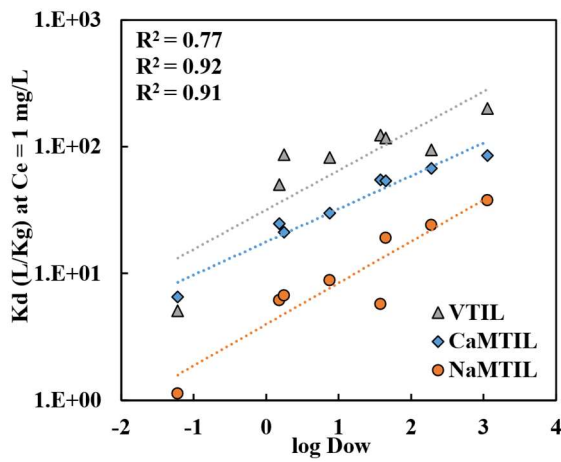
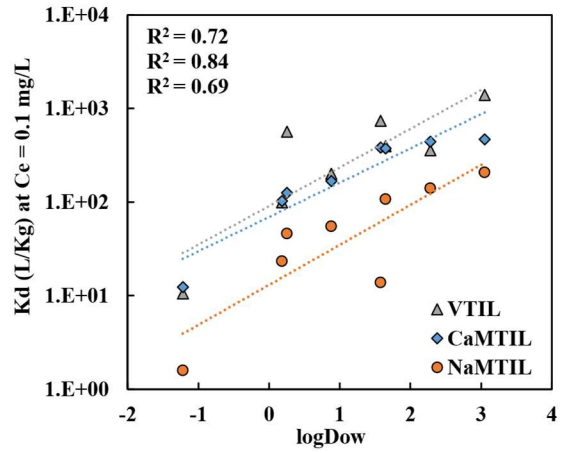


Figure 3.9 Fitted K_d values with $\log D_{ow}$ of PFAS for three IL-modified clays at representative C_e values ($C_e = 0.1, 1$ and 10 mg/L).

To investigate the relation between PFAS property and their adsorption onto the IL-modified clays, K_d values were calculated (at $C_e = 1$ mg/L for illustration) and plotted against $\log D_{ow}$ of PFAS for all the IL-modified clays (Figure 3.9). Interestingly, it appeared that for each organoclay, the $\log K_d$ exhibited a good linear relationship with the $\log D_{ow}$ (at pH 7) of PFAS. Similar trends were observed for $\log K_d$ values calculated using different C_e values (Figure 3.9). Meanwhile, much weaker correlation was found between $\log K_d$ and $\log K_{ow}$ values (Figure 3.10), suggesting that $\log D_{ow}$ may be better suited than $\log K_{ow}$ to describe PFAS adsorption behaviors, because of the ionic nature of the examined PFAS in aqueous solution. Notably, the adsorption of PFAS shared the same trends for all three IL-modified clays, indicating that $\log D_{ow}$ may be used as a general indicator for PFAS adsorption onto the IL-modified clays.

The change in total free energy related to PFAS adsorption onto IL-modified clays can be determined based on the K_d value at a given C_e concentration, as described in Equation 3.8 (F. Xiao et al. 2011). Based on the model developed by Xiao (F. Xiao et al. 2011, 2019), the thermodynamic contributions to the total adsorption energy can be divided into items for hydrophobic interactions ($G_{\text{hydrophobic}}$) and non-hydrophobic interactions ($G_{\text{non-hydrophobic}}$) (Equation 3.9). The hydrophobic contribution is linear with the number of $-\text{CF}_2$ moieties, as shown in Equation 3.10. Therefore, the relative contribution of non-hydrophobic interactions can be estimated by dividing $G_{\text{non-hydrophobic}}$ by the total Gibbs energy (G_{total}), as shown in Equation 3.11.

$$G_{\text{total}} = -RT \ln K_d \quad (3.8)$$

$$G_{\text{total}} = G_{\text{hydrophobic}} + G_{\text{non-hydrophobic}} \quad (3.9)$$

$$G_{\text{hydrophobic}} = m * G_{\text{-CF}_2} \quad (3.10)$$

$$\text{Contribution}_{\text{non-hydrophobic}} = G_{\text{non-hydrophobic}} / G_{\text{total}} \quad (3.11)$$

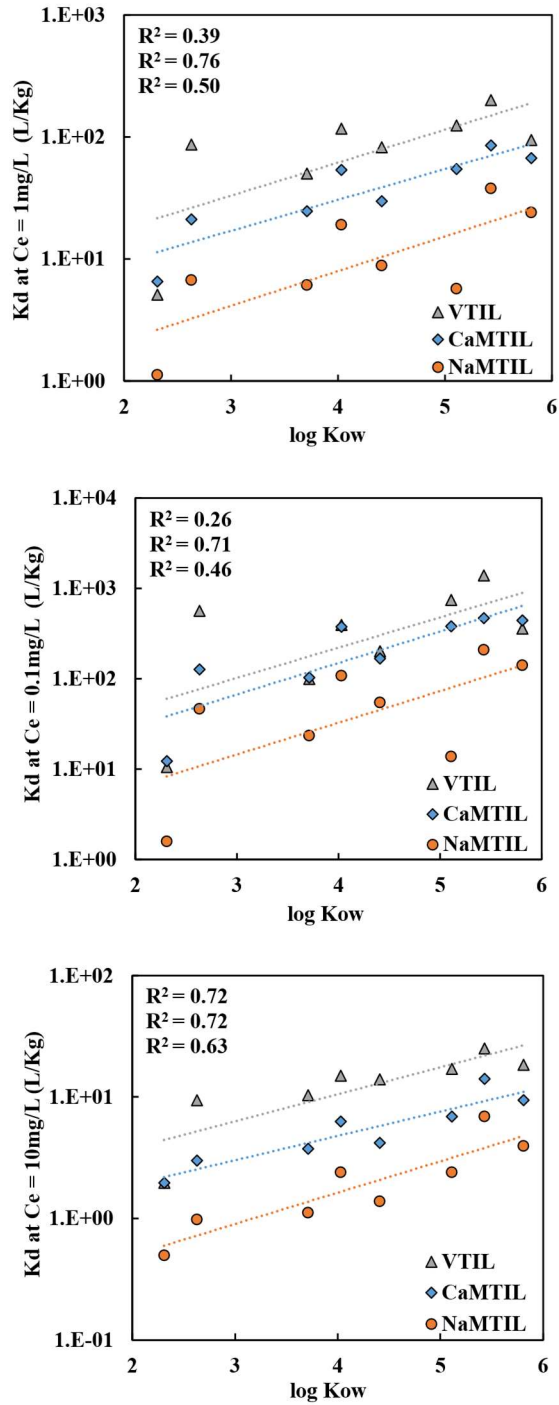


Figure 3.10 Fitted K_d values with $\log K_{ow}$ of PFAS for three IL-modified clays for representative C_e values ($C_e = 0.1, 1$ and 10 mg/L).

We computed the linear relationship between the carbon number of PFAS vs the G_{total} calculated based on the fitted K_d values at $C_e = 1$ mg/L to check the adsorption of PFAS onto different IL-modified clays (Figure 3.11). As mentioned above, the slope of the fitted line represented the contribution of hydrophobic interactions to the Gibbs free energy per $-\text{CF}_2$ moiety. It was interesting to note that for a given IL-modified clay, PFASs and PFCAs had different slopes, which suggested that the hydrophobic interactions induced by CF chains might also be affected by the end functional groups of PFAS. Moreover, while similar slopes were observed for PFASs onto all three IL-modified clays, the slope for PFCAs adsorption onto VTIL was different from those onto CaMTIL and NaMTIL. Previous research also suggested that the hydrophobic energy contribution per $-\text{CF}_2$ moiety was related to the composition of the adsorbents (F. Xiao et al. 2019, 2011). Overall, our results indicated that both hydrophobic and non-hydrophobic interactions governed PFAS adsorption onto IL-modified clays, and the relative contribution of non-hydrophobic interactions was affected by the structure and composition of the IL-modified clays.

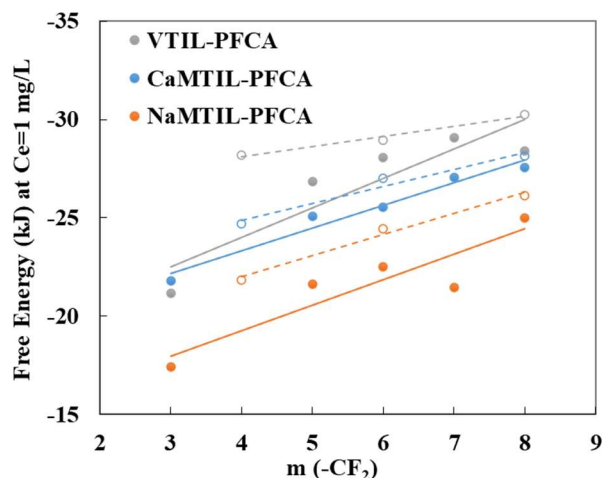


Figure 3.11 Linear relationship between the number of CF_2 (and CF_3) moiety and the adsorption free energy of PFAS at $C_e = 1$ mg/L onto three IL-modified clays. PFCA group and PFSA group were fitted separately and were shown with the solid and dash lines, respectively.

3.3.4 Adsorption of low-concentration PFAS mixture in various water matrices

Adsorption of the eight PFAA mixture was studied in two natural water matrices: a river water and a groundwater source, and results were compared with that from a simply lab-prepared solution (ultrapure water). In this study, the removal efficiency of PFAAs followed the same trend of lab solution > groundwater > river water for all three different IL-modified clays (Figure 3.12). Compared to that in lab solution, the removal of PFOS was not decreased in the groundwater and river water matrices. In contrast, the removal of short-chain PFAS such as PFBA, PFHxA, and PFBS by the three IL-modified clays was largely impacted in the groundwater due to the possible competitive adsorption of coexisting anions. Competitive adsorption has been reported to reduce the adsorption capacity of PFBA onto ionic exchange resins, which attracted PFAS primarily on electrostatic interactions (Maimaiti et al. 2018). Moreover, the river water showed stronger adverse effects on the adsorption of a wider range of PFAAs, probably due to its high NOM concentration (Table 3.3). Reduced PFAA adsorption by NOM was also found in ion exchange resins, activated carbon, and other materials due to competitive adsorption and size exclusion effect (J. Yu et al. 2012; Dixit, Barbeau, and Mohseni 2020). Compared to that in the lab solution, the removal efficiency of short- and medium-chain PFAAs (PFBA, PFBS, PFHxA, PFHpA) was substantially reduced in the river water matrix. Short- and medium-chain PFAAs may be possibly outcompeted and replaced by NOM and long-chain PFAAs due to their relatively lower affinity with the sorbents (Park, Wu, et al. 2020).

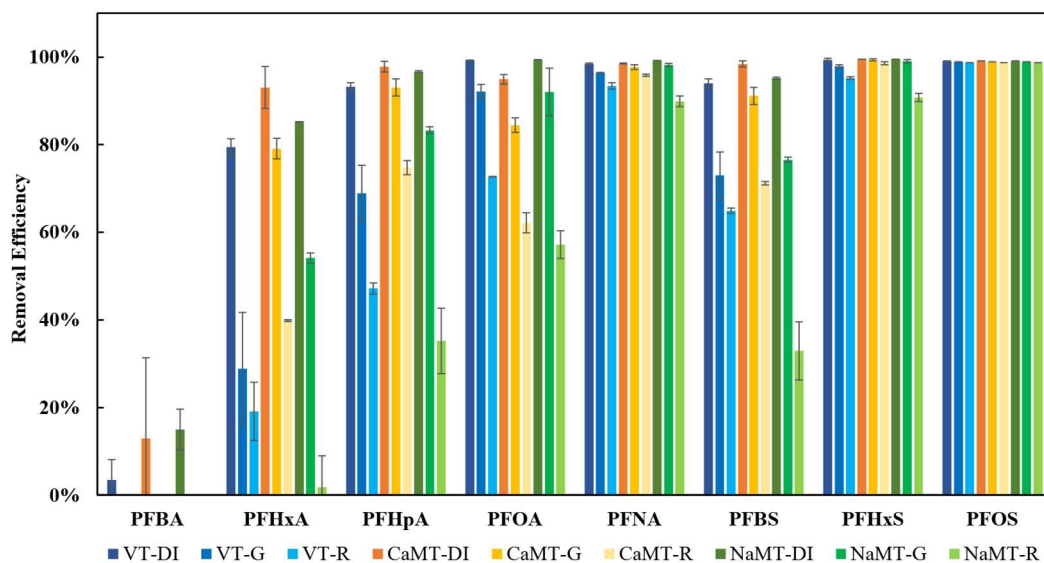


Figure 3.12 PFAS removal efficiency by three IL-modified clays (0.25 g/L) in low-concentration PFAS mixture experiments (1 $\mu\text{g/L}$ for each PFAS) under different water matrices.

In general, the removal efficiency of short-chain PFAAs followed the order of CaMTIL > VTIL \approx NaMTIL, while the three IL-modified clays exhibited comparable removal efficiency of long-chain PFAS. Compared to the adsorption isotherm results, the discrepancy of the materials performance in the low-concentration experiments may be related to the heterogenous nature of IL-modified clays. As mentioned above, K_d values of PFAS adsorption onto IL-modified clays decreased with increasing C_e values, and thus results of high-concentration experiments may show different trends from those of low-concentration experiments. Yan et al. previously found that PFAS adsorption onto organoclays followed stepwise adsorption isotherms, and the adsorption isotherm at low PFAS concentrations did not coincide with that obtained at high PFAS concentrations (Yan et al. 2020). Moreover, it should be acknowledged that the competitive adsorption among different PFAS in natural water may also cause the inconsistency with the single-PFAS adsorption results. Nevertheless, our work demonstrated the potential applicability

of IL-modified clays in PFAS removal under environmentally relevant conditions, especially for the treatment of long-chain PFAS.

3.4 Conclusions

Clay-based adsorbents hold promises in remediation of contaminated groundwater and soil. The present study provided a fundamental understanding on the impact of clay substrate composition and PFAS property on PFAS adsorption onto IL-modified clays. Notably, IL-modified clays could be easily prepared with minimal energy consumption, which may be readily scaled up.

Specifically, the adsorption behavior of eight selected PFAS was studied on IL-modified clays prepared with different clay substrates. The roles of structure and compositions of clay substrates and PFAS structure on adsorption capacity and affinity were investigated through equilibrium isotherm study and free energy analysis. The adsorption capacity of the IL-modified clays followed the order that $VTIL > CaMTIL > NaMTIL$, which was related to the CEC of the clay substrates. Furthermore, the adsorption affinity with PFAS was related to the surface charges of IL-modified clays and generally followed the order that $CaMTIL \approx VTIL > NaMTIL$.

Analysis of the isotherm results suggested that the adsorption capacity and affinity of PFAS onto IL-modified clays may be dependent on the physicochemical properties of PFAS, particularly the octanol-water distribution coefficient (D_{ow}). The optimal combination of CaMTIL and VTIL may deserve further study to achieve both high adsorption capacity and strong adsorption affinity.

Acknowledgement

This research was financially supported by the Department of Defense (DoD) Strategic Environmental Research and Development Program (SERDP, ER18-1289). All opinions expressed in this work are the authors' and do not necessarily reflect the views of DoD. We acknowledge the use of XRD in the Advanced Analysis Facility. XRF was analyzed in the Department of Geosciences. FTIR and Zeta potential measurements were performed in the Water Technology Accelerator at UWM. Water chemistry and solid C/N analysis was performed at the School of Freshwater and Science. LC-MS and LC-MS/MS analyses were conducted in the Shimadzu Laboratory for Advanced and Applied Analytical Chemistry at UWM. The authors declare no competing financial interest.

Chapter 4 Removal of Perfluoroalkyl Acids and Precursors with Silylated Clay: Efficient Adsorption and Enhanced Reuse

4.1 Introduction

Per- and polyfluoroalkyl substances (PFAS) are a group of synthetic chemicals containing the perfluoroalkyl moiety $C_nF_{2n+1}-$ in the structures (Buck et al. 2011; Z. Wang et al. 2021). The superior hydrophobic and oleophobic properties made PFAS very popular in synthesizing various commercial products such as the surface protector of food packaging, carpets, and the surfactants in aqueous film-forming foams (AFFF) (OECD 2013). Numerous PFAS such as perfluoroalkyl acids (PFAAs, i.e. carboxylates and sulfonates) have been detected frequently in the natural environment due to their resistance and recalcitrance (Backe, Day, and Field 2013; X. C. Hu et al. 2016; Lenka, Kah, and Padhye 2021; Vecitis et al. 2009). Most intractably, the endless use of substitutes of long chain PFAAs and their numerous precursors also contributes to the challenging and emerging concerns caused by PFAAs (M. Lu et al. 2017). After a production history of over half a century, perfluorooctyl sulfonate (PFOS), perfluorooctanoic acid (PFOA), and their related precursors are now listed under the Stockholm Convention on Persistent Organic Chemicals (UNEP 2019). Volatile PFCA precursors were also considered as the sink of remote terrestrial translocations of PFAS (Rankin et al. 2016). Recently, the US Environmental Protection Agency (EPA) has updated the health advisory for PFOA and PFOS in drinking water to sub ng/L level, which is much lower than 70 ng/L published in 2016 (OECD 2018; US EPA 2016b). Therefore, efficient and robust treatment approaches are in urgent need to face the vast application of PFAS and their precursors plus the stricter environmental standards.

Adsorption is an established approach for PFAS treatment that has gained great attention in research. Numerous adsorbents have been studied to remove PFAS such as ion exchange resin, activated carbon, covalent organic framework, polymer, organic modified layered double hydroxide, organoclay, et al. (Ateia, Arifuzzaman, et al. 2019; Gao et al. 2017b; Boyer et al. 2021; W. Ji et al. 2018; Deng et al. 2010b; Vu and Wu 2020; M. Wang et al. 2021; Wang 2019). Among various kinds of adsorbents, clay-based adsorbents could be readily amended with inorganic and organic modifiers, resulting in the development of efficient and economical adsorbents for PFAS control. For instance, hexadecyltrimethylammonium (HDTMA)-modified clay could adsorb over 90% of PFOS at neutral pH (Q. Zhou et al. 2010). Choline-modified montmorillonite showed high binding efficacy for PFOA and PFOS (M. Wang et al. 2021). By using imidazolium ionic liquid-modified clay, our earlier study showed that over 99% of PFOS and PFOA could be removed from water, and common anions and natural organic matter showed negligible impact on PFAS removal (Dong et al. 2021). While most of previous studies have concentrated on long-chain PFAAs, the performance of modified clay materials remains insufficiently understood for the removal of PFAA precursors.

PFAS adsorption mainly relies on the electrostatic and hydrophobic interactions with adsorbents. A positively charged organic modifier (e.g., quaternary ammonium salt) was commonly used to modified clay minerals through a conventional cation exchange approach to enhance the interaction with PFAS (Q. Zhou et al. 2010; Z. Du et al. 2016). However, because of the non-covalent bonding nature, the stability of the organic modifier within the organoclays has been a concern, especially during the solvent regeneration process and when used in complex matrices. For instance, previous research observed the decreased removal efficiency of PFOA with the use of regenerated IL-modified clay, due to the loss of IL modifiers during the regeneration process

(Dong et al. 2021). Silylation has been reported as a convenient process for clay modification with organic groups through covalent bonding (de Paiva, Morales, and Valenzuela Díaz 2008). However, to the best of our knowledge, development of organically functionalized clays through silylation have not been explored for the adsorption of PFAS.

The main objectives of this study were to (1) develop new silylated clay with organic functional groups covalently bonded to the clay substrate for PFAS adsorption; (2) investigate and compare the performance of silylated clay with organoclay prepared through conventional cation exchange approach for the removal of PFAAs and precursors under various water chemistry conditions; and (3) determine the regenerability and reusability of the silylated and conventional organoclays. Zr-pillared montmorillonite (ZrMT) was used as a representative clay substrate for organics modification because of the natural abundance and good expansion property of montmorillonite (Pająk-Komorowska 2003). Previous research found that intercalation with Zr species can expand the interlayer of montmorillonite and increase the accessibility of the interlayer sites (Huo, Min, and Wang 2021). The silylated clay was prepared by modifying ZrMT with an organosilane containing a long-chain quaternary ammonium group. For comparison purpose, a conventional organoclay was prepared through cation exchange approach using cetyltrimethyl ammonium bromide (CTAB) as an organic modifier because CTAB has been commonly applied to prepare organoclays (de Paiva, Morales, and Valenzuela Díaz 2008; Z. Zhang et al. 2013; dos Santos et al. 2018; Shah et al. 2013). PFOS and PFOA were selected as representative PFAAs because of their prevalence and recalcitrance in environment (Post et al. 2009; D. Cui, Li, and Quinete 2020; McMahon et al. 2022). 2H,2H,3H,3H-Perfluorooctanoic acid (5:3FTCA) and 1H,1H,2H,2H-perfluorooctanesulfonic acid (6:2FTS) were used as model PFAA precursors. In fish and sediment samples where was impacted by AFFF application, 5:3FTCA and 6:2FTS has been frequently

detected (Langberg et al. 2019). They also have the same carbon chain length as PFOS and PFOA (C8).

4.2 Materials and Methods

4.2.1 Materials

Calcium-rich montmorillonite (MT, STx-1, USA) was purchased from the Clay Minerals Society and used as a representative clay in the present work. The montmorillonite had a high cation exchange capacity (CEC) of 84 meq/100g. Detailed clay characterization was included in Table 4.1. Analytical grade zirconyl chloride octahydrate ($\text{ZrOCl}_2 \cdot 8\text{H}_2\text{O}$, Alfa-Aesar), sodium hydroxide (NaOH, DOT-Scientific), CTAB ($\text{C}_{19}\text{H}_{42}\text{BrN}$, CTAB, Sigma-Aldrich), dimethyloctadecyl[3-(trimethoxysilyl)propyl] ammonium chloride ($\text{C}_{26}\text{H}_{58}\text{ClNO}_3\text{Si}$, DTSACL, Gelest), methanol (CH_3OH , Optima™ Thermo Scientific), and ethanol ($\text{C}_2\text{H}_5\text{OH}$, VWR-BDH) were used to prepared the organically functionalized clays. PFOA (Alfa-Aesar), PFOS (Sigma-Aldrich), 5:3FTCA (Synquest-Laboratories), and 6:2FTS (Synquest-Laboratories) were used as representative PFAS. The CAS number and purity of the PFAS were shown in the Table 4.2. Sodium chloride (NaCl, Fisher-Scientific), sodium bicarbonate (NaHCO_3 , Fisher-Scientific), sodium sulfate decahydrate ($\text{Na}_2\text{SO}_4 \cdot 10\text{H}_2\text{O}$, Fisher Scientific), hydrochloric acid (HCl, VWR-BDH), and sodium nitrate (NaNO_3 , Fisher-Scientific) were used in the adsorption experiments. MS grade acetonitrile (CH_3CN , Optima™ Thermo Scientific), formic acid (HCOOH , Fisher-Scientific), and ammonium formate (NH_4HCO_2 , Fisher Scientific) were used for PFAS analysis. Suwannee River natural organic matter (NOM) was purchased from the International Humic

Substances Society. A stock solution of 50 mg C/L was prepared and calibrated with a Shimadzu TOC analyzer. Ultrapure water (resistivity > 18.2 MΩ·cm) was used for all experiments.

Table 4.1 Key characteristics of the clay mineral

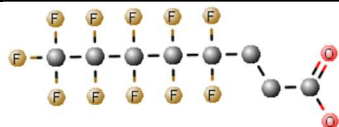
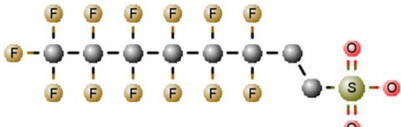
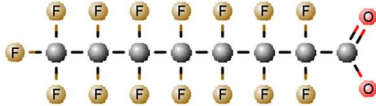
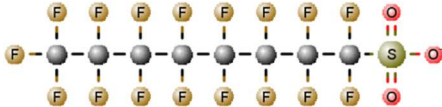
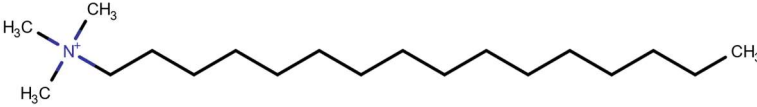
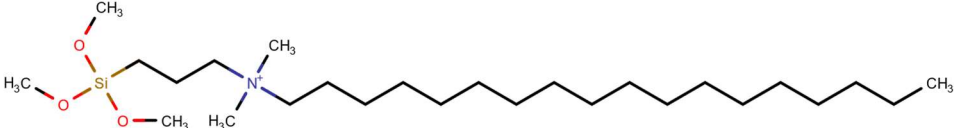
Materials	CEC (meq/100g)	AEC ^a (meq/100g)	Surface area m ² /g	Pore volume cm ³ /g	Pore size nm
MT	84	0.22	91.14	0.174	6.84

^a AEC stands for anion exchange capacity

Table 4.2 PFAS chemical list for adsorption experiments

Analyte	Abbreviation	CAS #	Purity	Manufacturer
2H,2H,3H,3H-perfluorooctanoic acid	5:3FTCA	914637-49-3	97%	Synquest-
1H,1H,2H,2H-Perfluorooctanesulfonic acid	6:2FTS	27619-97-2	97%	Laboratories
Heptadecafluorooctanesulfonic acid potassium salt	PFOS	2795-39-3	≥ 98%	Sigma-Aldrich
Perfluorooctanoic acid	PFOA	335-67-1	95%	Alfa-Aesar

Table 4.3 Structure and key parameters of PFAS and organic modifiers

Analyte	Structure ^a	Log D _{ow} ^{a, b}	pK _a ^a	Log K _{ow} ^a
5:3FTCA		0.18	0.72	3.7
6:2FTS		1.54	-2.72	3.92
PFOA		1.58	-4.2	5.11
PFOS		3.05	-3.32	5.43
CTAB				Br ⁻
DTSACl				Cl ⁻

^a Source from MarvinSketchTM

^b Log D_{ow} was determined at pH 7.

4.2.2 Preparation of organically functionalized clays

ZrMT substrate was prepared following our previously reported method (Huo, Min, and Wang 2021). Briefly, 5 g of MT was dispersed and stirred in 100 ml of water overnight. Then 4.833 g of ZrOC₂·8H₂O was added into the clay dispersion and the mixture was stirred for 4 h. The pH value was adjusted to 8–9 then by slowly adding 1 M NaOH solution to the mixture, followed by 24-h

aging process. The slurry was collected in the centrifuge tube and washed with ultrapure water until the pH became neutral. Finally, the materials were dried at 105 °C for 8 h to obtain the ZrMT.

The silylated clay was prepared by grafting ZrMT with an organosilane (DTSACl) through covalent bonding (Souza, Larocca, and Pessan 2016; Dean, Bateman, and Simons 2007). In a typical synthesis, ZrMT obtained from the procedure above was dispersed in 100 mL of methanol and water mixture (75/25) in a flask. Then a desired amount of DTSACl (1:1 CEC) was added dropwise in the flask where the temperature was maintained at 60 °C for 24 h. The pH was adjusted to 9 to facilitate the hydrolysis of silane. The synthesized silylated clay was collected using centrifugation and washed with 75% ethanol solution three times, followed by washing with 10 mM NaCl solution until the pH was neutral. After drying at 75 °C for 24 h, the final product was collected and labeled as ZrMD.

For comparison purpose, an organoclay was also prepared using the conventional cation exchange approach modified from previous research (Mojović et al. 2011). Briefly, a desired amount (1:1 CEC) of CTAB was added to the suspension of ZrMT, which was pre dispersed in water overnight. The mixture was stirred for 24 h to allow for the cation exchange reaction. The slurry was then collected through centrifugation and washed with water four times, followed by oven dried at 60 °C for 24 h. The obtained material was labeled as ZrMC.

4.2.3 Material Characterization

Powder X-ray diffraction (XRD) patterns of the materials were recorded on a Bruker D8 Discover A25 diffractometer using Cu-K α radiation equipped with a Lynx-Eye detector. The XRD pattern was scanned from 2 Θ values of 3–70° with the scan speed and step size of 6° per min and 0.02°,

respectively. Fourier transform infrared spectroscopy (FTIR) measurements were conducted on a Shimadzu IRTracer100 Spectrometer equipped with IR Solutions 6.0 software for Windows to acquire information about the surface functional groups of the materials. The transmission spectrum corresponding to the wavenumbers in the 600–4000 cm^{-1} range was collected with a resolution of 2 cm^{-1} . The zeta potential of materials was measured in the pH range from 3 to 11 using a Malvern Zetasizer Nano ZS 90. Nitrogen and carbon contents were analyzed on a Fisons NA 1500 NCS elemental analyzer to determine the loading of functional groups prior to and after the material regeneration. $\text{N}_{2(\text{g})}$ adsorption-desorption isotherms were measured to determine the surface area of raw and modified clays using a Micromeritics ASAP-2020 Accelerated Surface Area System. The analysis bath temperature was $-195.8\text{ }^{\circ}\text{C}$, and the relative pressure (P/P_0) ranged from 0.00 to 0.99. The surface area was calculated using the Brunauer-Emmett-Teller (BET) method of the adsorption branch.

4.2.4 Batch Sorption Experiments

The performance of ZrMC and ZrMD for PFAS adsorption was examined under batch mode and ambient temperature ($22 \pm 2\text{ }^{\circ}\text{C}$) with a sorbent loading of 0.25 g/L. The initial concentration of PFOA, PFOS, 5:3FTCA, or 6:2FTS was fixed at 1 mg/L for most experimental conditions unless otherwise specified. The relative high concentration in this study was analogous to the high PFAS level in some contaminated water and source zone where the concentrations have been observed ranging from 220 to $> 6000\text{ }\mu\text{g/L}$ (McGuire et al. 2014). The initial pH was adjusted to 7 ± 0.2 and remained stable throughout the adsorption experiment. In each experiment, 10 mg of an adsorbent was added to 40 mL of solution containing a single PFAS in a polypropylene tube, and the

suspension was placed immediately on an orbital shaker (Thermo Scientific, 300 rpm) to initiate the experiment. Experiments were conducted for 24 h to ensure that PFAS adsorption reached equilibrium, except for the kinetic studies where samples were collected at a series of pre-determined time intervals (i.e., 1 min – 24 h). To determine the maximum PFAS adsorption capacities, isotherm experiments were performed with a series of relatively high PFAS concentrations up to 75 mg/L. In addition, a separate set of adsorption experiments was carried out to study the effects of solution pH (3–11), ionic strength (provided by NaCl, 1–100 mM), co-existence of common anions (chloride, sulfate, nitrate, bicarbonate, 1 mM), and NOM (Suwannee River NOM, 1 mM as C). All experimental conditions were run in at least duplicates.

Regeneration of the spent adsorbents was evaluated using a methanol/water (50%/50%) mixture containing varied amounts of NaCl (0 – 10 wt%). PFAS-loaded ZrMD or ZrMC was first prepared in a solution consisting of 1 mg/L of a single PFAS with an adsorbent loading of 0.25 g/L for 24 h. The PFAS-loaded adsorbent was then collected and regenerated in a regenerating solution for 24 h. To determine the reusability of the adsorbents, the adsorption/desorption experiments were carried out for three consecutive cycles using methanol/water (50%/50%) mixture with 10% NaCl as the regenerating solution.

4.2.5 PFAS measurement

Samples collected in all experiments were immediately filtered with 0.22- μ m PES syringe filters (SLGPX13NK, Millipore), and the filtrates were diluted to 1:1 methanol/water mixture and preserved for PFAS analysis. No significant PFAS loss was found via the filtering process due to

the small filter diameter and the pre-rinsing step where the first three mL filtrate was discarded before sample collection.

The analysis of PFOA, PFOS, 5:3FTCA, and 6:2FTS was carried out using a high-performance liquid chromatography (HPLC, UltiMate3000, Thermo Scientific) coupled with single quadrupole mass spectrometry (ISQ EM, Thermo Scientific). Chromatography was performed using an XB-C18 column (Kinetex® 1.7 µm, 100 Å, 100 x 2.1 mm, Phenomenex) flushed with the mobile phase of (A) Milli-Q, which was washed with the mobile phase of (B) acetonitrile amended with 0.1% formic acid. Mass spectrometry analysis was performed using the single quadrupole MS with an ESI source operated in a negative polarity mode (SIM-). MS operating conditions was as follows: interface voltage, -4.5 V; interface temperature, 350 °C; desolvation temperature, 275 °C; drying gas flow, 42psi; and nebulizing gas flow, 2psi. Samples were injected at 4 µL volumes with a loading pump delivering at 400 µL/min of the mobile phase consisting of 50% B ramping up to 90% at 4 to 8 min and then back to 50% till the end of 12 min. The column temperature was held constant at 40 °C. Matrix-matched calibration standards were prepared for external calibration, and analytes were quantified from calibration standards based on the peak area by linear least-squares regression. The method had a detection limit for PFOA, PFOS, 5:3FTCA, and 6:2FTS of 1 µg/L individually.

The amount of adsorbed PFAS (q , mg/g) and removal efficiency ($Removal$, %) were determined based on Eqs. 4.1 and 4.2, respectively:

$$q = \frac{(c_0 - c_e) \times V}{W} \quad 4.1$$

$$Removal(\%) = (1 - c_e/c_0) \times 100\% \quad 4.2$$

where C_0 (mg/L) and C_e (mg/L) represent the initial PFAS concentration prior to sorption and the equilibrium concentration after sorption in solution, respectively, V (L) is the volume of the solution, and W (g) is the sorbent mass.

4.3 Results and Discussion

4.3.1 Material characterization

In the present study, ZrMD was prepared via post grafting using an organosilane, while ZrMC was prepared through the cation exchange with a surfactant CTAB. Various tools were applied to investigate the difference in the key physicochemical properties between ZrMD and ZrMC. In raw clay and ZrMT, three signature peaks at 3610 cm^{-1} , 1630 cm^{-1} and 1040 cm^{-1} were found (Figure 4.1a), attributing to the stretching of -OH, bending mode of absorbed water and stretching of Si-O group, respectively (Soltani et al. 2020; Avcı 2018). After organics modification, two peaks at $2950\text{-}2860\text{ cm}^{-1}$ caused by the stretching of CH_3 and CH_2 group were clearly observed in ZrMD and ZrMC (Avcı 2018). A new weak peak was also found at 1470 cm^{-1} that was attributed to the C-H bending (scissoring) in CH_3 groups for ZrMC and ZrMD (Kenne Dedzo and Detellier 2017). Additionally, a peak at 725 cm^{-1} assigned to the NC_4 stretch was found in ZrMC and ZrMD. The FTIR results indicated that both the grafting and cation exchange methods could introduce the organic functional groups to the clay substrates. Based on the C and N elemental analysis, ZrMD had a slightly higher modifier loading (0.53mmol/g) than ZrMC (0.47mmol/g).

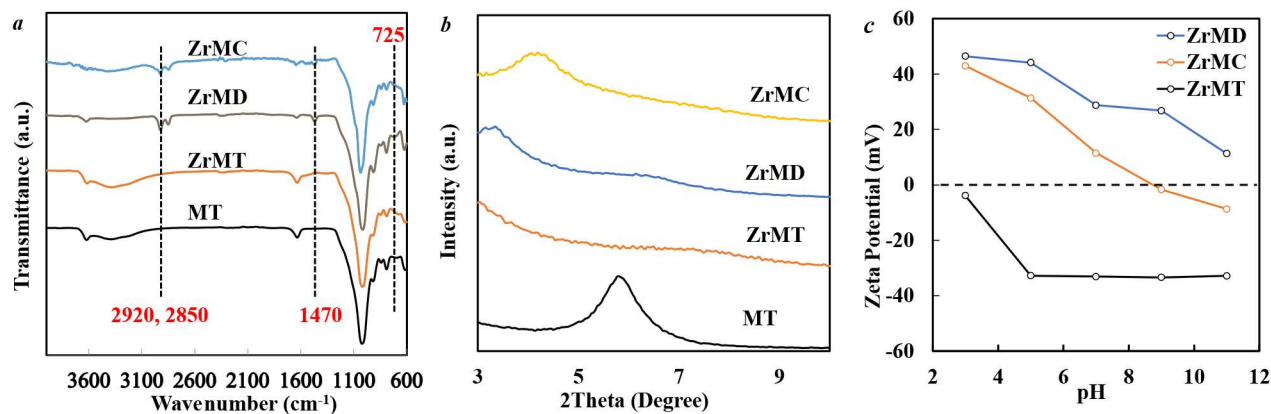


Figure 4.1 FTIR (a), small-angle XRD pattern (b) and zeta potential (c) of raw and organically modified clays.

The layer structure and basal spacing of the clay mineral prior to and after modification was studied using XRD. Signature peaks of modified clays were similar with the original one, indicating that modification did not change the crystal structure of clay mineral (Figure 4.2a). Intercalation of Zr species and modification with organic groups resulted in layer expansion to different extents. Due to the (001) reflection, a strong diffraction peak at 2θ of 5.8° was observed in the raw clay. After modification with Zr species, the (001) peak was almost invisible, suggesting that the layer structure became less ordered (Figure 4.1b). Huo et al. found that the (001) peak of MT became broader and less obvious with increased Zr loading, which was consistent with the observation in our study (Huo, Min, and Wang 2021). The less ordered layer structure of ZrMT resulted in the enlarged BET surface area in comparison to the raw clay (Table 4.4). A clear shift of the (001) peak was also observed after CTAB and DTSACl modification (Figure 4.1b), suggesting the successful intercalation of modifiers into the layer of clay substrate. Specifically, based on the Bragg equation, the basal spacing (d_{001}) of ZrMC and ZrMD was calculated as 2.1nm and 2.68nm respectively, larger than that of the raw clay (1.52 nm). The larger basal spacing of ZrMD than

ZrMC may be caused by the arrangement and deformation of ZrMD with the use of the longer chain organic modifier (Klapyta, Fujita, and Iyi 2001). Meanwhile, the surface area of ZrMD and ZrMC decreased after modification, due to the surface coverage of the modifiers (Table 4.4). Interestingly, compared to ZrMT, a more uniform and ordered layer structure was reformed through the modification with CTAB and DTSACl.

Table 4.4 Surface area of functionalized clay

Materials	Surface area m ² /g	Pore volume cm ³ /g	Pore size nm
ZrMT	160.22	0.221	5.52
ZrMC	78.57	0.141	7.20
ZrMD	37.88	0.130	13.73

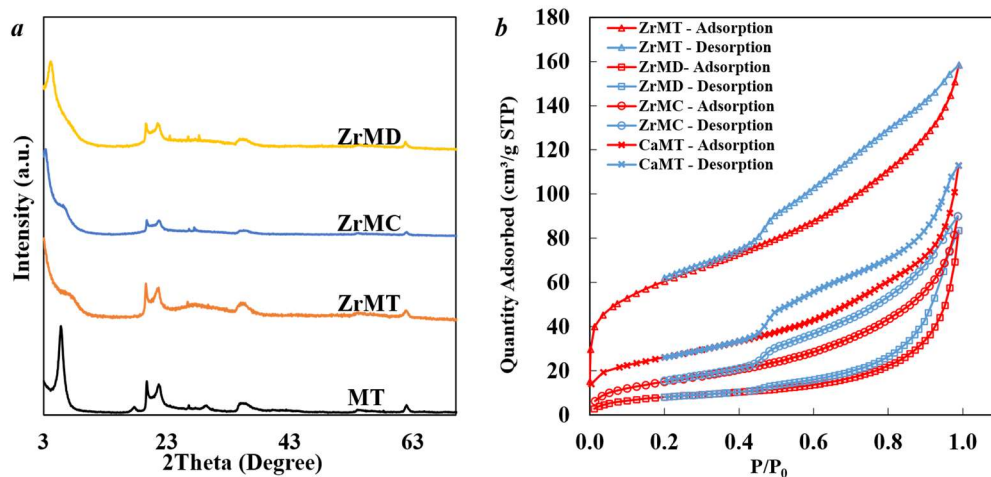


Figure 4.2 Wide angle XRD pattern (a) and simulated isotherms for nitrogen (b) of clay substrate and organically functionalized clay.

The surface charge of ZrMT and modified clays was determined based on zeta potential measurement. The surface of ZrMT was negatively charged in the pH range of 3–11 due to the isomorphous replacement of Si with Al within the clay structural layer, structure imperfection, and deprotonation of the surface hydroxyl groups of clay (Drits 2003). After modification with organic functional groups, the surface became positively charged under the acidic and mild alkaline conditions (Figure 4.1c). The silylation, moreover, resulted in a more positive surface charge on ZrMD, with a higher point of zero charge (PZC) at pH higher than 11, compared to ZrMC. At pH 7, ZrMD has a higher positive surface charge than ZrMC. Although CTAB and DTSACl had the same head group and similar alkyl chain length, ZrMD exhibited a higher PZC and stronger surface charge, which might be related to the following two reasons. First, ZrMD had a slightly higher organic group loading than that of ZrMC as indicated by the C/N analysis results. Additionally, because of the three carbons between Si and N (Table 4.3), the positive charge of the quaternary ammonium head in DTSACl might not be reduced by the negatively charged clay layer. In contrast, the negative clay interlayer may partially neutralize the CTAB head group's positive charge, resulting in a less strong surface charge (L. Wu, Yang, et al. 2014).

4.3.2 Adsorption kinetics

Adsorption kinetics were studied to compare the adsorption behavior of four PFAS onto the ZrMC and ZrMD. The adsorption of PFAS on ZrMT was negligible (Figure 4.3). Based on the kinetics experiments, both ZrMC and ZrMD exhibited a rapid PFAS uptake and reached equilibrium within 0.5 h except for the adsorption of 5:3FTCA onto ZrMC (Figure 4.4). 5:3 FTCA had two C-H that substituted C-F, which probably increased the hydrophilicity of 5:3 FTCA in comparison with PFOA. The low octanol-water distribution coefficient (D_{ow}) value of 5:3 FTCA also indicated the

low hydrophobicity of 5:3 FTCA. The kinetics data were fitted with the pseudo-second-order model and the fitted parameters are listed in Table 4.5. The adsorption kinetics constant values for four PFAS followed the same trend as PFOS > PFOA > 6:2FTS > 5:3FTCA for both ZrMC and ZrMD, although the differences were more subtle for ZrMD. Results suggested that both ZrMC and ZrMD showed fast adsorption kinetics for the examined PFAS.

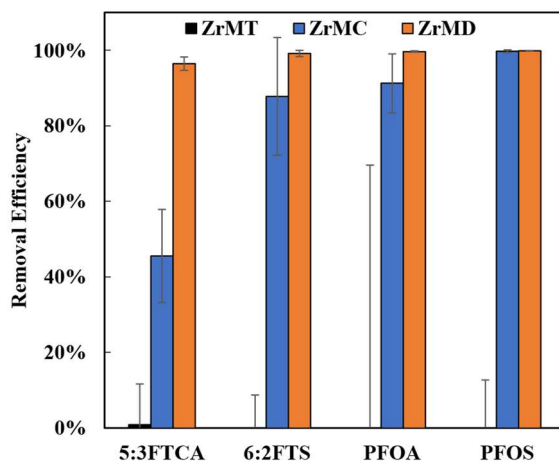


Figure 4.3 Removal of PFOA, PFOS, 6:2FTS and 5:3FTCA ($C_0=10$ mg/L) on clay substrate. Experiments were conducted at pH 7 with a sorbent loading of 0.25 g/L and a contact time of 24 h.

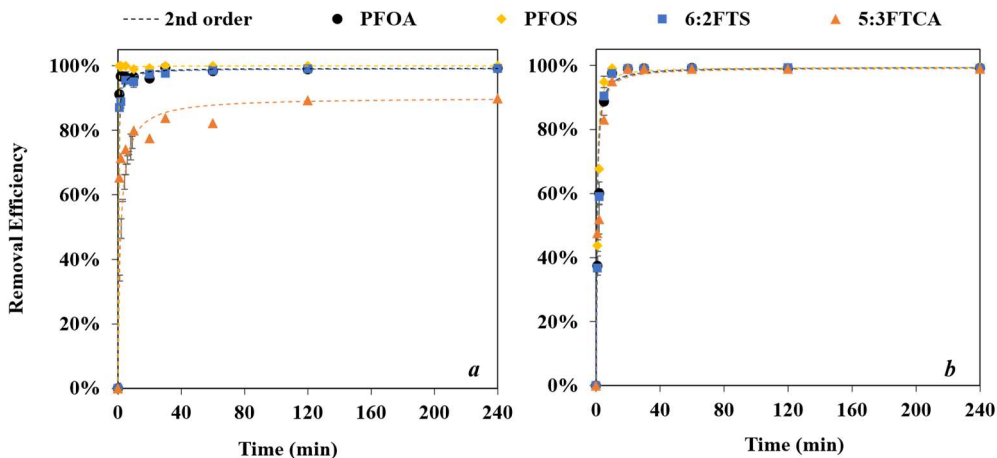


Figure 4.4 Pseudo-second-order fitted kinetics of PFOA, PFOS, 6:2FTS and 5:3FTCA on ZrMC (a) and ZrMD (b).

Table 4.5 Kinetics and isotherm fitting parameters for PFAS adsorption onto ZrMC and ZrMD.

		ZrMC			ZrMD		
		Q_m (mg/g)	K_L	r²	Q_m (mg/g)	K_L	r²
			(L/mg)			(L/mg)	
Langmuir							
isotherm	PFOA	104.17	1.88	0.99	114.94	4.35	0.99
model fit	PFOS	250	2.86	0.99	119.05	4.00	0.99
	6:2 FTS	70.42	1.38	0.99	78.74	5.77	0.99
	5:3 FTCA	32.47	0.29	0.98	61.73	4.76	0.99
		K_f	1/n	r²	K_f	1/n	r²
		mg/g·(L/mg)^{1/n}			mg/g·(L/mg)^{1/n}		
Freundlich							
isotherm	PFOA	40.89	0.44	0.92	58.87	0.27	0.80
model fit	PFOS	112.72	2.24	0.75	55.84	0.28	0.70
	6:2 FTS	27.19	0.35	0.93	42.8	0.27	0.81
	5:3 FTCA	8.32	0.39	0.95	32.44	0.25	0.68
		q_e (mg/g)	k (g/mg-	r²	q_e (mg/g)	k (g/mg-	r²
			min)			min)	
Pseudo-	PFOA	3.48	1.29	1.00	3.53	0.52	1.00
second	PFOS	4.31	7.70	1.00	4.32	0.59	1.00
order	6:2 FTS	3.67	1.02	1.00	4.40	0.43	1.00
kinetics	5:3 FTCA	4.21	0.15	1.00	3.90	0.42	1.00

4.3.3 Adsorption isotherms

Adsorption isotherms of individual PFAS on ZrMC and ZrMD were obtained to determine the equilibrium adsorption behavior of each PFAS. The adsorption of PFOA, PFOS and 6:2FTS on ZrMD and ZrMC all increased fast at the low concentration and then increased gradually till reaching plateau (Figure 4.5). Meanwhile, the adsorption of 5:3FTCA on ZrMC slowly reached plateau with the increased equilibrium concentrations, indicating the relatively weak adsorption affinity between 5:3FTCA and ZrMC. The classic Langmuir (Equation 4.3) and Freundlich (Equation 4.4) models were used to fit the adsorption isotherms.

$$q_e = \frac{Q_m K_L C_e}{1 + K_L C_e} \quad (4.3)$$

$$q_e = K_f C_e^{\frac{1}{n}} \quad (4.4)$$

Where q_e (mg/g) and C_e (mg/L) represent PFAS adsorbed onto the modified clays and in aqueous solution at equilibrium, respectively. K_L is the Langmuir adsorption constant and Q_m (mg/g) is the maximum sorption capacity. K_f (mg/g·(L/mg)^{1/n}) is the Freundlich constant and $1/n$ is a dimensionless indicator related to the sorbent surface heterogeneity.

The fitting parameters were shown in Table 4.5. Generally, the Langmuir model fitted the experimental results better than the Freundlich model. Based on the Langmuir model, the adsorption capacities substantially increased from 5:3FTCA to PFOS on ZrMC. The adsorption capacity increased with the hydrophobicity of PFAS in the order of PFOS > PFOA > 6:2FTS > 5:3FTCA, suggesting that the hydrophobic interaction could be an important driving force between PFAS and ZrMC (Figure 4.6a). Due to the hydrophobicity, PFAS were compelled from the water phase to a more hydrophobic surface through the tail-tail interaction (Z. W. Du et al. 2014).

Through the hydrophobic interaction, the molecular long axes adhere closely and parallel to the surfaces to minimize the interaction between water molecules and C–F chains. The higher adsorption capacity with increased hydrophobicity of PFAS was frequently found in the adsorption of PFAS on activated carbon where the hydrophobic interaction was predominant (Q. Yu et al. 2009; Deng et al. 2015; L. Liu et al. 2020; D. Zhang et al. 2016). In the present work, a nice linear relationship of $\log Q_m$ vs $\log D_{ow}$ was observed for PFAS adsorption onto ZrMC (Figure 4.6b).

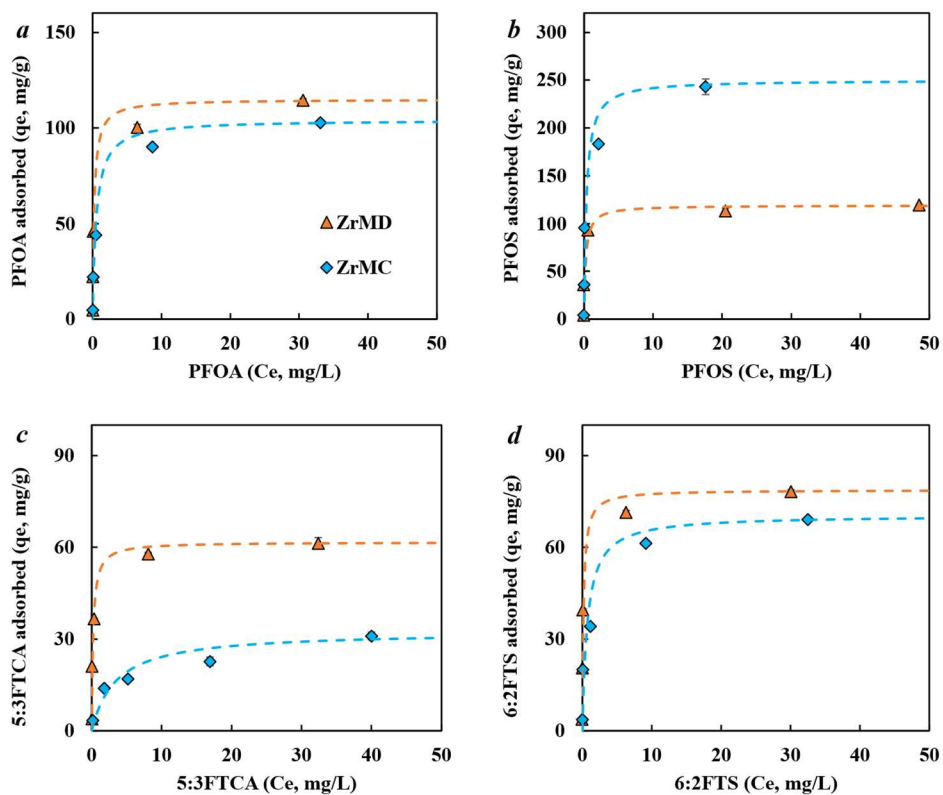


Figure 4.5 Adsorption isotherms of (a) PFOA, (b) PFOS, (c) 5:3FTCA, and (d) 6:2FTS onto ZrMD and ZrMC. Experiments were conducted at pH 7 with an organoclay loading of 0.25 g/L. Dash lines represent Langmuir model fits.

The adsorption capacity of different PFAS was similar on ZrMD, indicating that charge interaction between PFAS and ZrMD may play a more important role than that of ZrMC. Park and co-authors suggested that the charge interaction played more important roles than the hydrophobic interactions in ion exchange resin processes, based on density functional theory calculations (Park, Daniels, et al. 2020). Similar to the anion exchange resins, the quaternary ammonium group within ZrMD may provide strong electrostatic interactions with the negatively charged PFAS. The strong PFAS-ZrMD interactions were supported by the similar K_L values for different PFAS onto ZrMD, which indicated the adsorption affinity (Table 4.5). Meanwhile, the $\log Q_m$ of PFAS onto ZrMD only had a relatively weak linear relationship with $\log D_{ow}$ of PFAS. The adsorption isotherm results suggested that ZrMD may have generally stronger interaction with PFAS than that of ZrMC.

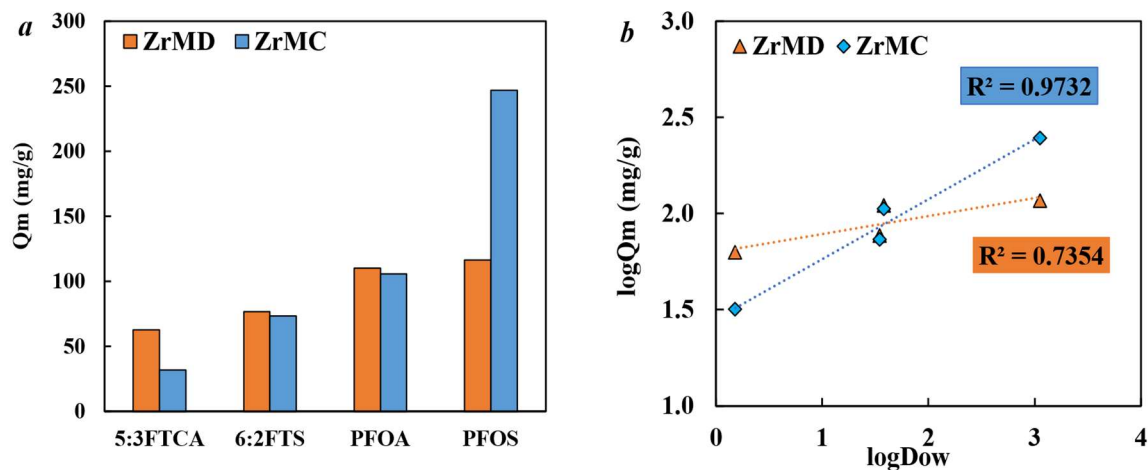


Figure 4.6 (a) Fitted adsorption capacity (mg/g) of 5:3FTCA, 6:2FTS, PFOA and PFOS on ZrMD and ZrMC. (b) The linear regression of $\log D_{ow}$ and $\log Q_m$ (fitted adsorption capacity by Langmuir mode) of selected PFAS on ZrMD and ZrMC.

4.3.4 Effect of water chemistry parameters

The adsorption of four PFAS in the presence of anions, NOM, and different ionic strengths was compared between ZrMC and ZrMD. From Figure 4.7a, it is shown that the removal of PFOS on ZrMC was not impacted by the co-anions and NOM, while the removal of 5:3FTCA was largely impacted by NOM. As mentioned before, PFOS has the highest hydrophobicity among the examined PFAS, resulting in the strongest affinity with ZrMC. In general, the presence of co-anions did not show much impact on PFAS removal, indicating the strong non-electrostatic interactions between PFAS and ZrMC. NOM was usually regarded as a negatively charged hydrophobic moiety and showed strong inhibitory effect on PFOS and PFOA removal by activated carbons (J. Yu et al. 2012). In the present work, NOM showed moderate inhibition on PFOA and 6:2FTS and strong inhibition on 5:3FTCA adsorption onto ZrMC (Figure 4.7a), which may be caused by the competition of adsorption sites. The level of NOM inhibition was consistent with the hydrophobicity of PFAS.

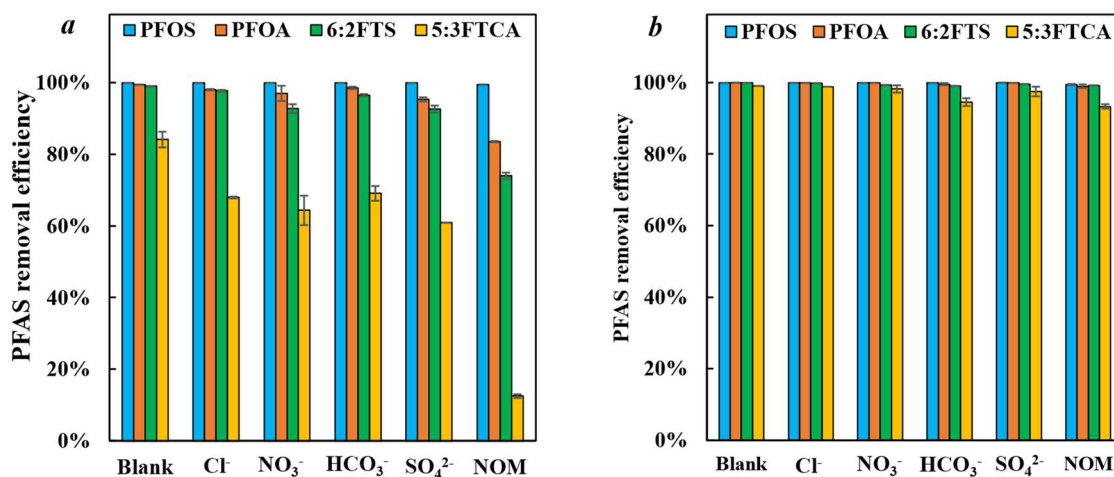


Figure 4.7 Effect of common anions (1 mM) and NOM (1 mM as C) on the adsorption of PFAS onto (a) ZrMD and (b) ZrMC. Experiments were conducted at pH 7 with a PFAS concentration of 1 mg/L and organoclay loading of 0.25 g/L.

As shown in Figure 4.8, the removal of PFOA, PFOS, and 6:2 FTS was not impacted by the elevated ionic strength on ZrMC and ZrMD. The removal efficiency of 5:3FTCA decreased with the increase of the ionic strength on ZrMC but not ZrMD. High ionic strength usually impaired the electrostatic interactions between the adsorbents and adsorbates by compressing the electric double layer. Therefore, the robust adsorption performance of both ZrMD and ZrMC suggested that in addition to electrostatic interactions, they may also have strong hydrophobic interactions with PFAS, due to the long alkyl chain of the modified organic functional group. Notably, despite the slightly different alkyl chain length (C16 of CTAB vs C18 of DTSACl), they may possess similar hydrophobicity. Meanwhile, since 5:3FTCA has the lowest hydrophobicity among four studied PFAS, increasing the ionic strength may substantially reduce the affinity between 5:3FTCA and ZrMC, resulting in the reduced removal efficiency.

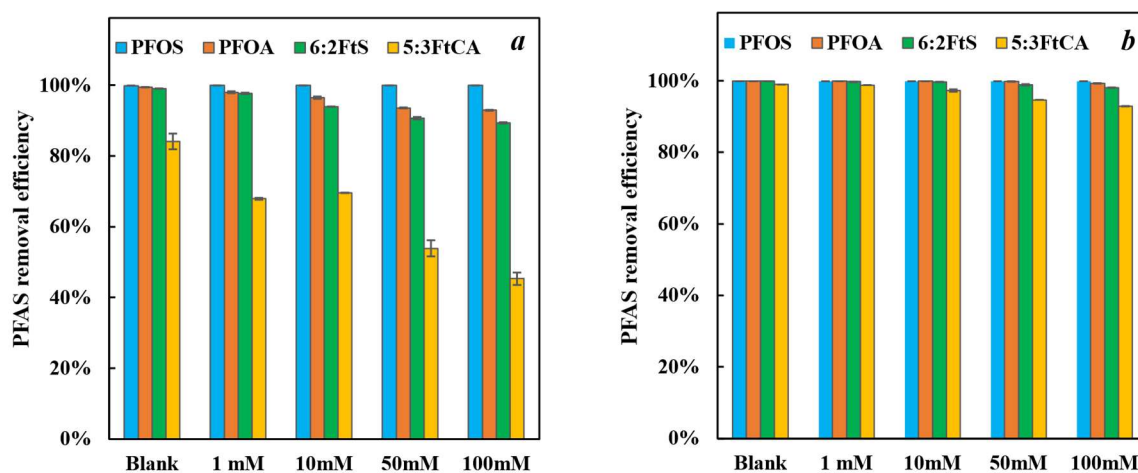


Figure 4.8 Removal of PFOS, PFOA, 6:2FTS, and 5:3FTCA by ZrMC (a) and ZrMD (b) with different ionic strengths (provided by NaCl).

The performance of ZrMD was also very stable in a wide pH range (Figure 4.9). Compared to ZrMC, ZrMD had a larger PZC value and a higher zeta potential at a given pH (Figure 4.1c), indicating that it may have stronger electrostatic interactions with PFAS. Although the zeta potential of ZrMC and ZrMD fast approached zero or even became negative at pH 11, they showed high removal efficiency of PFOS, PFOA, and 6:2FTS, which was likely due to the strong hydrophobic interactions. The stronger impact on 5:3FTCA adsorption may be attributed to the smallest hydrophobicity of 5:3FTCA in comparison to the other examined PFAS, resulting in the weakest affinity with the adsorbents at elevated pH conditions.

Overall, the performance of clay on PFAS removal was largely enhanced through the covalent bonding with organosilane. Both hydrophobic and electrostatic interactions played important roles in PFAS adsorption on the two organically modified clays. Compared with ZrMC, the adsorption of PFAS onto ZrMD was not impacted under various water chemistry conditions, indicating the stronger interaction between ZrMD and PFAS.

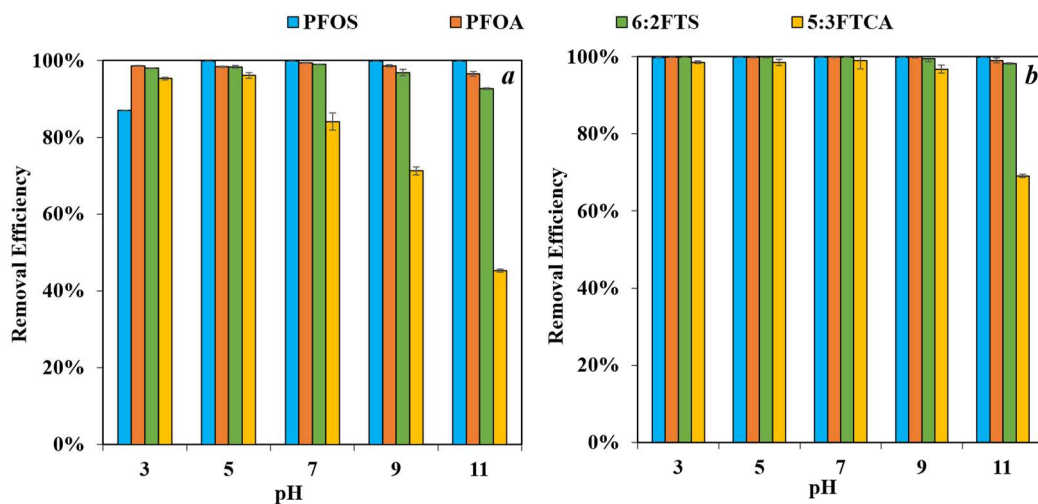


Figure 4.9 Removal of PFOS, PFOA, 6:2FTS, and 5:3FTCA by ZrMC (a) and ZrMD (b) in a wide range of pH (3-11).

4.3.5 Regeneration and reuse

The regeneration efficiency of spent ZrMC and ZrMD varied when using regenerants with different compositions. The regenerant was selected based on those commonly reported in literature for regeneration of various adsorbents (methanol/water (50%/50%) mixture with 0–10% NaCl) (Dixit et al. 2020; Ateia, Arifuzzaman, et al. 2019). Methanol could slacken the hydrophobic interaction between PFAS and adsorbents, while the inorganic anions may reduce the electrostatic interactions (Gagliano et al. 2020). When a methanol/water (50%/50%) mixture was applied, only 0 – 20% of PFAS was desorbed from ZrMD (Figure 4.10a), validating the strong electrostatic interactions between ZrMD and PFAS. Meanwhile, the same regenerant resulted in more facile PFAS desorption from ZrMC (data not shown), indicating that the interaction between PFAS and ZrMC was not as strong as that of ZrMD. The regeneration of ZrMD was highly improved with the aid of salt solutions. It was observed that the recovery of PFOS, one of the most difficult contaminants to desorb, increased as the NaCl concentration increased. Using methanol/water (50%/50%) mixture with 10% NaCl resulted in efficient desorption of all PFAS and thus regeneration of ZrMD. Previous studies have demonstrated that strong salt or hydroxide solutions were required to rehabilitate the ion exchange resins by reducing electrostatic forces between the resins and PFAS to regain their adsorption capacity (Deng et al. 2010; Dixit et al. 2020). Similarly, PFAS-loaded ZrMC can also be efficiently regenerated using 50%/50% methanol/water mixture with 10% NaCl (Figure 4.10b). The results of the regeneration study may further support the different PFAS adsorption mechanisms onto ZrMD and ZrMC, and ZrMD generally had stronger electrostatic interactions with PFAS than that of ZrMC.

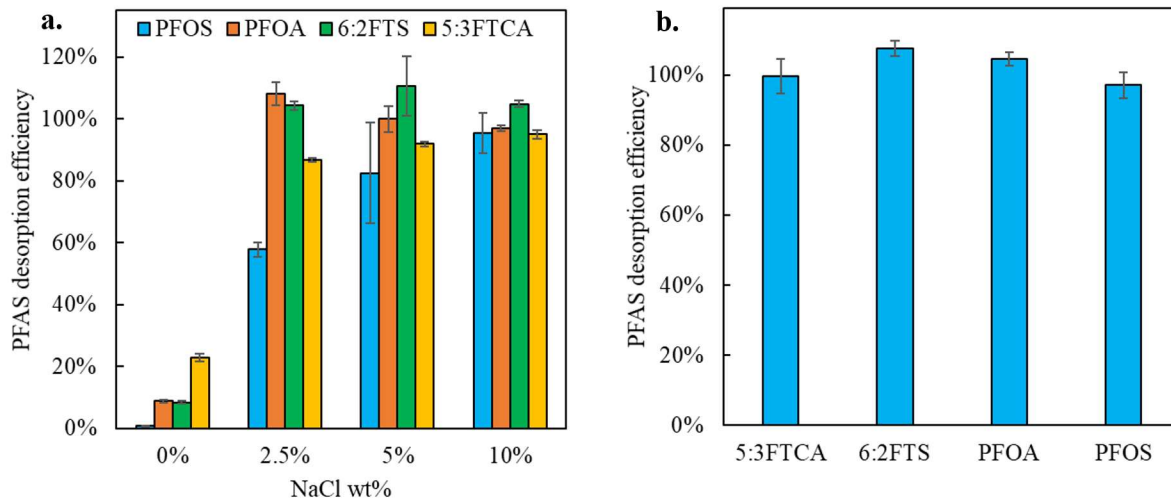


Figure 4.10 Regeneration of (a) PFAS-loaded ZrMD using 50%/50% methanol/water mixture with varied concentrations of NaCl and (b) PFAS-loaded ZrMC using 50%/50% methanol/water mixture with 10% NaCl.

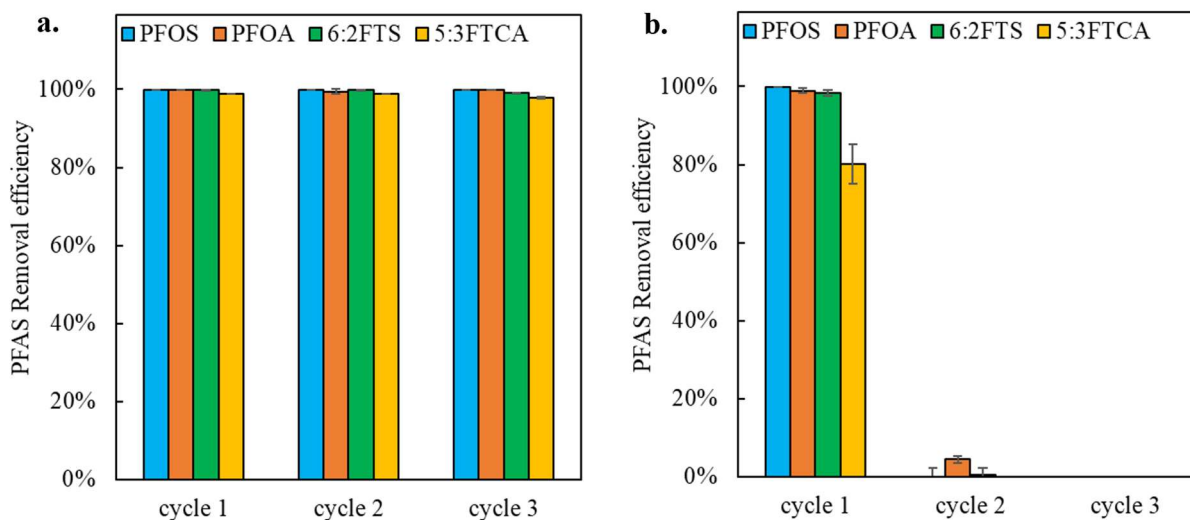


Figure 4.11 Reuse of (a) ZrMD and (b) ZrMC for PFAS removal (1 mg/L) at pH 7 with an adsorbent loading of 0.25 g/L. The organoclays were regenerated after PFAS adsorption in each cycle using a 50%/50% methanol/water mixture with 10% NaCl.

We regenerated the spent clay minerals using methanol/water (50%/50%) mixture with 10% NaCl and reused them for a new cycle of PFAS adsorption. The regeneration and reuse processes were repeated three times. As shown in Figure 4.11a, after continuous regeneration, ZrMD maintained almost the same adsorption efficiency as before for all four PFAS. Although ZrMC could be regenerated, the adsorption of PFAS on ZrMC was negligible after material regeneration. The content of organic functional group of ZrMD and ZrMC was measured based on C/N elemental analysis after material regeneration. No organic functional groups were retained in ZrMC after regeneration using methanol/water (50%/50%) mixture with 10% NaCl. Since the organic functional groups (i.e., CTAB) were introduced to ZrMC through ion exchange, they may have insufficient interaction with the clay substrate and be washed out during the regeneration process. The nearly complete loss of organic functional groups after regeneration may account for the negligible PFAS removal of ZrMC during reuse. In contrast, minimal loss of the organic functional groups was observed for ZrMD after regeneration, because of the covalent bonding between the organic functional groups and the clay substrate through silylation. Thus, ZrMD can be efficiently reused for multiple cycles without compromised performance. The robust regeneration and reuse ability may largely facilitate the practical application of ZrMD for *ex situ* environmental remediation.

4.4 Conclusion

The adsorption of four selected PFAS with similar chain lengths but different structures was studied on ZrMD and ZrMC to examine the impact of preparation methods on the performance of organoclay. In summary, both ZrMC and ZrMD exhibited fast PFAS adsorption kinetics. ZrMD outcompeted ZrMC in terms of the strong affinity with PFAS and reusability. Compared to ZrMC,

water chemistry parameters such as co-anions, NOM, and ionic strength had negligible impact on PFAS adsorption onto ZrMD. Results suggested that while hydrophobic interactions played an important role in PFAS adsorption onto both ZrMD and ZrMC, ZrMD may exhibit stronger electrostatic interactions with PFAS, resulting in stronger affinity with PFAS than that of ZrMC. Further, ZrMD can be conveniently regenerated and reused for PFAS adsorption, because of the stable covalent bonding between the modified organic functional groups and clay substrate. In contrast, although ZrMC could be regenerated, it could not be reused because of the loss of organic functional groups during the regeneration process. Overall, results of this chapter suggested that ZrMD may hold promises for *ex situ* treatment of PFAS-contaminated waters.

Acknowledgements

This research was financially supported by the Department of Defense (DoD) Strategic Environmental Research and Development Program (SERDP, ER18-1289). All opinions expressed in this work are the authors' and do not necessarily reflect the views of DoD. We acknowledge the use of XRD and BET in the Advanced Analysis Facility. C/N elemental analysis was performed in the School of Freshwater and Sciences at UWM. FTIR and Zeta potential measurements were performed in the Water Technology Accelerator at UWM.

Chapter 5 Conclusions and Recommendations

5.1 Conclusions

This research focused on a series of activities to improve the removal efficiency and reusability of clay-based adsorbents from the following three aspects: 1) develop IL-modified clay with enhanced adsorption of PFAS, 2) investigate the role of clay substrate on the performance of IL-modified clay for PFAS sorption, and 3) develop organosilane-modified clay with enhanced reusability for PFAS removal.

In Task 1, a family of IL-modified clays were prepared using imidazolium-type ILs with varied alkyl chain lengths and were evaluated for the sorption of PFOA and PFOS for the first time. The alkyl chain length of the IL strongly affected the surface charge and interlayer spacing of the corresponding IL-modified clay, and thus the sorption of PFOA and PFOS. Compared to clays modified with shorter-chain ILs (C4, C6 and C10), CaMTC16 exhibited high removal efficiency for both PFOA and PFOS, probably due to the strong hydrophobic and electrostatic interactions. Detailed sorption experiments revealed that CaMTC16 had fast sorption kinetics and high affinity with PFOA and PFOS, as well as robust performance under various water chemistry conditions. In addition, CaMTC16 was very effective for the simultaneous removal of numerous PFAAs. Our results highlighted the important role of IL structure in the performance of the IL-modified clay, and clay modified with the optimal IL may be an efficient sorbent for PFAS capture and removal.

In Task 2, we have evaluated IL-modified clays prepared with different clay substrates, including CaMT, NaMT, and VT for the sorption of eight selected PFAS to explore the roles of structure and composition of clay substrate in the adsorption behaviors of PFAS. The adsorption

capacity of the IL-modified clays followed the order that VTIL > CaMTIL > NaMTIL, which was significantly related to the cation exchange capacity of the clay substrates and the IL loading of the IL-modified clays. Further, the PFAS adsorbent-water partition coefficients were related to the properties of the IL-modified clays such as the surface charge and decreased over the increasing equilibrium concentrations of PFAS in aqueous phase, suggesting the heterogeneous nature of the IL-modified clays. Analysis of the isotherm results suggested that the adsorption capacity and affinity of PFAS with IL-modified clays may be dependent on the physicochemical properties of PFAS, particularly the octanol-water distribution coefficient (D_{ow}). Results of this study suggested that the performance of IL-modified clays was strongly affected by the composition of the clay substrates, and IL-modified clays may hold promises for the removal of PFAS, especially long-chain ones, under various water matrices.

In Task 3, we reported the development of a new organically-functionalized clay (ZrMD) by grafting pillared clay substrate with an organosilane through covalent bonding. The performance of ZrMD was systematically compared with an organoclay (ZrMC) prepared from the conventional ion exchange approach for the removal of two legacy PFAAs including PFOA and PFOS, as well as two precursor compounds, 5:3FTCA and 6:2FTS. Both ZrMC and ZrMD exhibit fast removal of the four PFAS. More importantly, ZrMD outcompeted ZrMC regarding the strong affinity with PFAS and convenient reusability. Results from the combined material characterization and PFAS adsorption/desorption experiments suggested that PFAS adsorption onto ZrMD and ZrMC may follow different mechanisms. While hydrophobic interactions were expected to play an important role in PFAS adsorption onto both materials, ZrMD exhibited stronger electrostatic interactions with PFAS than those of ZrMC. Specifically, ZrMD showed robust performance for PFAS adsorption in the presence of co-existing anions, NOM, and elevated

ionic strengths, indicating a strong interaction between ZrMD and the selected PFAS. In contrast, the presence of NOM strongly reduced PFAS adsorption onto ZrMC, particularly for 5:3FTCA. Moreover, ZrMD could be conveniently regenerated and readily reused for multiple times without reduced performance, likely due to the retaining of the covalently bonded organic functional groups during the regeneration process. In contrast, ZrMC showed minimal PFAS removal after regeneration because of the loss of organic functional groups during the regeneration process. Overall, compared to the conventional organoclays, ZrMD prepared through grafting reactions showed improved performance for PFAS removal in terms of both adsorption affinity and material reusability, which may represent the next-generation organoclay adsorbents for various PFAS treatment applications.

5.2 Recommendations for future work

To promote technology development, future research may focus on (1) examination of the adsorption of a wider spectrum of PFAS structures onto organoclays; (2) elucidation of the adsorption mechanisms of various PFAS structures onto organoclays based on molecular level characterizations and simulations; (3) development of improved strategies to promote the *in situ* regeneration of organoclays; (4) determination of the long-term performance of organoclays under challenging conditions relevant to field applications; (5) evaluation the technical and economic feasibility of the technology; and (6) demonstration of organoclay performance in pilot- and full-scale validation studies.

Reference

- Ahmed, A., Y. Chaker, El H. Belarbi, O. Abbas, J. N. Chotard, H. B. Abassi, A. Nguyen Van Nhien, M. El Hadri, and S. Bresson. 2018a. "XRD and ATR/FTIR Investigations of Various Montmorillonite Clays Modified by Monocationic and Dicationic Imidazolium Ionic Liquids." *Journal of Molecular Structure* 1173: 653–64. <https://doi.org/10.1016/j.molstruc.2018.07.039>.
- Al-ghouti, Mohammad A, and Dana A Da. 2020. "Guidelines for the Use and Interpretation of Adsorption Isotherm Models : A Review." *Journal of Hazardous Materials* 393 (January): 122383. <https://doi.org/10.1016/j.jhazmat.2020.122383>.
- Alsaiee, Alaaeddin, Brian J. Smith, Leilei Xiao, Yuhang Ling, Damian E. Helbling, and William R. Dichtel. 2016. "Rapid Removal of Organic Micropollutants from Water by a Porous β -Cyclodextrin Polymer." *Nature* 529 (7585): 190–94. <https://doi.org/10.1038/nature16185>.
- Alshameri, Aref, Hongping He, Jianxi Zhu, Yunfei Xi, Runliang Zhu, Lingya Ma, and Qi Tao. 2018. "Adsorption of Ammonium by Different Natural Clay Minerals: Characterization, Kinetics and Adsorption Isotherms." *Applied Clay Science* 159 (November): 83–93. <https://doi.org/10.1016/j.clay.2017.11.007>.
- Appleman, Timothy D., Eric R.V. Dickenson, Christopher Bellona, and Christopher P. Higgins. 2013. "Nanofiltration and Granular Activated Carbon Treatment of Perfluoroalkyl Acids." *Journal of Hazardous Materials* 260: 740–46. <https://doi.org/10.1016/j.jhazmat.2013.06.033>.
- Appleman, Timothy D., Christopher P. Higgins, Oscar Quiñones, Brett J. Vanderford, Chad Kolstad, Janie C. Zeigler-Holady, and Eric R.V. Dickenson. 2014. "Treatment of Poly- and Perfluoroalkyl Substances in U.S. Full-Scale Water Treatment Systems." *Water Research* 51: 246–55. <https://doi.org/10.1016/j.watres.2013.10.067>.
- Arias Espana, Victor Andres, Megharaj Mallavarapu, and Ravi Naidu. 2015. "Treatment Technologies for Aqueous Perfluorooctanesulfonate (PFOS) and Perfluorooctanoate (PFOA): A Critical Review with an Emphasis on Field Testing." *Environmental Technology and Innovation* 4: 168–81. <https://doi.org/10.1016/j.eti.2015.06.001>.
- Arvaniti, Olga S., and Athanasios S. Stasinakis. 2015. "Review on the Occurrence, Fate and Removal of Perfluorinated Compounds during Wastewater Treatment." *Science of the Total Environment* 524–525: 81–92. <https://doi.org/10.1016/j.scitotenv.2015.04.023>.
- Ateia, Mohamed, Alaaeddin Alsaiee, Tanju Karanfil, and William Dichtel. 2019. "Efficient PFAS Removal by Amine-Functionalized Sorbents: Critical Review of the Current Literature." *Environmental Science and Technology Letters* 6 (12): 688–95. <https://doi.org/10.1021/acs.estlett.9b00659>.
- Ateia, Mohamed, Md Arifuzzaman, Steven Pellizzeri, Mohamed F. Attia, Nishanth Tharayil, Jeffrey N. Anker, and T. Karanfil. 2019. "Cationic Polymer for Selective Removal of GenX and Short-Chain PFAS from Surface Waters and Wastewaters at ng/L Levels." *Water Research* 163. <https://doi.org/10.1016/j.watres.2019.114874>.
- Ateia, Mohamed, Mohamed F. Attia, Amith Maroli, Nishanth Tharayil, Frank Alexis, Daniel C. Whitehead, and Tanju Karanfil. 2018. "Rapid Removal of Poly- and Perfluorinated Alkyl Substances by Poly(Ethylenimine)-Functionalized Cellulose Microcrystals at Environmentally Relevant Conditions." *Environmental Science and Technology Letters* 5 (12): 764–69. <https://doi.org/10.1021/acs.estlett.8b00556>.

- Ateia, Mohamed, Amith Maroli, Nishanth Tharayil, and Tanju Karan. 2019. "The Overlooked Short- and Ultrashort-Chain Poly- and Per fluorinated Substances: A Review." *Chemosphere* 220: 866–82. <https://doi.org/10.1016/j.chemosphere.2018.12.186>.
- Avci, Betül. 2018. "Comparative Theology and Scriptural Reasoning: A Muslim's Approach to Interreligious Learning". *Religions* 9(10). <https://doi.org/10.3390/rel9100297>.
- Backe, Will J., Thomas C. Day, and Jennifer A. Field. 2013. "Zwitterionic, Cationic, and Anionic Fluorinated Chemicals in Aqueous Film Forming Foam Formulations and Groundwater from U.S. Military Bases by Nonaqueous Large-Volume Injection HPLC-MS/MS." *Environmental Science and Technology* 47 (10): 5226–34. <https://doi.org/10.1021/es3034999>.
- Badrudodoza, Abu Zayed Md, Bikash Bhattarai, and Rominder P.S. Suri. 2017. "Environmentally Friendly β -Cyclodextrin-Ionic Liquid Polyurethane-Modified Magnetic Sorbent for the Removal of PFOA, PFOS, and Cr(VI) from Water." *ACS Sustainable Chemistry and Engineering* 5 (10): 9223–32. <https://doi.org/10.1021/acssuschemeng.7b02186>.
- Barshad, I. 1955. "Absorptive and Swelling Properties of Clay-Water System." *Clays and Clay Minerals* 1(1): 70–77. <https://doi.org/10.1346/CCMN.1952.0010108>.
- Bartell, Scott M, Antonia M Calafat, Christopher Lyu, Kayoko Kato, P Barry Ryan, and Kyle Steenland. 2010. "Rate of Decline in Serum PFOA Concentrations after Granular Activated Carbon Filtration at Two Public Water Systems in Ohio and West Virginia". *Environmental health perspectives* 118 (2): 222–28. <https://doi.org/10.1289/ehp.0901252>.
- Blesic, Marijana, Maria Helena Marques, Natalia V. Plechkova, Kenneth R. Seddon, Luís Paulo N. Rebelo, and António Lopes. 2007. "Self-Aggregation of Ionic Liquids: Micelle Formation in Aqueous Solution." *Green Chemistry* 9 (5): 481–90. <https://doi.org/10.1039/b615406a>.
- Boyer, Treavor H., Yida Fang, Anderson Ellis, Rebecca Dietz, Youn Jeong Choi, Charles E. Schaefer, Christopher P. Higgins, and Timothy J. Strathmann. 2021. "Anion Exchange Resin Removal of Per- and Polyfluoroalkyl Substances (PFAS) from Impacted Water: A Critical Review." *Water Research* 200: 117244. <https://doi.org/10.1016/j.watres.2021.117244>.
- Buck, Robert C, James Franklin, Urs Berger, Jason M Conder, Ian T Cousins, Pim De Voogt, Allan Astrup Jensen, et al. 2011. "Perfluoroalkyl and Polyfluoroalkyl Substances in the Environment: Terminology, Classification, and Origins". *Integrated environmental assessment and management*, 7(4): 513–41. <https://doi.org/10.1002/ieam.258>.
- Cao, Huimin, Weilan Zhang, Cuiping Wang, and Yanna Liang. 2020. "Sonochemical Degradation of Poly- and Perfluoroalkyl Substances – A Review." *Ultrasonics Sonochemistry* 69 (2020): 105245. <https://doi.org/10.1016/j.ultsonch.2020.105245>.
- Cardona, Wilson, Pablo Richter, Jhon A. Fiscal-Ladino, Luis F. Giraldo, Mónica Obando-Ceballos, Milton Rosero-Moreano, and Diego F. Montaña. 2016. "Ionic Liquids Intercalated in Montmorillonite as the Sorptive Phase for the Extraction of Low-Polarity Organic Compounds from Water by Rotating-Disk Sorptive Extraction." *Analytica Chimica Acta* 953: 23–31. <https://doi.org/10.1016/j.aca.2016.11.067>.
- Carter, Margaret C., James E. Kilduff, and Walter J. Weber. 1995. "Site Energy Distribution Analysis of Preloaded Adsorbents." *Environmental Science and Technology* 29 (7): 1773–80. <https://doi.org/10.1021/es00007a013>.
- Chang, Po Hsiang, Wei Teh Jiang, and Zhaohui Li. 2019. "Removal of Perfluorooctanoic Acid from Water Using Calcined Hydrotalcite – A Mechanistic Study." *Journal of Hazardous Materials* 368

- (2019): 487–95. <https://doi.org/10.1016/j.jhazmat.2019.01.084>.
- Chen, Meng Jia, Shang Lien Lo, Yu Chi Lee, Jeff Kuo, and Chung Hsin Wu. 2016. “Decomposition of Perfluorooctanoic Acid by Ultraviolet Light Irradiation with Pb-Modified Titanium Dioxide.” *Journal of Hazardous Materials* 303: 111–18. <https://doi.org/10.1016/j.jhazmat.2015.10.011>.
- Clark, Chelsea A., Kimberly N. Heck, Camilah D. Powell, and Michael S. Wong. 2019. “Highly Defective UiO-66 Materials for the Adsorptive Removal of Perfluorooctanesulfonate.” *ACS Sustainable Chemistry and Engineering* 7 (7): 6619–28. <https://doi.org/10.1021/acssuschemeng.8b05572>.
- Cousins, Ian T., Jamie C. Dewitt, Juliane Glüge, Gretta Goldenman, Dorte Herzke, Rainer Lohmann, Mark Miller, et al. 2020. “Strategies for Grouping Per- and Polyfluoroalkyl Substances (PFAS) to Protect Human and Environmental Health.” *Environmental Science: Processes and Impacts* 22 (7): 1444–60. <https://doi.org/10.1039/d0em00147c>.
- Cui, Danni, Xuerong Li, and Natalia Quinete. 2020. “Occurrence, Fate, Sources and Toxicity of PFAS: What We Know So Far in Florida and Major Gaps.” *TrAC Trends in Analytical Chemistry* 130: 115976. <https://doi.org/10.1016/j.trac.2020.115976>.
- Cui, Junkui, Panpan Gao, and Yang Deng. 2020. “Destruction of Per- and Polyfluoroalkyl Substances (PFAS) with Advanced Reduction Processes (ARPs): A Critical Review.” *Environmental Science and Technology* 54 (7): 3752–66. <https://doi.org/10.1021/acs.est.9b05565>.
- Dai, Chengna, Jie Zhang, Chongpin Huang, and Zhigang Lei. 2017. “Ionic Liquids in Selective Oxidation: Catalysts and Solvents.” *Chemical Reviews* 117 (10): 6929–83. <https://doi.org/10.1021/acs.chemrev.7b00030>.
- Dean, Katherine M., Stuart A. Bateman, and Ranya Simons. 2007. “A Comparative Study of UV Active Silane-Grafted and Ion-Exchanged Organo-Clay for Application in Photocurable Urethane Acrylate Nano- and Micro-Composites.” *Polymer* 48 (8): 2231–40. <https://doi.org/10.1016/j.polymer.2007.02.044>.
- Deng, Shubo, Yao Nie, Ziwen Du, Qian Huang, Pingping Meng, Bin Wang, Jun Huang, and Gang Yu. 2015. “Enhanced Adsorption of Perfluorooctane Sulfonate and Perfluorooctanoate by Bamboo-Derived Granular Activated Carbon.” *Journal of Hazardous Materials* 282: 150–57. <https://doi.org/10.1016/j.jhazmat.2014.03.045>.
- Deng, Shubo, Qiang Yu, Jun Huang, and Gang Yu. 2010. “Removal of Perfluorooctane Sulfonate from Wastewater by Anion Exchange Resins: Effects of Resin Properties and Solution Chemistry.” *Water Research* 44 (18): 5188–95. <https://doi.org/10.1016/j.watres.2010.06.038>.
- Dixit, Fuhar, Benoit Barbeau, and Madjid Mohseni. 2018. “Characteristics of Competitive Uptake between Microcystin-LR and Natural Organic Matter (NOM) Fractions Using Strongly Basic Anion Exchange Resins.” *Water Research* 139: 74–82. <https://doi.org/10.1016/j.watres.2018.03.074>.
- Dixit, Fuhar, Benoit Barbeau, and Madjid Mohseni. 2020. “Impact of Natural Organic Matter Characteristics and Inorganic Anions on the Performance of Ion Exchange Resins in Natural Waters.” *Water Science and Technology: Water Supply* 20 (8): 3107–19. <https://doi.org/10.2166/ws.2020.197>.
- Dixit, Fuhar, Benoit Barbeau, Shadan Ghavam Mostafavi, and Madjid Mohseni. 2020. “Removal of Legacy PFAS and Other Fluorotelomers: Optimized Regeneration Strategies in DOM-Rich Waters.” *Water Research* 183: 116098. <https://doi.org/10.1016/j.watres.2020.116098>.
- Dixit, Fuhar, Rahul Dutta, Benoit Barbeau, Pierre Berube, and Madjid Mohseni. 2021. “PFAS Removal

- by Ion Exchange Resins: A Review.” *Chemosphere* 272: 129777.
<https://doi.org/10.1016/j.chemosphere.2021.129777>.
- Dogan, A. Umran, Meral Dogan, Muserref Omal, Yuksel Sarikaya, Aktham Aburub, and Dale Eric Wurster. 2006. “Baseline Studies of The Clay Minerals Society Source Clays: Specific Surface Area by Brunauer Emmett Teller (BET) Method.” *Clays and Clay Minerals* 54 (1): 62–66.
<https://doi.org/10.1346/CCMN.2006.0540108>.
- Dong, Qianqian, Xiaopeng Min, Jingwan Huo, and Yin Wang. 2021. “Efficient Sorption of Perfluoroalkyl Acids by Ionic Liquid-Modified Natural Clay.” *Chemical Engineering Journal Advances* 7 (2021): 100135. <https://doi.org/10.1016/j.cej.2021.100135>.
- Drits, V. A. 2003. “Structural and Chemical Heterogeneity of Layer Silicates and Clay Minerals.” *Clay Minerals* 38 (4): 403–32. <https://doi.org/10.1180/0009855033840106>.
- Du, Ziwen, Shubo Deng, Youguang Chen, Bin Wang, Jun Huang, Yujue Wang, and Gang Yu. 2015. “Removal of Perfluorinated Carboxylates from Washing Wastewater of Perfluorooctanesulfonyl Fluoride Using Activated Carbons and Resins.” *Journal of Hazardous Materials* 286: 136–43.
<https://doi.org/10.1016/j.jhazmat.2014.12.037>.
- Du, Ziwen, Shubo Deng, Siyu Zhang, Bin Wang, Jun Huang, Yujue Wang, Gang Yu, and Baoshan Xing. 2016. “Selective and High Sorption of Perfluorooctanesulfonate and Perfluorooctanoate by Fluorinated Alkyl Chain Modified Montmorillonite.” *Journal of Physical Chemistry C* 120 (30): 16782–90. <https://doi.org/10.1021/acs.jpcc.6b04757>.
- Du, Ziwen, Shubo Deng, Siyu Zhang, Wei Wang, Bin Wang, Jun Huang, Yujue Wang, Gang Yu, and Baoshan Xing. 2017. “Selective and Fast Adsorption of Perfluorooctanesulfonate from Wastewater by Magnetic Fluorinated Vermiculite.” *Environmental Science and Technology* 51 (14): 8027–35.
<https://doi.org/10.1021/acs.est.6b06540>.
- Du, Ziwen W, Shubo B Deng, Yue Bei, Qian Huang, Bin Wang, Jun Huang, and Gang Yu. 2014. “Adsorption Behavior and Mechanism of Perfluorinated Compounds on Various Adsorbents-A Review.” *Journal of Hazardous Materials* 274: 443–54.
<https://doi.org/10.1016/j.jhazmat.2014.04.038>.
- Elsherbiny, Abeer S., Mohamed A. Salem, and Azza A. Ismail. 2012. “Influence of the Alkyl Chain Length of Cyanine Dyes on Their Adsorption by Na⁺-Montmorillonite from Aqueous Solutions.” *Chemical Engineering Journal* 200–202: 283–90. <https://doi.org/10.1016/j.cej.2012.06.050>.
- Evich, Marina G., Mary J.B. Davis, James P. McCord, Brad Acrey, Jill A. Awkerman, Detlef R.U. Knappe, Andrew B. Lindstrom, et al. 2022. “Per- and Polyfluoroalkyl Substances in the Environment.” *Science* 375 (6580). <https://doi.org/10.1126/science.abg9065>.
- Fang, C.; M.; Megharaj, and R. Naidu. 2017. “Electrochemical Advanced Oxidation Processes (EAOP) to Degrade per- and Polyfluoroalkyl Substances (PFASs).” *Journal of Advanced Oxidation Technologies* 20 (2). <https://doi.org/10.1515/jaots-2017-0014>.
- Fernandez, Nerea Abad, Lucia Rodriguez-Freire, Manish Keswani, and Reyes Sierra-Alvarez. 2016. “Effect of Chemical Structure on the Sonochemical Degradation of Perfluoroalkyl and Polyfluoroalkyl Substances (PFASs).” *Environmental Science: Water Research and Technology* 2 (6): 975–83. <https://doi.org/10.1039/c6ew00150e>.
- Fluoride Action Network Pesticide Project. 2006. “Timeline for PFOS and PFOS Perfluorinated Chemicals.” 2021.8.20.
<http://www.fluoridealert.org/wpcontent/pesticides/effect.pfos.class.timeline.htm>.

- Foo, Keng Yuen, and Bassim H. Hameed. 2010. "Insights into the Modeling of Adsorption Isotherm Systems." *Chemical Engineering Journal* 156 (1): 2–10. <https://doi.org/10.1016/j.cej.2009.09.013>.
- Gagliano, Erica, Massimiliano Sgroi, Pietro P. Falciglia, Federico G.A. Vagliasindi, and Paolo Roccaro. 2020. "Removal of Poly- and Perfluoroalkyl Substances (PFAS) from Water by Adsorption: Role of PFAS Chain Length, Effect of Organic Matter and Challenges in Adsorbent Regeneration." *Water Research* 171: 115381. <https://doi.org/10.1016/j.watres.2019.115381>.
- Gao, Yanxin, Shubo Deng, Ziwen Du, Kai Liu, and Gang Yu. 2017. "Adsorptive Removal of Emerging Polyfluoroalkyl Substances F-53B and PFOS by Anion-Exchange Resin: A Comparative Study." *Journal of Hazardous Materials* 323 (April 2016): 550–57. <https://doi.org/10.1016/j.jhazmat.2016.04.069>.
- Giri, R. R., H. Ozaki, T. Morigaki, S. Taniguchi, and R. Takanami. 2011. "UV Photolysis of Perfluorooctanoic Acid (PFOA) in Dilute Aqueous Solution." *Water Science and Technology* 63 (2): 276–82. <https://doi.org/10.2166/wst.2011.050>.
- Giri, Rabindra Raj, Hiroaki Ozaki, Tatsuya Okada, Shogo Taniguchi, and Ryohei Takanami. 2012. "Factors Influencing UV Photodecomposition of Perfluorooctanoic Acid in Water." *Chemical Engineering Journal* 180: 197–203. <https://doi.org/10.1016/j.cej.2011.11.049>.
- Grim, Ralph Early, Roger Hammond Bray, and William Frank Bradley. "The mica in argillaceous sediments." *American Mineralogist: Journal of Earth and Planetary Materials* 22, no. 7 (1937): 813–829.
- Golubeva, O. Yu, and V. V. Gusarov. 2007. "Layered Silicates with a Montmorillonite Structure: Preparation and Prospects for the Use in Polymer Nanocomposites." *Glass Physics and Chemistry* 33 (3): 237–41. <https://doi.org/10.1134/S108765960703008X>.
- Haouzi, Ahmed, Ibn Khaldoun Lefkaier, Mohamed Kharroubi, Mouffok Abdessamad, Sebastien Balme, Abdeljabbar Belbel, and Jean-Marc Janot. 2018. "Preparation and Characterization of Homoionic Montmorillonite Modified with Ionic Liquid: Application in Dye Adsorption." *Colloids and Surfaces A: Physicochemical and Engineering Aspects* 558 (2018): 219–27. <https://doi.org/10.1016/j.colsurfa.2018.08.080>.
- He, Yuxuan, Liming Zhang, Xiao An, Gengping Wan, Wenjie Zhu, and Yongming Luo. 2019. "Enhanced Fluoride Removal from Water by Rare Earth (La and Ce) Modified Alumina: Adsorption Isotherms, Kinetics, Thermodynamics and Mechanism." *Science of the Total Environment* 688: 184–98. <https://doi.org/10.1016/j.scitotenv.2019.06.175>.
- Herkert, Nicholas J., John Merrill, Cara Peters, David Bollinger, Sharon Zhang, Kate Hoffman, P. Lee Ferguson, Detlef R.U. Knappe, and Heather M. Stapleton. 2020. "Assessing the Effectiveness of Point-of-Use Residential Drinking Water Filters for Perfluoroalkyl Substances (PFASs)." *Environmental Science and Technology Letters* 7 (3): 178–84. <https://doi.org/10.1021/acs.estlett.0c00004>.
- Higgins, Christopher P., and Richard G. Luthy. 2006. "Sorption of Perfluorinated Surfactants on Sediments." *Environmental Science and Technology* 40 (23): 7251–56. <https://doi.org/10.1021/es061000n>.
- Ho, Yuh-Shan, and Gordon McKay. 1999. "Pseudo-Second Order Model for Sorption Processes." *Process Biochemistry* 34 (5): 451–65.
- Houtz, Erika F., Rebecca Sutton, June Soo Park, and Margaret Sedlak. 2016. "Poly- and Perfluoroalkyl Substances in Wastewater: Significance of Unknown Precursors, Manufacturing Shifts, and Likely

- AFFF Impacts.” *Water Research* 95: 142–49. <https://doi.org/10.1016/j.watres.2016.02.055>.
- Houtz, Erika F, Christopher P Higgins, Jennifer A Field, and David L Sedlak. 2013. “Persistence of Perfluoroalkyl Acid Precursors in AFFF-Impacted Groundwater and Soil.” *Environmental Science & Technology* 47 (15): 8187–95. <https://doi.org/10.1021/es4018877>.
- Hu, Xindi C., David Q. Andrews, Andrew B. Lindstrom, Thomas A. Bruton, Laurel A. Schaider, Philippe Grandjean, Rainer Lohmann, et al. 2016. “Detection of Poly- and Perfluoroalkyl Substances (PFASs) in U.S. Drinking Water Linked to Industrial Sites, Military Fire Training Areas, and Wastewater Treatment Plants.” *Environmental Science and Technology Letters* 3 (10): 344–50. <https://doi.org/10.1021/acs.estlett.6b00260>.
- Hu, Zhihao, Xin Song, Changlong Wei, and Jianguo Liu. 2017. “Behavior and Mechanisms for Sorptive Removal of Perfluorooctane Sulfonate by Layered Double Hydroxides.” *Chemosphere* 187: 196–205. <https://doi.org/10.1016/j.chemosphere.2017.08.082>.
- Huang, Yanmei, Haiyan Li, Mindong Bai, and Xiaojia Huang. 2018. “Efficient Extraction of Perfluorocarboxylic Acids in Complex Samples with a Monolithic Adsorbent Combining Fluorophilic and Anion-Exchange Interactions.” *Analytica Chimica Acta* 1011: 50–58. <https://doi.org/10.1016/j.aca.2018.01.032>.
- Huo, Jingwan, Xiaopeng Min, and Yin Wang. 2021. “Zirconium-Modified Natural Clays for Phosphate Removal: Effect of Clay Minerals.” *Environmental Research* 194. <https://doi.org/10.1016/j.envres.2020.110685>.
- Ismadji, Suryadi, Felycia Edi Soetaredjo, and Aning Ayucitra. 2015. “Natural Clay Minerals as Environmental Cleaning Agents BT - Clay Materials for Environmental Remediation.” In *Clay materials for environmental remediation*, pp. 5–37. Springer, Cham. https://doi.org/10.1007/978-3-319-16712-1_2.
- Ji, Bin, Peiying Kang, Ting Wei, and Yaqian Zhao. 2020. “Challenges of Aqueous Per- and Polyfluoroalkyl Substances (PFASs) and Their Foreseeable Removal Strategies.” *Chemosphere* 250: 126316. <https://doi.org/10.1016/j.chemosphere.2020.126316>.
- Ji, Woojung, Leilei Xiao, Yuhan Ling, Casey Ching, Michio Matsumoto, Ryan P. Bisbey, Damian E. Helbling, and William R. Dichtel. 2018. “Removal of GenX and Perfluorinated Alkyl Substances from Water by Amine-Functionalized Covalent Organic Frameworks.” *Rapid-communication. Journal of the American Chemical Society* 140 (40): 12677–81. <https://doi.org/10.1021/jacs.8b06958>.
- Ji, Xiaoyuan, Lanlan Ge, Chuang Liu, Zhongmin Tang, Yufen Xiao, Wei Chen, Zhouyue Lei, et al. 2021. “Capturing Functional Two-Dimensional Nanosheets from Sandwich-Structure Vermiculite for Cancer Theranostics.” *Nature Communications* 12 (1): 1–17. <https://doi.org/10.1038/s41467-021-21436-5>.
- Jia, Xiaohui, Hongfei Cheng, Yi Zhou, Shilong Zhang, and Qinghe Liu. 2019. “Time-Efficient Preparation and Mechanism of Methoxy-Grafted Kaolinite via Acid Treatment and Heating.” *Applied Clay Science* 174 (126): 170–77. <https://doi.org/10.1016/j.clay.2019.04.001>.
- Kenne Dedzo, Gustave, and Christian Detellier. 2017. “Characterization and Applications of Kaolinite Robustly Grafted by an Ionic Liquid with Naphthyl Functionality.” *Materials*, 10(9) 1006. <https://doi.org/10.3390/ma10091006>.
- Kim, Seung-Kyu, Young Lim Kho, Mahiba Shoeib, Kyoung-Soo Kim, Kyung-Ryul Kim, Jong-Eun Park, and Yong-Seung Shin. 2011. “Occurrence of Perfluorooctanoate and Perfluorooctanesulfonate in the

- Korean Water System: Implication to Water Intake Exposure.” *Environmental Pollution* 159 (5): 1167–73.
- Kłapyta, Z., A. Gawęł, T. Fujita, and N. Iyi. 2003. “Structural Heterogeneity of Alkylammonium-Exchanged, Synthetic Fluorotetrasilicic Mica.” *Clay Minerals* 38 (2): 151–60. <https://doi.org/10.1180/0009855033820085>.
- Kłapyta, Zenon, Taketoshi Fujita, and Nobuo Iyi. 2001. “Adsorption of Dodecyl- and Octadecyltrimethylammonium Ions on a Smectite and Synthetic Micas.” *Applied Clay Science* 19 (1–6): 5–10. [https://doi.org/10.1016/S0169-1317\(01\)00059-X](https://doi.org/10.1016/S0169-1317(01)00059-X).
- Klemes, Max J., Yuhan Ling, Casey Ching, Congyue Wu, Leilei Xiao, Damian E. Helbling, and William R. Dichtel. 2019. “Reduction of a Tetrafluoroterephthalonitrile- β -Cyclodextrin Polymer to Remove Anionic Micropollutants and Perfluorinated Alkyl Substances from Water.” *Angewandte Chemie - International Edition* 58 (35): 12049–53. <https://doi.org/10.1002/anie.201905142>.
- Kolpin, Dana W., Laura E. Hubbard, David M. Cwiertny, Shannon M. Meppelink, Darrin A. Thompson, and James L. Gray. 2021. “A Comprehensive Statewide Spatiotemporal Stream Assessment of Per- And Polyfluoroalkyl Substances (PFAS) in an Agricultural Region of the United States.” *Environmental Science and Technology Letters* 8 (11): 981–88. <https://doi.org/10.1021/acs.estlett.1c00750>.
- Kotthoff, Matthias, Josef Müller, Heinrich Jüriling, Martin Schlummer, and Dominik Fiedler. 2015. “Perfluoroalkyl and Polyfluoroalkyl Substances in Consumer Products.” *Environmental Science Pollutant Research* 22 (19): 14546–59. <https://doi.org/10.1007/s11356-015-4202-7>.
- Kucharzyk, Katarzyna H., Ramona Darlington, Mark Benotti, Rula Deeb, and Elisabeth Hawley. 2017. “Novel Treatment Technologies for PFAS Compounds: A Critical Review.” *Journal of Environmental Management* 204: 757–64. <https://doi.org/10.1016/j.jenvman.2017.08.016>.
- Kunacheva, Chinagarn, Shigeo Fujii, Shuhei Tanaka, STMLD Seneviratne, Nguyen Pham Hong Lien, Munehiro Nozoe, Koji Kimura, Binaya Raj Shivakoti, and Hidenori Harada. 2012. “Worldwide Surveys of Perfluorooctane Sulfonate (PFOS) and Perfluorooctanoic Acid (PFOA) in Water Environment in Recent Years.” *Water Science and Technology* 66 (12): 2764–71.
- Lang, Johnsie R., B. Mc Kay Allred, Jennifer A. Field, James W. Levis, and Morton A. Barlaz. 2017. “National Estimate of Per- and Polyfluoroalkyl Substance (PFAS) Release to U.S. Municipal Landfill Leachate.” *Environmental Science and Technology* 51 (4): 2197–2205. <https://doi.org/10.1021/acs.est.6b05005>.
- Langberg, Håkon A., Gijs D. Breedveld, Hege M. Grønning, Marianne Kvennås, Bjørn M. Jenssen, and Sarah E. Hale. 2019. “Bioaccumulation of Fluorotelomer Sulfonates and Perfluoroalkyl Acids in Marine Organisms Living in Aqueous Film-Forming Foam Impacted Waters.” *Environmental Science and Technology* 53 (18): 10951–60. <https://doi.org/10.1021/acs.est.9b00927>.
- Lee, Seung Mok, and Diwakar Tiwari. 2012. “Organo and Inorgano-Organo-Modified Clays in the Remediation of Aqueous Solutions: An Overview.” *Applied Clay Science* 59–60: 84–102. <https://doi.org/10.1016/j.clay.2012.02.006>.
- Lenka, Swadhina Priyadarshini, Melanie Kah, and Lokesh P. Padhye. 2021. “A Review of the Occurrence, Transformation, and Removal of Poly- and Perfluoroalkyl Substances (PFAS) in Wastewater Treatment Plants.” *Water Research* 199: 117187. <https://doi.org/10.1016/j.watres.2021.117187>.
- Li, Fan, Jun Duan, Shuting Tian, Haodong Ji, Yangmo Zhu, Zongsu Wei, and Dongye Zhao. 2020.

- “Short-Chain per- and Polyfluoroalkyl Substances in Aquatic Systems: Occurrence, Impacts and Treatment.” *Chemical Engineering Journal* 380 (2020). <https://doi.org/10.1016/j.cej.2019.122506>.
- Li, Yin Ming, and Fu Shen Zhang. 2014. “Characterization of a Cetyltrimethyl Ammonium Bromide-Modified Sorbent for Removal of Perfluorooctane Sulphonate from Water.” *Environmental Technology (United Kingdom)* 35 (20): 2556–68. <https://doi.org/10.1080/09593330.2014.912253>.
- Liu, Kai, Siyu Zhang, Xiyue Hu, Kunyang Zhang, Ajay Roy, and Gang Yu. 2015. “Understanding the Adsorption of PFOA on MIL-101(Cr)-Based Anionic-Exchange Metal-Organic Frameworks: Comparing DFT Calculations with Aqueous Sorption Experiments.” *Environmental Science and Technology* 49 (14): 8657–65. <https://doi.org/10.1021/acs.est.5b00802>.
- Liu, Longfei, Yanli Liu, Bin Gao, Rong Ji, Chengliang Li, and Shengsen Wang. 2020. “Removal of Perfluorooctanoic Acid (PFOA) and Perfluorooctane Sulfonate (PFOS) from Water by Carbonaceous Nanomaterials: A Review.” *Critical Reviews in Environmental Science and Technology* 50 (22): 2379–2414. <https://doi.org/10.1080/10643389.2019.1700751>.
- Loos, Robert, Raquel Carvalho, Diana C. António, Sara Comero, Giovanni Locoro, Simona Tavazzi, Bruno Paracchini, et al. 2013. “EU-Wide Monitoring Survey on Emerging Polar Organic Contaminants in Wastewater Treatment Plant Effluents.” *Water Research* 47 (17): 6475–87. <https://doi.org/10.1016/j.watres.2013.08.024>.
- Lu, Dingnan, Sha Sha, Jiayue Luo, Zhuangrong Huang, and Xiaoqi Zhang Jackie. 2020. “Treatment Train Approaches for the Remediation of Per- and Polyfluoroalkyl Substances (PFAS): A Critical Review.” *Journal of Hazardous Materials* 386: 121963. <https://doi.org/10.1016/j.jhazmat.2019.121963>.
- Lu, Mengnan, Giovanni Cagnetta, Kunlun Zhang, Jun Huang, and Gang Yu. 2017. “Mechanochemical Mineralization of ‘Very Persistent’ Fluorocarbon Surfactants – 6:2 Fluorotelomer Sulfonate (6:2FTS) as an Example.” *Scientific Reports* 7 (1): 17180. <https://doi.org/10.1038/s41598-017-17515-7>.
- Lv, Guocheng, Zhaohui Li, Wei Teh Jiang, Shangping Xu, and Travis E. Larson. 2014. “Ionic Liquid Modification of Zeolite and Its Removal of Chromate from Water.” *Green Chemistry Letters and Reviews* 7 (2): 191–98. <https://doi.org/10.1080/17518253.2014.923518>.
- Mahinroosta, Reza, and Lalantha Senevirathna. 2020. “A Review of the Emerging Treatment Technologies for PFAS Contaminated Soils.” *Journal of Environmental Management* 255: 109896. <https://doi.org/10.1016/j.jenvman.2019.109896>.
- Maimaiti, Ayiguli, Shubo Deng, Pingping Meng, Wei Wang, Bin Wang, Jun Huang, Yujue Wang, and Gang Yu. 2018. “Competitive Adsorption of Perfluoroalkyl Substances on Anion Exchange Resins in Simulated AFFF-Impacted Groundwater.” *Chemical Engineering Journal* 348: 494–502. <https://doi.org/10.1016/j.cej.2018.05.006>.
- Martín, Julia, María del Mar Orta, Santiago Medina-Carrasco, Juan Luis Santos, Irene Aparicio, and Esteban Alonso. 2018. “Removal of Priority and Emerging Pollutants from Aqueous Media by Adsorption onto Synthetic Organo-Functionalized High-Charge Swelling Micas.” *Environmental Research* 164: 488–94. <https://doi.org/10.1016/j.envres.2018.03.037>.
- McGuire, Meghan E., Charles Schaefer, Trenton Richards, Will J. Backe, Jennifer A. Field, Erika Houtz, David L. Sedlak, Jennifer L. Guelfo, Assaf Wunsch, and Christopher P. Higgins. 2014. “Evidence of Remediation-Induced Alteration of Subsurface Poly- and Perfluoroalkyl Substance Distribution at a Former Firefighter Training Area.” *Environmental Science and Technology* 48 (12): 6644–52. <https://doi.org/10.1021/es5006187>.

- McMahon, Peter B., Andrea K. Tokranov, Laura M. Bexfield, Bruce D. Lindsey, Tyler D. Johnson, Melissa A. Lombard, and Elise Watson. 2022. "Perfluoroalkyl and Polyfluoroalkyl Substances in Groundwater Used as a Source of Drinking Water in the Eastern United States." *Environmental Science and Technology* 56 (4): 2279–88. <https://doi.org/10.1021/acs.est.1c04795>.
- Merino, Nancy, Yan Qu, Rula A. Deeb, Elisabeth L. Hawley, Michael R. Hoffmann, and Shaily Mahendra. 2016. "Degradation and Removal Methods for Perfluoroalkyl and Polyfluoroalkyl Substances in Water." *Environmental Engineering Science* 33 (9): 615–49. <https://doi.org/10.1089/ees.2016.0233>.
- Mermut, Ahmet R., and Angel Faz Cano. 2001. "Baseline Studies of The Clay Minerals Society Source Clays: Chemical Analyses of Major Elements." *Clays and Clay Minerals* 49 (5): 381–86.
- Michael Hawthorne. 2003. "Internal Warnings Industry Memos Show DUPONT Knew for Decades That a Chemical Used to Make Teflon Is Polluting Workers and Neighbors." *The Columbus Dispatch* (Ohio). 2021.7.20. <http://www.fluoridealert.org/wp-content/pesticides/effect.pfos.class.news.7.htm>.
- Min, Xiaopeng, Dulay Trujillo, Jingwan Huo, Qianqian Dong, and Yin Wang. 2020. "Amine-Bridged Periodic Mesoporous Organosilica Nanomaterial for Efficient Removal of Selenate." *Chemical Engineering Journal* 396: 125278. <https://doi.org/10.1016/j.cej.2020.125278>.
- Mojović, Z., N. Jović-Jovičić, A. Milutinović-Nikolić, P. Banković, A. Abu Rabi-Stanković, and D. Jovanović. 2011. "Phenol Determination on HDTMA-Bentonite-Based Electrodes." *Journal of Hazardous Materials* 194: 178–84. <https://doi.org/10.1016/j.jhazmat.2011.07.084>.
- Moriwaki, Hiroshi, Youichi Takagi, Masanobu Tanaka, Kenshiro Tsuruho, Kenji Okitsu, and Yasuaki Maeda. 2005. "Sonochemical Decomposition of Perfluorooctane Sulfonate and Perfluorooctanoic Acid." *Environmental Science and Technology* 39 (9): 3388–92. <https://doi.org/10.1021/es040342v>.
- Naidu, R., R. S. Kookana, M. E. Sumner, R. D. Harter, and K. G. Tiller. 1997. "Cadmium Sorption and Transport in Variable Charge Soils: A Review." *Journal of Environmental Quality* 26 (3): 602–17. <https://doi.org/10.2134/jeq1997.00472425002600030004x>.
- Nicole, Wendee. 2013. "News | Science Selections PFOA and Cancer in a Highly Exposed Community." *Science Selections*.
- OECD. 2013. "Per- and Polyfluorinated OECD / UNEP Global PFC Group Synthesis Paper on per- and Polyfluorinated Chemicals (PFCs)." *Environment, Health and Safety, Environment Directorate, OECD.*, 1–60.
- OECD. 2018. "Toward a New Comprehensive Global Database of Per- and Polyfluoroalkyl Substances (PFASs): Summary Report on Updating the OECD 2007 List of per- and Polyfluoroalkyl Substances (PFASs)." *Series on Risk Management* (39): 1–24. [http://www.oecd.org/officialdocuments/publicdisplaydocumentpdf/?cote=ENV-JM-MONO\(2018\)7&doclanguage=enKEMI](http://www.oecd.org/officialdocuments/publicdisplaydocumentpdf/?cote=ENV-JM-MONO(2018)7&doclanguage=enKEMI).
- Oloyede, Olukayode Gideon, Umar Omeiza Aroke, Saidat Olanipekun Giwa, and Alexander Asanja Jock. 2021. "Characterisation of Natural and HDTMA-Br Modified Dijah-Monkin Bentonite Clay: FTIR, XRF, XRD and SEM." *Path of Science* 7 (5): 2010–18. <https://doi.org/10.22178/pos.70-12>.
- Paiva, Lucilene Betega de, Ana Rita Morales, and Francisco R. Valenzuela Díaz. 2008. "Organoclays: Properties, Preparation and Applications." *Applied Clay Science* 42 (1–2): 8–24. <https://doi.org/10.1016/j.clay.2008.02.006>.
- Pajak-Komorowska, Agnieszka. 2003. "Swelling, Expansion and Shrinkage Properties of Selected Clays in the Mazowsze Province, Central Poland." *Geological Quarterly* 47 (1): 55–62.

- Pan, Meng Meng, Qinying Li, and Li Xu. 2020. "Efficient Adsorption of Perfluoroalkyl Acids by the Quaternized Hierarchically Porous Polystyrene-Divinylbenzene." *Chemical Engineering Journal* 386. <https://doi.org/10.1016/j.cej.2019.123990>.
- Park, Minkyu, Kevin D. Daniels, Shimin Wu, Austin D. Ziska, and Shane A. Snyder. 2020. "Magnetic Ion-Exchange (MIEX) Resin for Perfluorinated Alkyl Substance (PFAS) Removal in Groundwater: Roles of Atomic Charges for Adsorption." *Water Research* 181: 115897. <https://doi.org/10.1016/j.watres.2020.115897>.
- Park, Minkyu, Shimin Wu, Israel J Lopez, Joseph Y Chang, Tanju Karan, and Shane A Snyder. 2020. "Adsorption of Perfluorinated Alkyl Substance (PFAS) in Groundwater by Granular Activated Carbons : Roles of Hydrophobicity of PFAS and Carbon Characteristics." *Water Research* 170.
- Paul, Alexander G., Kevin C. Jones, and Andrew J. Sweetman. 2009. "A First Global Production, Emission, and Environmental Inventory for Perfluorooctane Sulfonate." *Environmental Science and Technology* 43 (2): 386–92. <https://doi.org/10.1021/es802216n>.
- Pauletto, Paola S., and Teresa J. Bandosz. 2022. "Activated Carbon versus Metal-Organic Frameworks: A Review of Their PFAS Adsorption Performance." *Journal of Hazardous Materials* 425: 127810. <https://doi.org/10.1016/j.jhazmat.2021.127810>.
- Podder, Aditi, A. H.M.Anwar Sadmani, Debra Reinhart, Ni Bin Chang, and Ramesh Goel. 2021. "Per and Poly-Fluoroalkyl Substances (PFAS) as a Contaminant of Emerging Concern in Surface Water: A Transboundary Review of Their Occurrences and Toxicity Effects." *Journal of Hazardous Materials* 419: 126361. <https://doi.org/10.1016/j.jhazmat.2021.126361>.
- Post, Gloria B, Judith B Louis, Keith R Cooper, Betty Jane Boros-Russo, and R Lee Lippincott. 2009. "Occurrence and Potential Significance of Perfluorooctanoic Acid (PFOA) Detected in New Jersey Public Drinking Water Systems." *Environmental Science & Technology* 43 (12): 4547–54. <https://doi.org/10.1021/es900301s>.
- R. Zambare, X. Song, S. Bhuvana, J.S. Antony Prince, P. Nemade. 2017. "Ultrafast Dye Removal Using Ionic Liquid–Graphene Oxide Sponge." *ACS Sustainable Chemistry & Engineering*, 5(7): 6026-6035. <https://doi.org/10.1021/acssuschemeng.7b00867>.
- Radjenovic, Jelena, Nick Duinslaeger, Shirin Saffar Avval, and Brian P. Chaplin. 2020. "Facing the Challenge of Poly- And Perfluoroalkyl Substances in Water: Is Electrochemical Oxidation the Answer?" *Environmental Science and Technology* 54 (23): 14815–29. <https://doi.org/10.1021/acs.est.0c06212>.
- Rahman, Mohammad Feisal, Sigrid Peldszus, and William B. Anderson. 2014. "Behaviour and Fate of Perfluoroalkyl and Polyfluoroalkyl Substances (PFASs) in Drinking Water Treatment: A Review." *Water Research* 50: 318–40. <https://doi.org/10.1016/j.watres.2013.10.045>.
- Rankin, Keegan, Scott A. Mabury, Thomas M. Jenkins, and John W. Washington. 2016. "A North American and Global Survey of Perfluoroalkyl Substances in Surface Soils: Distribution Patterns and Mode of Occurrence." *Chemosphere* 161: 333–41. <https://doi.org/10.1016/j.chemosphere.2016.06.109>.
- Ross, Ian, Jeffrey McDonough, Jonathan Miles, Peter Storch, Parvathy Thelakkat Kochunarayanan, Erica Kalve, Jake Hurst, Soumitri S. Dasgupta, and Jeff Burdick. 2018. "A Review of Emerging Technologies for Remediation of PFASs." *Remediation* 28 (2): 101–26. <https://doi.org/10.1002/rem.21553>.
- Saleh, Navid B., Arsalan Khalid, Yuhao Tian, Craig Ayres, Indu V. Sabaraya, Jaana Pietari, David

- Hanigan, Indranil Chowdhury, and Onur G. Apul. 2019. "Removal of Poly- and per-Fluoroalkyl Substances from Aqueous Systems by Nano-Enabled Water Treatment Strategies." *Environmental Science: Water Research and Technology* 5 (2): 198–208. <https://doi.org/10.1039/c8ew00621k>.
- Sánchez-Martín, M. J., M. C. Dorado, C. del Hoyo, and M. S. Rodríguez-Cruz. 2008. "Influence of Clay Mineral Structure and Surfactant Nature on the Adsorption Capacity of Surfactants by Clays." *Journal of Hazardous Materials* 150 (1): 115–23. <https://doi.org/10.1016/j.jhazmat.2007.04.093>.
- Şans, Bala Ekinçi, Onur Güven, Fahri Esenli, and Mehmet S. Çelik. 2017. "Contribution of Cations and Layer Charges in the Smectite Structure on Zeta Potential of Ca-Bentonites." *Applied Clay Science* 143: 415–21. <https://doi.org/10.1016/j.clay.2017.04.016>.
- Santos, A. dos, M. F. Viante, D. J. Pochapski, A. J. Downs, and C. A.P. Almeida. 2018. "Enhanced Removal of P-Nitrophenol from Aqueous Media by Montmorillonite Clay Modified with a Cationic Surfactant." *Journal of Hazardous Materials* 355: 136–44. <https://doi.org/10.1016/j.jhazmat.2018.02.041>.
- Sato, Tsutomu, Takashi Watanabe, and Ryohei Otsuka. 1992. "Effects of Layer Charge, Charge Location, and Energy Change on Expansion Properties of Dioctahedral Smectites." *Clays and Clay Minerals* 40 (1): 103–13. <https://doi.org/10.1346/CCMN.1992.0400111>.
- Shah, Kinjal J., Manish Kumar Mishra, Atindra D. Shukla, Toyoko Imae, and Dinesh O. Shah. 2013. "Controlling Wettability and Hydrophobicity of Organoclays Modified with Quaternary Ammonium Surfactants." *Journal of Colloid and Interface Science* 407: 493–99. <https://doi.org/10.1016/j.jcis.2013.05.050>.
- Sharma, Maya, and Anjali Bajpai. 2018. "Superabsorbent Nanocomposite from Sugarcane Bagasse, Chitin and Clay: Synthesis, Characterization and Swelling Behaviour." *Carbohydrate Polymers* 193: 281–88. <https://doi.org/10.1016/j.carbpol.2018.04.006>.
- Shin, Hyeong Moo, Verónica M. Vieira, P. Barry Ryan, Russell Detwiler, Brett Sanders, Kyle Steenland, and Scott M. Bartell. 2011. "Environmental Fate and Transport Modeling for Perfluorooctanoic Acid Emitted from the Washington Works Facility in West Virginia." *Environmental Science and Technology* 45 (4): 1435–42. <https://doi.org/10.1021/es102769t>.
- Simonin, Jean Pierre. 2016. "On the Comparison of Pseudo-First Order and Pseudo-Second Order Rate Laws in the Modeling of Adsorption Kinetics." *Chemical Engineering Journal* 300: 254–63. <https://doi.org/10.1016/j.cej.2016.04.079>.
- Singh, Raj Kamal, Sujana Fernando, Sadjad Fakouri Baygi, Nicholas Multari, Selma Mededovic Thagard, and Thomas M. Holsen. 2019. "Breakdown Products from Perfluorinated Alkyl Substances (PFAS) Degradation in a Plasma-Based Water Treatment Process." *Environmental Science and Technology* 53 (5): 2731–38. <https://doi.org/10.1021/acs.est.8b07031>.
- Singh, Sandip K., and Anthony W. Savoy. 2020. "Ionic Liquids Synthesis and Applications: An Overview." *Journal of Molecular Liquids* 297: 112038. <https://doi.org/10.1016/j.molliq.2019.112038>.
- Soltani, Roozbeh, Azam Marjani, Mina Hosseini, and Saeed Shirazian. 2020. "Synthesis and Characterization of Novel N-Methylimidazolium-Functionalized KCC-1: A Highly Efficient Anion Exchanger of Hexavalent Chromium." *Chemosphere* 239: 124735. <https://doi.org/10.1016/j.chemosphere.2019.124735>.
- Souza, Michelle Andrade, Nelson Marcos Larocca, and Luiz Antonio Pessan. 2016. "Highly Thermal Stable Organoclays of Ionic Liquids and Silane Organic Modifiers and Effect of Montmorillonite

- Source.” *Journal of Thermal Analysis and Calorimetry* 126 (2): 499–509.
<https://doi.org/10.1007/s10973-016-5501-z>.
- Stepnowski, Piotr, Wojciech Mrozik, and Joanna Nichthauser. 2007. “Adsorption of Alkylimidazolium and Alkylpyridinium Ionic Liquids onto Natural Soils.” *Environmental Science and Technology* 41 (2): 511–16. <https://doi.org/10.1021/es062014w>.
- Tang, Heqing, Qingqing Xiang, Min Lei, Jingchun Yan, Lihua Zhu, and Jing Zou. 2012. “Efficient Degradation of Perfluorooctanoic Acid by UV-Fenton Process.” *Chemical Engineering Journal* 184: 156–62. <https://doi.org/10.1016/j.cej.2012.01.020>.
- Taylor, Publisher, Kimberly E Carter, James Farrell, Kimberly E Carter, and James Farrell. 2010. “Removal of Perfluorooctane and Perfluorobutane Sulfonate from Water via Carbon Adsorption and Ion Exchange.” *Separation Science and Technology* 45(6): 37–41.
<https://doi.org/10.1080/01496391003608421>.
- Tichonovas, Martynas, Edvinas Krugly, Dalia Jankunaite, Viktoras Racys, and Dainius Martuzevicius. 2017. “Ozone-UV-Catalysis Based Advanced Oxidation Process for Wastewater Treatment.” *Environmental Science and Pollution Research* 24 (21): 17584–97. <https://doi.org/10.1007/s11356-017-9381-y>.
- Trojanowicz, Marek, Anna Bojanowska-Czajka, Iwona Bartosiewicz, and Krzysztof Kulisa. 2018. “Advanced Oxidation/Reduction Processes Treatment for Aqueous Perfluorooctanoate (PFOA) and Perfluorooctanesulfonate (PFOS) – A Review of Recent Advances.” *Chemical Engineering Journal* 336: 170–99. <https://doi.org/10.1016/j.cej.2017.10.153>.
- Tzabar, Nir, and H. J. M. Ter Brake. 2016. “Adsorption Isotherms and Sips Models of Nitrogen, Methane, Ethane, and Propane on Commercial Activated Carbons and Polyvinylidene Chloride.” *Adsorption* 22 (7): 901–14. <https://doi.org/10.1007/s10450-016-9794-9>.
- UNEP. 2019. “The New POPs under the Stockholm Convention.” Stockholm Convention. 2021.8.
<http://chm.pops.int/TheConvention/ThePOPs/TheNewPOPs/tabid/2511/Default.aspx>.
- US EPA. 2016a. “Drinking Water Health Advisory for Perfluorooctanoic Acid (PFOA).”
- US EPA. 2019. “Per- and Polyfluoroalkyl Substances (PFAS) Using External Standard Calibration and Multiple Reaction Monitoring (MRM) Liquid Chromatography/Tandem Mass Spectrometry (LC/MS/MS).” <https://doi.org/10.1037/0033-2909.126.1.78>.
- US EPA, OW. 2016b. “Drinking Water Action Plan.” 2021.6.12. <https://www.epa.gov/ground-water-and-drinking-water/drinking-water-action-plan>.
- Vecitis, Chad D., Hyunwoong Park, Jie Cheng, Brian T. Mader, and Michael R. Hoffmann. 2009. “Treatment Technologies for Aqueous Perfluorooctanesulfonate (PFOS) and Perfluorooctanoate (PFOA).” *Frontiers of Environmental Science and Engineering in China* 3 (2): 129–51.
<https://doi.org/10.1007/s11783-009-0022-7>.
- Venkataraman, N. V., and S. Vasudevan. 2002. “Characterization of Alkyl Chain Conformation in an Intercalated Cationic Lipid Bilayer by IR Spectroscopy.” *Journal of Physical Chemistry B* 106 (32): 7766–73. <https://doi.org/10.1021/jp025743g>.
- Verma, Sanny, Bineyam Mezgebe, Endalkachew Sahle-Demessie, and Mallikarjuna N. Nadagouda. 2021. “Photooxidative Decomposition and Defluorination of Perfluorooctanoic Acid (PFOA) Using an Innovative Technology of UV-Vis/ZnxCu1-XFe2O4/Oxalic Acid.” *Chemosphere* 280: 1–11.
<https://doi.org/10.1016/j.chemosphere.2021.130660>.

- Vu, Chi Thanh, and Tingting Wu. 2020. "Adsorption of Short-Chain Perfluoroalkyl Acids (PFAAs) from Water/Wastewater." *Environmental Science: Water Research and Technology* 6 (11): 2958–72. <https://doi.org/10.1039/d0ew00468e>.
- Wang, Jiaxuan, Lei Wang, Changqing Xu, Rui Zhi, Rui Miao, Tong Liang, Xianglei Yue, Yongtao Lv, and Tingting Liu. 2018. "Perfluorooctane Sulfonate and Perfluorobutane Sulfonate Removal from Water by Nanofiltration Membrane: The Roles of Solute Concentration, Ionic Strength, and Macromolecular Organic Foulants." *Chemical Engineering Journal* 332 (July 2017): 787–97. <https://doi.org/10.1016/j.cej.2017.09.061>.
- Wang, Lan, Xu Wang, Jiao Yin, and Chuanyi Wang. 2016. "Insights into the Physicochemical Characteristics from Vermiculite to Silica Nanosheets." *Applied Clay Science* 132–133: 17–23. <https://doi.org/10.1016/j.clay.2016.05.006>.
- Wang, Meichen, Asuka A. Orr, Joseph M. Jakubowski, Kelsea E. Bird, Colleen M. Casey, Sara E. Hearon, Phanourios Tamamis, and Timothy D. Phillips. 2021. "Enhanced Adsorption of Per- and Polyfluoroalkyl Substances (PFAS) by Edible, Nutrient-Amended Montmorillonite Clays." *Water Research* 188: 116534. <https://doi.org/10.1016/j.watres.2020.116534>.
- Wang, Shana, Qi Yang, Fei Chen, Jian Sun, Kun Luo, Fubing Yao, Xiaolin Wang, Dongbo Wang, Xiaoming Li, and Guangming Zeng. 2017. "Photocatalytic Degradation of Perfluorooctanoic Acid and Perfluorooctane Sulfonate in Water: A Critical Review." *Chemical Engineering Journal* 328: 927–42. <https://doi.org/10.1016/j.cej.2017.07.076>.
- Wang, Ting, Shali Ai, Yaoyu Zhou, Zirui Luo, Chunhao Dai, Yuan Yang, Jiachao Zhang, Hongli Huang, Shuang Luo, and Lin Luo. 2018. "Adsorption of Agricultural Wastewater Contaminated with Antibiotics, Pesticides and Toxic Metals by Functionalized Magnetic Nanoparticles." *Journal of Environmental Chemical Engineering* 6 (5): 6468–78. <https://doi.org/https://doi.org/10.1016/j.jece.2018.10.014>.
- Wang, Wei; Maimaiti Ayiguli; Shi Huilan; Wu Rongrong; Wang Run; Li Zelun; Qi Delin; Yu Gang; Deng Shubo. 2019. "Adsorption Behavior and Mechanism of Emerging Perfluoro-2-Propoxypropanoic Acid (GenX) on Activated Carbons and Resins." *Chemical Engineering Journal* 364: 132–38. <https://doi.org/10.1037/0033-2909.126.1.78>.
- Wang, Xiaoyu, Orhan Ozdemir, Marc A Hampton, Anh V Nguyen, and Duong D Do. 2012. "The Effect of Zeolite Treatment by Acids on Sodium Adsorption Ratio of Coal Seam Gas Water." *Water Research* 46 (16): 5247–54. <https://doi.org/https://doi.org/10.1016/j.watres.2012.07.006>.
- Wang, Yuan, Pengyi Zhang, Gang Pan, and Hao Chen. 2008. "Ferric Ion Mediated Photochemical Decomposition of Perfluorooctanoic Acid (PFOA) by 254 Nm UV Light." *Journal of Hazardous Materials* 160 (1): 181–86. <https://doi.org/10.1016/j.jhazmat.2008.02.105>.
- Wang, Zhanyun, Andreas M. Buser, Ian T. Cousins, Silvia Demattio, Wiebke Drost, Olof Johansson, Koichi Ohno, et al. 2021. "A New OECD Definition for Per- And Polyfluoroalkyl Substances." *Environmental Science and Technology* 55 (23): 15575–78. <https://doi.org/10.1021/acs.est.1c06896>.
- Wang, Zhanyun, Jamie C. Dewitt, Christopher P. Higgins, and Ian T. Cousins. 2017. "A Never-Ending Story of Per- and Polyfluoroalkyl Substances (PFASs)?" *Environmental Science and Technology* 51 (5): 2508–18. <https://doi.org/10.1021/acs.est.6b04806>.
- Wanninayake, Dushanthi M. 2021. "Comparison of Currently Available PFAS Remediation Technologies in Water: A Review." *Journal of Environmental Management* 283: 111977. <https://doi.org/10.1016/j.jenvman.2021.111977>.

- Ward, A. F. H., and L. Tordai. 1946. "Standard Entropy of Adsorption." *Nature* 158 (4012): 416.
- Watanabe, Nobuhisa, Shusuke Takemine, Katsuya Yamamoto, Yuki Haga, and Mitsuyasu Takata. 2016. "Residual Organic Fluorinated Compounds from Thermal Treatment of PFOA, PFHxA and PFOS Adsorbed onto Granular Activated Carbon (GAC)." *Journal of Material Cycles and Waste Management* 18 (4): 625–30. <https://doi.org/10.1007/s10163-016-0532-x>.
- Baird, Rodger B., Andrew D. Eaton, and Lenore S. Clesceri. Standard methods for the examination of water and wastewater. Edited by Eugene W. Rice. Vol. 10. Washington, DC: American public health association, 2012.
- Weng, Chih-Huang, Cha-Zen Tsai, Sue-Hua Chu, and Yogesh C Sharma. 2007. "Adsorption Characteristics of Copper(II) onto Spent Activated Clay." *Separation and Purification Technology* 54 (2): 187–97. <https://doi.org/https://doi.org/10.1016/j.seppur.2006.09.009>.
- Wilkes, John S. 2002. "A Short History of Ionic Liquids - From Molten Salts to Neoteric Solvents." *Green Chemistry* 4 (2): 73–80. <https://doi.org/10.1039/b110838g>.
- Winchell, Lloyd J., John J. Ross, Martha J.M. Wells, Xavier Fonoll, John W. Norton, and Katherine Y. Bell. 2021. "Per- and Polyfluoroalkyl Substances Thermal Destruction at Water Resource Recovery Facilities: A State of the Science Review." *Water Environment Research* 93 (6): 826–43. <https://doi.org/10.1002/wer.1483>.
- Wu, Boran, Shilai Hao, Younjeong Choi, Christopher P. Higgins, Rula Deeb, and Timothy J. Strathmann. 2019. "Rapid Destruction and Defluorination of Perfluorooctanesulfonate by Alkaline Hydrothermal Reaction." *Environmental Science and Technology Letters* 6 (10): 630–36. <https://doi.org/10.1021/acs.estlett.9b00506>.
- Wu, Dan, Xukai Li, Yiming Tang, Ping Lu, Weirui Chen, Xiaoting Xu, and Laisheng Li. 2017. "Mechanism Insight of PFOA Degradation by ZnO Assisted-Photocatalytic Ozonation: Efficiency and Intermediates." *Chemosphere* 180: 247–52. <https://doi.org/10.1016/j.chemosphere.2017.03.127>.
- Wu, Limei, Libing Liao, Guocheng Lv, Faxiang Qin, and Zhaohui Li. 2014. "Microstructure and Process of Intercalation of Imidazolium Ionic Liquids into Montmorillonite." *Chemical Engineering Journal* 236: 306–13. <https://doi.org/10.1016/j.cej.2013.09.063>.
- Wu, Limei, Chengxue Yang, Lefu Mei, Faxiang Qin, Libing Liao, and Guocheng Lv. 2014. "Microstructure of Different Chain Length Ionic Liquids Intercalated into Montmorillonite: A Molecular Dynamics Study." *Applied Clay Science* 99: 266–74. <https://doi.org/10.1016/j.clay.2014.07.004>.
- Xiao, Feng. 2017. "Emerging Poly- and Perfluoroalkyl Substances in the Aquatic Environment: A Review of Current Literature." *Water Research* 124: 482–95. <https://doi.org/10.1016/j.watres.2017.07.024>.
- Xiao, Feng, Bosen Jin, Svetlana A. Golovko, Mikhail Y. Golovko, and Baoshan Xing. 2019. "Sorption and Desorption Mechanisms of Cationic and Zwitterionic Per- And Polyfluoroalkyl Substances in Natural Soils: Thermodynamics and Hysteresis." *Environmental Science and Technology* 53 (20): 11818–27. <https://doi.org/10.1021/acs.est.9b05379>.
- Xiao, Feng, Pavankumar Challa Sasi, Bin Yao, Alena Kubátová, Svetlana A. Golovko, Mikhail Y. Golovko, and Dana Soli. 2020. "Thermal Stability and Decomposition of Perfluoroalkyl Substances on Spent Granular Activated Carbon." *Environmental Science and Technology Letters* 7 (5): 343–50. <https://doi.org/10.1021/acs.estlett.0c00114>.
- Xiao, Feng, Xiangru Zhang, Lee Penn, John S. Gulliver, and Matt F. Simcik. 2011. "Effects of

- Monovalent Cations on the Competitive Adsorption of Perfluoroalkyl Acids by Kaolinite: Experimental Studies and Modeling.” *Environmental Science and Technology* 45 (23): 10028–35. <https://doi.org/10.1021/es202524y>.
- Xiao, Leilei, Yuhan Ling, Alaaeddin Alsbaiee, Chenjun Li, Damian E. Helbling, and William R. Dichtel. 2017. “ β -Cyclodextrin Polymer Network Sequesters Perfluorooctanoic Acid at Environmentally Relevant Concentrations.” *Journal of the American Chemical Society* 139 (23): 7689–92. <https://doi.org/10.1021/jacs.7b02381>.
- Xu, Yi, Xuefeng Liang, Yingming Xu, Xu Qin, Qingqing Huang, Lin Wang, and Yuebing Sun. 2017. “Remediation of Heavy Metal-Polluted Agricultural Soils Using Clay Minerals: A Review.” *Pedosphere* 27 (2): 193–204. [https://doi.org/10.1016/S1002-0160\(17\)60310-2](https://doi.org/10.1016/S1002-0160(17)60310-2).
- Yan, Bei, Gabriel Munoz, Sébastien Sauvé, and Jinxia Liu. 2020. “Molecular Mechanisms of Per- and Polyfluoroalkyl Substances on a Modified Clay: A Combined Experimental and Molecular Simulation Study.” *Water Research* 184: 116166. <https://doi.org/10.1016/j.watres.2020.116166>.
- Yan, Bei, Jian Wang, and Jinxia Liu. 2021. “STXM-XANES and Computational Investigations of Adsorption of per- and Polyfluoroalkyl Substances on Modified Clay.” *Water Research* 201: 117371. <https://doi.org/10.1016/j.watres.2021.117371>.
- Yang, Liping, Lingyan Zhu, and Zhengtao Liu. 2011. “Occurrence and Partition of Perfluorinated Compounds in Water and Sediment from Liao River and Taihu Lake, China.” *Chemosphere* 83 (6): 806–14.
- Yang, Yiqiong, Zenghui Zheng, Wenqing Ji, Jingcheng Xu, and Xiaodong Zhang. 2020. “Insights to Perfluorooctanoic Acid Adsorption Micro-Mechanism over Fe-Based Metal Organic Frameworks: Combining Computational Calculation with Response Surface Methodology.” *Journal of Hazardous Materials* 395: 122686. <https://doi.org/10.1016/j.jhazmat.2020.122686>.
- Ye, Jianshe, Xiao Chen, Chao Chen, and Bate Bate. 2019. “Emerging Sustainable Technologies for Remediation of Soils and Groundwater in a Municipal Solid Waste Landfill Site – A Review.” *Chemosphere* 227: 681–702. <https://doi.org/10.1016/j.chemosphere.2019.04.053>.
- Yu, Jing, Lu Lv, Pei Lan, Shujuan Zhang, Bingcai Pan, and Weiming Zhang. 2012. “Effect of Effluent Organic Matter on the Adsorption of Perfluorinated Compounds onto Activated Carbon.” *Journal of Hazardous Materials* 226: 99–106. <https://doi.org/10.1016/j.jhazmat.2012.04.073>.
- Yu, Liang, Xiaodong Liu, and Zulin Hua. 2022. “Occurrence, Distribution, and Risk Assessment of Perfluoroalkyl Acids in Drinking Water Sources from the Lower Yangtze River.” *Chemosphere* 287 (P1): 132064. <https://doi.org/10.1016/j.chemosphere.2021.132064>.
- Yu, Qiang, Ruiqi Zhang, Shubo Deng, Jun Huang, and Gang Yu. 2009. “Sorption of Perfluorooctane Sulfonate and Perfluorooctanoate on Activated Carbons and Resin: Kinetic and Isotherm Study.” *Water Research* 43 (4): 1150–58. <https://doi.org/10.1016/j.watres.2008.12.001>.
- Zhang, D.Q., W.L. Zhang, and Y.N. Liang. 2019. “Adsorption of Perfluoroalkyl and Polyfluoroalkyl Substances (PFASs) from Aqueous Solution - A Review.” *Science of The Total Environment* 694: 133606. <https://doi.org/10.1016/j.scitotenv.2019.133606>.
- Zhang, Di, Qi Luo, Bin Gao, Sheau Yun Dora Chiang, David Woodward, and Qingguo Huang. 2016. “Sorption of Perfluorooctanoic Acid, Perfluorooctane Sulfonate and Perfluoroheptanoic Acid on Granular Activated Carbon.” *Chemosphere* 144: 2336–42. <https://doi.org/10.1016/j.chemosphere.2015.10.124>.
- Zhang, Rui, and P. Somasundaran. 2006. “Advances in Adsorption of Surfactants and Their Mixtures at

- Solid/Solution Interfaces.” *Advances in Colloid and Interface Science* 123–126 (SPEC. ISS.): 213–29. <https://doi.org/10.1016/j.cis.2006.07.004>.
- Zhang, Zepeng, Jichu Zhang, Libing Liao, and Zhiguo Xia. 2013. “Synergistic Effect of Cationic and Anionic Surfactants for the Modification of Ca-Montmorillonite.” *Materials Research Bulletin* 48 (5): 1811–16. <https://doi.org/10.1016/j.materresbull.2013.01.029>.
- Zhao, Lixia, Jingna Bian, Yahui Zhang, Lingyan Zhu, and Zhengtao Liu. 2014. “Comparison of the Sorption Behaviors and Mechanisms of Perfluorosulfonates and Perfluorocarboxylic Acids on Three Kinds of Clay Minerals.” *Chemosphere* 114 (May 2009): 51–58. <https://doi.org/10.1016/j.chemosphere.2014.03.098>.
- Zhao, Mei, Li Wei, Yunkai Zheng, Mengping Liu, Junliang Wang, and Yuping Qiu. 2019. “Structural Effect of Imidazolium-Type Ionic Liquid Adsorption to Montmorillonite.” *Science of the Total Environment* 666: 858–64. <https://doi.org/10.1016/j.scitotenv.2019.02.297>.
- Zhou, Qin, Shubo Deng, Qiang Yu, Qiaoying Zhang, Gang Yu, Jun Huang, and Hongping He. 2010. “Sorption of Perfluorooctane Sulfonate on Organo-Montmorillonites.” *Chemosphere* 78 (6): 688–94. <https://doi.org/10.1016/j.chemosphere.2009.12.005>.
- Zhou, Zhen, Yong Liang, Yali Shi, Lin Xu, and Yaqi Cai. 2013. “Occurrence and Transport of Perfluoroalkyl Acids (PFAAs), Including Short-Chain PFAAs in Tangxun Lake, China.” *Environmental Science and Technology* 47 (16): 9249–57. <https://doi.org/10.1021/es402120y>.

CURRICULUM VITAE

Qianqian Dong

Education

- Feb 2017-present Ph.D. Environmental Engineering (Water Chemistry and Technology)
University of Wisconsin-Milwaukee
- Dissertation: Adsorption of Perfluoroalkyl Substances (PFAS) on
Functionalized Clay Minerals: Effects of Modifier Property and Clay Mineral
Structure
Advisor: Professor Yin Wang
- Sep 2012-Mar 2014 M.S. Environmental Engineering, Aquatic Pollution Ecology
Tongji University, China
Advisor: Professor Qinghui Huang
- Feb 2013-May 2013 Graduate Certificate, Ecoservices
Venice International University, Italy
- Sep 2007-May 2011 B.S. Environmental Science
Henan University of Urban Construction, China

Research specializations

Water chemistry and technology
Analytical chemistry
Aquatic Pollution Ecology

Publications

Refereed journal articles

- 2022 **Qianqian Dong**, Xiaopeng Min, Yanan Zhao, Wenxin Zhang, Yin Wang. Removal of Perfluoroalkyl Acids and Precursors with Silylated Clay: Efficient Adsorption and Enhanced Reuse. Will submit to *Chemical Engineering Journal*.
- 2022 **Qianqian Dong**, Xiaopeng Min, Jingwan Huo, Yanan Zhao, Yin Wang. The effect of clay composition and PFAS structure on the adsorption of PFAS by ionic liquid-modified clays. Will submit to *Science of Total Environment*.
- 2022 Jingwan Huo, Xiaopeng Min, **Qianqian Dong**, Shangping Xu, and Yin Wang. Comparison of Zn–Al and Mg–Al layered double hydroxides for adsorption of perfluorooctanoic acid. *Chemosphere* (2022).
- 2021 **Qianqian Dong**, Xiaopeng Min, Jingwan Huo, and Yin Wang. Efficient Sorption of Perfluoroalkyl Acids by Ionic Liquid-Modified Natural Clay. *Chemical Engineering Journal Advances* (2021).

- 2020 Xiaopeng Min, Dulay Trujillo, Jingwan Huo, **Qianqian Dong**, and Yin Wang. Amine-bridged periodic mesoporous organosilica nanomaterial for efficient removal of selenate. *Chemical Engineering Journal* (2020).
- 2020 Zhou, Guihua, Bing Jin, Yale Wang, **Qianqian Dong**, Arnab Maity, Jingbo Chang, Ren Ren et al. Ultrasensitive sensors based on aluminum oxide-protected reduced graphene oxide for phosphate ion detection in real water. *Molecular Systems Design & Engineering* (2020).
- 2019 Huang, Xingkang, Xiaoru Guo, **Qianqian Dong**, Lianjun Liu, Rebecca Tallon, and Junhong Chen. Zero-Wastewater Capacitive Deionization: Selective Removal of Heavy Metal Ions in Tap Water Assisted by Phosphate Ions. *Environmental Science: Nano* (2019).
- 2018 **Qianqian Dong**⁺, Xiaoru Guo⁺, Xingkang Huang, Lianjun Liu, Rebecca Tallon, Bruce Taylor, and Junhong Chen. Selective removal of lead ions through capacitive deionization: Role of ion-exchange membrane. *Chemical Engineering Journal* (2018).
- 2018 **Qianqian Dong**, Feng Wang, Yihua Xiao, Penghui Li, and Qinghui Huang. Effects of elevated production of autochthonous dissolved organic matter on the freely dissolved concentration of cadmium. *Environmental Science: Processes & Impacts* (2018).
- 2014 **Qianqian Dong**, Penghui Li, Qinghui Huang, Ahmed A. Abdelhafez, Ling Chen. Occurrence, Polarity and Bioavailability of Dissolved Organic Matter in the Huangpu River, China. *Journal of Environmental Science*, 2014, 26: [DOI: 10.1016/j.jes.2014.06.020].
- 2014 **Qianqian Dong**, Ai Zhang, Yongmei Li, Ling Chen, Qinghui Huang. Linking Optical Properties of Dissolved Organic Matter with NDMA Formation Potential in the Huangpu River. *Environmental Science*, 2014, 35(3).

Posters & Presentations

- 2019 **Qianqian Dong**, Yin Wang. Sorption of PFOA and PFOS on organic-modified clay: Effect of modifier structure. *Emerging Contaminants Short Course. Marquette University, WI, USA.*
- 2019 **Qianqian Dong**, Yin Wang. Functionalized mineral adsorbents for the removal of per-fluorinated chemicals. *257th American Chemistry Society National Meeting and Exposition. Orlando, FL, USA.*

Projects

- | | |
|-------------------|---|
| 2018-present | Treatment of legacy and emerging fluoroalkyl contaminants in groundwater with integrated approaches: rapid and regenerable adsorption and UV-induced defluorination
<i>DoD Strategic Environmental Research and Development Program, USA</i> |
| 2017-2018 | The impact of ion-exchange membranes on lead removal by capacitive deionization (CDI) technology
<i>NSF I/UCRC Water Equipment and Policy Center, Milwaukee</i> |
| 2017-2018 | Ultra-sensitive novel Graphene-Based Transistor Sensors for orthophosphate ions detection
<i>NSF GOALI grant CBET-1606057</i> |
| 2021-2022 | Novel Iron-based electrocoagulation-peroxidation treatment process for removal of PFAS
<i>NSF I/UCRC Water Equipment and Policy Center, Milwaukee</i> |
| Sep 2011-Mar 2014 | Behavior and Effects of Dissolved Organic Matter (DOM) Driven by Eutrophication in River Plume Zones
<i>National Natural Science Foundation of China</i> |

Mar 2012-Mar 2014	Development of an Environmental Specimen Bank in the Yangtze River Delta and Study on the Spatial Distribution of Typical Pollutants <i>Fundamental Research Funds for the Central Universities</i>
Oct 2010-May 2011	Preparation and Performance Study of Floating Magnetic Tio ₂ Photo Catalyst <i>Undergraduate thesis</i>

Employment

2017-present	University of Wisconsin Milwaukee Research Assistant: PFAS removal with regenerable and functionalized clay minerals (2018-2022), US drinking water crisis (2019), Lead removal with CDI technology (2017-2018) Teaching Assistant: Computer Based Engineering Analysis (2018)
Mar 2014-Apr 2015	Shanghai Cyeco Environmental Technology Co., Ltd. Assistant Environmental Engineer
Sep 2011-Mar 2014	Tongji University Research Assistant, IESD Office Assistance

Awards

2018-2022	Chancellor graduate award <i>UW Milwaukee, USA</i>
2019	Graduate Student Travel Award <i>UW Milwaukee, USA</i>
2019	Academic Excellence Award <i>Central State Water Environment Association, USA</i>
2015	Outstanding Employee Award <i>Cyeco Environmental Technology Company, China</i>
2013	Italian Governmental Scholarship <i>Venice International University, Italy</i>
2011	Full tuition scholarship <i>Tongji University, China</i>
2009	Chinese National Scholarship <i>Ministry of Education, China</i>

Skills

Instrumental Chemical Analysis (proficient) Liquid Chromatography-Spectrometry, Solid Phase Extraction, Total Organic Carbon Analyzer, Double-beam Spectrophotometer, Fluorescence Spectrophotometer, Gel Permeation Chromatography, X-ray Powder Diffraction, Fourier Transform Electron Microscope, Scanning Electron Microscope